

RUPTURE PHENOMENA IN VISCOELASTIC MATERIALS

Thesis by
Wolfgang Gustav Knauss

In Partial Fulfillment of the Requirements
For the Degree of
Doctor of Philosophy

California Institute of Technology
Pasadena, California

1963

To my patient wife

ACKNOWLEDGEMENTS

It is a pleasure to express my appreciation to Professor M. L. Williams for suggesting this interesting problem area and for his valuable comments, especially during the latter stages of this work.

I wish to thank Dr. R. F. Landel of the California Institute of Technology Jet Propulsion Laboratory for making his laboratory facilities so readily available for the determination of the material properties. The experimental material was supplied by Drs. R. B. Kruse and T. A. Neely of the Thiokol Chemical Corporation, Huntsville, Alabama.

My thanks are also due to Mrs. R. Lees and Mr. K. Hebert of the California Institute of Technology Computing Center for their continuing advice and assistance during the programming of the numerical calculations for an IBM 7090 computer.

I am indebted to Mrs. Elizabeth Fox and Miss Helen Burrus for their excellent work in typing this manuscript and to Mrs. Betty Wood for her assistance in lettering the figures.

Two National Aeronautics and Space Administration Fellowships during the course of this research are also gratefully acknowledged. Part of this research was supported by the National Aeronautics and Space Administration Research Grant NsG-172-60.

ABSTRACT

A failure theory for high polymers is developed from the hypothesis that weak regions exist in the material. Defects nucleate in these regions through bond rupture until the defects reach a size which is critical for the applied boundary loading. This critical condition is based on energy balance considerations,

By considering the relaxation of the polymer chain in terms of the phenomenological stress-strain behavior and the rupture of chemical bonds in terms of an Arrhenius type rate law, the theory is able to accommodate an arbitrary stress or strain history, and shows reasonably good agreement with experiments which cover a large range of conditions.

In addition the stress analysis of a special crack geometry is presented. The geometry consists of a thin infinite strip containing a semi-infinite crack, For a uniform separation of the infinite boundaries an infinitesimal elasticity solution is obtained with the help of the Fourier transform and Wiener-Hopf techniques. The effect of large strains on the stresses near the crack tip is studied experimentally and a surprising correlation with the infinitesimal elasticity solution is found,

TABLE OF CONTENTS

PART	TITLE	PAGE
I	THE RUPTURE OF POLYMERIC MATERIALS	1
A.	MECHANICAL BEHAVIOR OF VISCOELASTIC MATERIALS	8
1.1	Representation of Stress-Strain Behavior	8
1.2	Time-Temperature Equivalence	12
1.3	Effect of Finite Strain	14
1.4	Isothermal vs. Adiabatic Rupture Properties	16
B.	THE PHENOMENOLOGICAL DESCRIPTION OF THE RUPTURE PROCESS	19
1.5	The Molecular Structure of Polymers	19
a.	The polymer chain	20
b.	Effect of chain slipping	21
c.	The chemical bond	23
d.	Atmospheric effects	25
1.6	Microscopic Aspects	26
a.	The nature of polymer defects	28
b.	The effect of volume size upon rupture properties	29
1.7	Macroscopic Considerations	31
a.	Fracture markings	32
b.	Effect of the multiaxial stress state	36
c.	Energetics of crack growth	39
C.	THE RUPTURE MODEL	42
1.8	Defect Growth	44
1.9	A Condition of Critical Loading	49

TABLE OF CONTENTS (Cont'd)

PART	TITLE	PAGE
D.	APPLICATION TO RUPTURE PREDICTION	54
	1.10 The Constant Strain Rate Test	56
	1.11 Rupture Initiation Time	58
	1.12 Crack Propagation at Constant Velocity	62
	a. Analytical considerations	63
	b. Experimental analysis	68
	1.13 Suggested Applications of the Failure Theory	69
	a. Crack acceleration	72
	b. Cumulative damage in the constant strain rate test	75
	c. The dual strain rate test	76
	d. Stress cycling	78
	1.14 Filled Polymer Systems	81
E.	EXAMINATION OF THE FRACTURE MODEL	82
F.	CONCLUSION	86
II	STRESS ANALYSIS OF A SPECIAL CRACK GEOMETRY	89
A.	CLASSICAL ELASTICITY SOLUTION	91
	2.1 Statement of the Mathematical Problem	92
	2.2 Solution	94
	2.3 Evaluation of Stress and Displacement Integrals	102
	2.4 Numerical Evaluation	105
B.	EXPERIMENTAL ANALYSIS OF THE STRESSES IN A SLIT RUBBER SHEET	109
	2.5 Large Deformation Stress Analysis	110

TABLE OF CONTENTS (Cont'd)

PART	TITLE	PAGE
	2.6 Experimental Procedure	114
	2.7 Numerical Evaluation	115
C.	CONCLUSION	120
	REFERENCES	122
	FIGURES	129
	APPENDIX A	157
	APPENDIX B	161

INTRODUCTION

In the past, investigators have tended to explain material failure by establishing the criticality of various stress or strain combinations, or by the energy instability concept pioneered by Griffith. Since in their usual application these criteria are rate and thus time independent they have been of restricted usefulness for materials possessing strongly time dependent mechanical properties. Excepting the analysis of creep deformations, this deficiency has been of little practical concern because the usual engineering metals possess only limited rate dependence. But with the increasing incorporation of viscoelastic materials such as the organic glasses and rubbers in structural design, as well as the use of metals at higher and higher temperatures, an extension of the presently existing knowledge to rate dependent failure processes is believed timely .

Depending upon the temperature and the rate of load application, viscoelastic materials can exhibit such different behavior as brittle rupture response or viscous flow and non-recoverable permanent set. In this regard they constitute a class of materials that form a transition between the essentially rigid engineering metals and the highly deformable liquids. One would therefore expect their failure characteristics to reflect certain features of one or the other limit states.

In the following development we shall use the conceptual similarity to metallic behavior in explaining certain aspects of failure. As an important corollary, and because such a similarity

should not be one-sided, one would also expect that the study of rupture phenomena in viscoelastic materials might also aid in elucidating some, possibly yet undetermined, phenomena in metal fracture. Although a metallurgist and a physical chemist may be sceptical of an association of dislocations and chemo-molecular bonds it is, nevertheless, an accepted fact that the high mobility both of dislocations in crystals and of molecular configurations in amorphous polymers are at the origin of fracture behavior in the respective materials. It appears therefore that the study of rupture phenomena in viscoelastic materials may not only consist of an important extension of existing fracture knowledge *per se*, but also provide an important source of new ideas for understanding rupture in the engineering metals.

Since the analysis of viscoelastic rupture includes the analysis of stresses and strains in the fracturing solid, a part of this dissertation is devoted to the stress analysis of a test geometry employed here in crack propagation studies. Inasmuch as this stress analysis can apply also to materials which are not viscoelastic it has been separated from the rupture analysis in a second part of this dissertation,

Part I is thus concerned with the rupture analysis of viscoelastic materials. Following the presentation of background information, a rupture model is deduced which is subsequently used to predict rupture in some selected test situations.

Part II contains the stress analysis for the stretching of a thin sheet containing a semi-infinite crack, Although the

physical situation treated in Part I actually requires the consideration of large deformation effects the theoretical analysis is based on the theory of classical elasticity. The influence of large deformations and non-linear stress-strain behavior is then examined in an experimental study on a rubber sheet of the same geometry.

PART I

THE RUPTURE OF POLYMERIC MATERIALS

Initially the exploration of rupture in polymeric materials was related to the strength characteristics of natural and synthetic textile fibers; but recently this problem has obtained new impetus from developments in solid propellant rocket technology where the fracture threshold and its control is of major production and design importance.

Solid propellant materials consist of a physical mixture of oxidizer granules and a rubber matrix filling the interstitial spaces between the oxidizer particles. Their characteristic behavior arises from both the viscoelastic nature of the rubber and the relaxation effects associated with the restricted motion of the oxidizer particles. More specifically, the rupture behavior is complicated by the irregular separation of the rubber from the hard filler grains prior to gross fracture. In order to avoid such effects of the interaction between filler and rubber matrix, it seems prudent for an initial investigation of viscoelastic rupture to consider only a one phase system such as a pure rubber. Building upon this foundation one then hopes to extend the results to a two phase system, and eventually to solid propellant fuels, by judicious extrapolation and continuing research.

This dissertation will therefore be concerned with the time dependent failure of viscoelastic materials which can be considered as macroscopically amorphous and homogeneous.

The most extensive study of rate dependent rupture behavior has been made by Rivlin, Thomas, and Greensmith (1-8). These authors have investigated the tear behavior of rubbers by extending the Griffith concept so as to include a rate dependent tearing energy which plays a role analogous to that of surface energy in Griffith's fracture criterion for brittle materials. Such an approach requires an estimate or calculation of the energy in the whole structure which is often a difficult undertaking. Furthermore, the experimental nature of the tearing energy and its dependence on the stress or strain history place severe restrictions on the application of this concept to the variety of situations encountered in practice.

It is therefore pertinent to explore a more fundamental description of the time dependent failure process which admits an arbitrary stress history without necessitating an experimental simulation of the failure history to determine the tearing energy. This approach to failure characterization is also found amenable to the prediction of rupture from a knowledge of the local stress field near notches and inclusions, thus obviating the often intractable energy analysis of the whole structure,

The essential feature of this dissertation is thus the study of fracture as a local, time dependent phenomenon from the basis of a judicious combination of microscopic and macroscopic considerations.

Attempts in this direction have been made previously by several investigators, notably Tobolsky and Eyring (9), and

F. Bueche (10). In both attempts difficult mathematical obstacles were circumvented by simplifications tantamount to a restatement of initial assumptions which would not necessarily appear physically reasonable. But, more importantly, only implicit cognizance has been taken of the energetic aspects of gross rupture without incorporating them explicitly in even an approximate manner. As a result the theories have been applicable only to relatively small ranges of experimental test conditions, The present work, however, eliminates these deficiencies and in addition considers a more detailed model of the rupture process than employed by the previous authors.

Apart from hypothesizing the source and nature of material defects inherent in polymeric materials, the present development of rupture prediction draws upon the general knowledge of polymer chemistry and fracture mechanics. Although the failure of polymers is a much more complicated process than envisaged in the rupture model of this work it appears prudent to investigate initially only the role of the basic mechanisms in polymer fracture. For this reason the dissertation is concerned only with those aspects of fracture which are common to polymers in general while effects arising from particular chemical formulations are excluded from the analysis. Having established the importance of the mechanisms included in the analysis it should be relatively easy to extend the results to specific materials provided their detailed rupture behavior is known.

In the following chapters we provide first the background required to deduce a failure model and to formulate it mathematically.

Not all the information presented there is included directly in establishing the rupture model, but it is nevertheless necessary for the qualitative understanding of viscoelastic rupture and illustrates simultaneously the variety of processes that influence fracture.

Following the general description and mathematical formulation of the failure model, fracture calculations are presented for specific situations. In this manner the use of the theory is demonstrated while providing a check on the validity of the modelled rupture process through comparison with experimental data. Since rupture often occurs under conditions which are not readily duplicated in the laboratory it is of practical interest to develop an understanding of the rupture process which permits an engineering appraisal of fracture behavior in more general situations. For this purpose some preliminary comments relating to progressive accumulation of rupture, or internal damage, have been included as a guide for future experimental work, although no conclusive experimental work is yet available which would substantiate the theoretical results.

Finally a section is devoted to testing the applicability of the theory to filled polymers by comparing calculated failure behavior with experimental data on a solid rocket propellant material.

A. MECHANICAL BEHAVIOR OF VISCOELASTIC MATERIALS

The mechanical properties of linearly viscoelastic materials and their mathematical representation have been discussed in detail in the literature (11-15). In contrast, the viscoelastic effects associated with large and non-linear deformations are as yet poorly understood and it is appropriate in this context to review briefly the work of other investigators. Following a brief presentation of the mechanical behavior of linearly viscoelastic solids we shall therefore consider the effects of large deformations on the material properties and discuss simultaneously some approximations which make the subsequent analysis of viscoelastic failure more tractable.

1.1 Representation of Stress-Strain Behavior

The distinguishing feature of viscoelastic materials is the incorporation of time effects in the stress-strain relation. Instead of the time independent Hooke's law, relating the stress σ linearly to the strain ϵ through the time independent modulus E

$$\sigma = E \epsilon \quad (1.1)$$

the viscoelastic stress strain law can be written in differential time operator notation as

$$\left\{ \sum_{n=0}^N a_n \frac{\partial^n}{\partial t^n} \right\} \sigma = \left\{ \sum_{n=0}^N b_n \frac{\partial^n}{\partial t^n} \right\} \epsilon \quad (1.2)$$

In this form the material behavior is embodied in the constants* a_n

*We assume for the present that the temperature does not change with time. Its effect upon viscoelastic material response is considered below.

and b_n instead of a simple characteristic Young's modulus E . If, for example, $N \approx 1$ and $b_1 \approx 0$ then the stress resulting from a step strain in time of magnitude ϵ_0 would be given by

$$\sigma(t) = \frac{b_0}{a_1} \epsilon_0 \exp\left\{-t \frac{a_1}{a_0}\right\} \quad (1.3)$$

The observation that this relation represents also the force experienced in a series arrangement of a linear spring and a Newtonian dashpot due to a step strain has led to the representation of viscoelastic material properties by mechanical spring-dashpot models (see fig. 1A). The mechanical model of a spring and dashpot in series is called a Maxwell model. Unfortunately the simple relation 1.3 is usually inadequate to represent actual material behavior so that $N > 1$ is required. This can be shown, however, to be tantamount to a mechanical model consisting of a parallel array of N Maxwell elements, as shown in fig. 1B, the number of elements, N , depending on the time scale of the material response and the accuracy of representation required. The stress response for the described strain history is termed the relaxation modulus and is of fundamental importance since with its help the stress response to an arbitrarily prescribed timewise varying strain history can be obtained through the use of Duhamel's Integral.

If in the stress strain law, equation 1.2, N is again equal to unity but $a_1 = 0$ instead of $b_1 \approx 0$ the prescription of a step stress in time permits the calculation of the time dependent strain. Again the strain behavior can be represented by a mechanical model, but now with the spring and dashpot in parallel; this second

configuration is called a Voigt element and its characteristics are shown in fig. 2A. The representation of actual material properties requires again the multiple combination of such Voigt models in series (see fig. 2B). Similar to the relaxation modulus the material response to a timewise step stress, usually referred to as the creep compliance, is of fundamental importance in the calculation of strain response under a more generally prescribed stress history.

The measured relaxation modulus and the creep compliance for the H-C rubber employed in this work have been represented by their respective 18 element models and are shown in figs. 3 and 4*.

As an alternate way of representing the mechanical behavior of viscoelastic materials the integral formulation of the stress-strain response has proven useful in the analysis of viscoelastic structures. To illustrate this approach by way of example consider the simple expression 1.3 for the relaxation modulus

$$E(t) \equiv \frac{\sigma(t)}{\epsilon_0} = m \exp\left\{-\frac{t}{\tau}\right\} \quad (1.4)$$

where $m = b_0/a_1$ and $\tau = a_0/a_1$. As pointed out previously the more general and more realistic case corresponding to the mechanical model in fig. 1B is represented by the summation expression

$$E(t) = m_e + \sum_{n=0}^N m_n \exp\left\{-\frac{t}{\tau_n}\right\} \quad (1.5)$$

* A detailed account of the procurement of the material properties is given in reference 16.

where m_e is the modulus of the viscosity degenerate Maxwell element and m_n and τ_n are, respectively, the spring constant and relaxation time of the n^{th} element. As the accuracy of representation increases with the number of elements N , it is convenient to consider N so large that the sum can be replaced by an integral expression in the form

$$E(t) = m_e + \int_0^{\infty} H(\tau) \exp\left(-\frac{t}{\tau}\right) d(\ln \tau). \quad (1.6)$$

Here τ is in the nature of a continuously varying relaxation time and $H(\tau)$ represents a continuous distribution of spring constants analogous to the set of m_n in the finite element model.

While this integral representation of material properties is very useful in some stress analysis problems, in particular those involving time varying temperature fields it has no advantage over the mechanical model representation for the purposes of the present work. Because the analysis of viscoelastic rupture involves the concept of elastically stored energy as distinct from dissipated energy, the mechanical model offers the simplicity of identifying the elastic energy physically with the energy stored in the model springs. But, more significantly, the numerical evaluation of the elastic energy is much easier when using a finite element model instead of the integral formulation. For these reasons we have made exclusive use of mechanical model theory in the following work.

1.2 Time-Temperature Equivalence

Beyond the dependence of the material properties on time, viscoelastic materials exhibit a strong dependence upon temperature. In contrast to the metals which are rather insensitive to appreciable deviations from ambient temperature, many viscoelastic materials change their response to stress or strain radically for only moderate temperature changes. But closer investigation shows that the primary effect of temperature is reflected in the change of the material response time, that is, in the viscous nature of the material. Indeed, it has been shown for a large class of viscoelastic materials, that lowering of the temperature corresponds to an expansion of the time scale, and the raising of the temperature to a compression of the time scale; the factor which determines this change of scale is a function of the temperature commonly denoted by $a_T(T)$, and is called the shift factor* (17). The change in time scale is then given by

$$dt' = \frac{1}{a_T(\tau)} dt \quad (1.7)$$

where dt' denotes the effective time increment if the material is instantaneously at a temperature T , different from the reference temperature T_0 , and dt is the corresponding time increment if the material were at the reference temperature. If the temperature does not change with time relation 1.7 can be written in total form as

* The term shift factor refers to the multiplicative nature of the function $a_T(T)$ in the time temperature relation, which on a logarithmic time scale corresponds to a temperature dependent shift along the logarithmic time scale.

$$t' = \frac{t}{a_T(\tau)}. \quad (1.8)$$

Figure 5 shows the dependence of the shift factor a_T on the temperature as determined from constant strain rate data on the H-C rubber employed in the experimental work (see reference 16); from this and equation 1.8 the compressive or expansive effect of temperature upon the time scale is readily apparent.

We shall later make reference to the glass transition temperature of polymers. This temperature is a characteristic of each polymer and indicates the narrow temperature range ($\pm 5^\circ\text{K}$) in which upon cooling the polymer changes its behavior from a rubberlike to a glasslike character. But the more general significance of this temperature lies in the fact that the behavior of many polymers is very similar if the individual polymers are at the same temperature with respect to their glass transition temperatures. For example, the shift factor can thus be expressed approximately for many different polymers by the same equation

$$\log_{10} a_T = - \frac{8.86 [T - (T_g + 50)]}{101.8 + [T - (T_g + 50)]} \quad (1.9)$$

where T_g is the glass transition temperature and T the temperature in $^\circ$ Centigrade. Relation 1.9 was determined empirically by Williams, Landel and Ferry (17) and is therefore commonly referred to as the WLF equation; it is shown as the dotted curve in fig. 5.

Although there are many interesting consequences of the shift factor principle and of the role of the glass transition temperature in viscoelastic material behavior, such a discussion lies

beyond the present scope. Instead, special observations and comments will be deferred until needed in the context.

1.3 Effect of Finite Strain

No mention has been made so far of the effect of large strains on the viscous response of the material. Since rupture may be associated with large strains, such considerations could play an important role in the prediction of material failure.

Landel and Stedry (18) have studied the relaxation of SBR rubber at large strains and found for strains up to 500% that within the requirements of usual engineering analysis the time and strain dependence of the stress could be factored in the form

$$\sigma(\epsilon, t) = E_r(t) \cdot f(\epsilon) \quad (1.10)$$

where $E_r(t)$ is the relaxation modulus and $f(\epsilon)$ is a non-linear function of the strain ϵ which reduces to ϵ for small strains and approaches thus the proper limit of the linearly viscoelastic stress-strain law. Becker and Rademacher (19) have found the same result for crystalline polyethylene for strains up to 11%. In a more extensive study on an SBR rubber Smith (20) substantiated essentially the factorizability of the stress dependence on time and strain in constant strain rate tests. He found, however, that while the factorization is reasonable at strains smaller than 100% for all temperatures tested it is applicable at larger strains only above a certain temperature and not jointly at high strains and low temperatures (below -32°C).

In order to circumvent a detailed study of similar large

deformation effects and to concentrate on the investigation of the rupture behavior of viscoelastic rubbers rather than their constitutive law it has proven useful in this work to assume that the factorization of strain-temperature-time effects is uniformly valid and to neglect possible deviations as found by Smith. This assumption affords a simple description of the mechanical material properties and is consistent with the qualitative linear stress analysis employed in the rupture calculations.

It will be found within the framework of the theory proposed in this dissertation that the calculation of the critical rupture stress or strain involves only the elastically stored energy in the material. Although the stress-strain relationship for a rubbery material may be nonlinear the functional dependence of the strain energy density upon stress or strain, is not markedly different from that calculated by using a linear stress-strain law. This is a consequence of the fact that the energy density is an integral quantity of the stress-strain behavior. For example, if $W_t(\sigma)$ is the true energy density in a uniaxial tensile specimen under large strain and E is the initial slope of the stress-strain curve then

$$W_t(\sigma) = \alpha \frac{\sigma^2}{2E} \quad (1.11)$$

where α is a numerical factor which is chosen so as to minimize the error in the approximation 1, 11. This can be achieved, for example, by minimizing the square error in the stress range of interest or simply by graphically fitting the right hand side of equation

1.11 to experimental data:: As an example, fig. 6 shows the energy density in a uniaxial tensile test for a neo-Hookean solid** in comparison with the right hand side of equation 1.11 for a convenient choice of $\alpha = 2$. The good approximation of the strain energy by the modified expression of linear elasticity theory is apparent. While a detailed analysis of rupture under large strains would require a careful analysis of these large deformation effects it seems nevertheless that the indicated simplifications permit a reasonably tractable treatment of the problem with presently available analysis tools.

1.4 Isothermal vs. Adiabatic Rupture Properties

Finally it is in order to comment on the presentation of ultimate tensile properties of viscoelastic solids. Because the

* This procedure is, of course, equivalent to approximating the non-linear stress-strain law by a linear one with an appropriately averaged Young's Modulus. However, the above interpretation is chosen because the viscoelastic material properties are determined in that range where the stress-strain behavior is essentially linear, i.e., near zero stress.

** The neo-Hookean solid is defined in terms of the strain energy function

$$W = \frac{E}{6} \{ \lambda_1^2 - \lambda_2^2 - \lambda_3^2 - 3 \}$$

with the side condition (incompressibility) that $\lambda_1 \lambda_2 \lambda_3 = 1$. Here the λ_i are stretch ratios in the three directions of principal strain. For example, in terms of a uniaxial strain ϵ , the stretch ratio is expressed as $\lambda = 1 + \epsilon$ and under consideration of the incompressibility condition $\lambda_1 \lambda_2 \lambda_3 = 1$, the corresponding strain energy function is

$$W_{\text{uniaxial}} = \frac{E}{6} \left\{ (1 + \epsilon)^2 - \frac{2}{1 + \epsilon} - 3 \right\}.$$

Note that for $\epsilon \rightarrow 0$ $W_{\text{uniaxial}} \rightarrow \frac{E \epsilon^2}{2}$ corresponding to the energy density expression for linear infinitesimal elasticity.

range of time and rate over which viscoelastic material properties vary is usually much larger than can be accommodated by mechanical testing devices, recourse is taken to the time-temperature shift factor principle described above to exchange a variation in temperature for high or low loading rates. Although the resulting failure curves are smooth within experimental accuracy a question arises as to the true meaning of the curves.

Consider, for instance, the H-C rubber characterized in figs. 3, 4 and 12 to be initially at -20°C and subjected to a strain rate of 10^4 in/in/min. This strain rate is sufficiently high to prevent effective heat transfer from the sample to the surroundings within the duration of the test so that essentially adiabatic conditions prevail. The ensuing energy dissipation can be estimated to raise the specimen temperature by at least 20°C at 100% strain which should have a pronounced effect upon the material behavior as predicted by the temperature dependence of the shift factor in fig. 5.

This consideration is complicated by the fact that the shift factor is really associated with the so-called free volume (12)* of polymeric materials which in turn depends upon the temperature through a time and rate dependent coefficient of expansion. If the strain rate is sufficiently high the free volume cannot grow fast

* We are anticipating here the development of the molecular structure considered in section 1.5. Briefly the free volume is that part of the polymer volume which could be occupied by polymer molecules but is not. It is a qualitative measure of the freedom with which polymer molecules can move relative to each other. The cited reference gives a detailed account of this concept.

enough to permit the shift factor to change appreciably during the test. Hence only the molecular bond strength of the polymer molecules is affected through the temperature rise and the net result may not be as pronounced as estimated from the equilibrium shift factor in fig. 5. For example, Jones (21) has found in preliminary tests that the shift factor principle does apply within engineering accuracy when the strain rates vary over approximately 6 decades.

Nevertheless, until this question of strain rate induced temperature effects is resolved more conclusively some care is indicated when applying isothermal rupture data to situations favoring adiabatic conditions.

B. THE PHENOMENOLOGICAL DESCRIPTION OF THE RUPTURE PROCESS

During the extensive study of ductile and brittle fracture two concepts have evolved which today are considered of fundamental importance: On the molecular level the dislocation concept of Taylor (22), Orowan (23) and Follani (24) describes the failure initiation stage while on a macroscopic scale the energy balance concept of Griffith permits, in principle, the prediction of gross fracture initiation. Conceptually it will be similarly useful when considering the fracture of polymeric materials to describe the rupture process in terms of molecular and macroscopic dimensions, thus emphasizing the difference in the molecular structure of metals and polymers on the one hand and the similarity as macroscopic continua on the other. We therefore proceed now to examine the process of rupture at the molecular, microscopic and macroscopic level where typical characteristic lengths are measured in Angstroms, microns, and centimeters, respectively,

1.5 The Molecular Structure of Polymers

The physio-chemical structure of high polymers has been the subject of extensive studies and is described in detail in the literature (25, 11-14)*. For our present purposes it suffices to state only the elementary concepts that relate to the initiation and propagation of rupture

* These references contain exhaustive bibliographies on the subject.

a. The polymer chain. Polymer molecules consist of long chains of atoms and chemical groups of atoms, the number of such elements in a chain ranging from a few hundred to a few hundred thousand; the mechanical properties of a macroscopic sample are determined to the largest extent by the average length of the polymer chains.

When a chain grows it assumes a spatial configuration that is compatible with its already existing length and with other chains growing adjacent to it. Due to the large number of chain elements and the relative freedom of direction in which the chain can grow, this spatial arrangement leads to severe entanglements of groups of chains.

If no chemical bond formation occurs between entangled chains the macroscopic strength characteristics are derived primarily from the nature of the mechanical entanglements::' which in turn depends strongly upon the molecular weight, i. e., the number of atoms or groups in the polymer chain. The material is then commonly called a plastic or linear polymer.

On the other hand, if bonding does occur between molecular chains this chemical crosslinking effect influences the material strength by restricting any motion that tends to untangle the polymer chains. In this case a sample of the material consists in principle of a single molecule which fills its macroscopic space by a huge, irregular network of connected polymer chains. Such

* The term "mechanical entanglement" implies, of course, the analog representation of the polymer chain by a string or linked chain.

a material is called an elastomer or rubber and is largely characterized by the number of groups in a chain between cross links, Since this number is typically on the order of 10^4 the network is not tightly knit, but permits the chain segments between cross links to move with relative freedom. Thus rubbers behave in certain respects like uncrosslinked polymers, and vice versa, the difference being restricted to the mechanical response which involves the untangling of the molecule chains. This dissimilarity will become more evident during the following discussion of the effect of chain slippage.

b. Effect of chain slipping. Because the absence of chemical bonds between polymer chains does not inhibit the motion of the chains relative to each other linear polymers can undergo large permanent deformations due to the viscous flow of the molecule chains past each other, However, if the molecular weight is sufficiently high the mechanical entanglements can act as effective crosslinks and consequently the flow phenomenon is observed only at temperatures approximately 100°C above the glass transition temperature, where the thermal motion of the molecule chains permits relatively high rates of viscous flow*. Of course, the material will rupture before chain flow can occur if the applied load is too large; in this respect linear polymers behave like the crosslinked polymers. In our further discussion

* The time-temperature shift principle implies the same behavior at long times and lower temperatures.

we shall exclude polymer flow phenomena and restrict ourselves conceptually to the rupture behavior of rubbers.

Within this restriction failure can occur only through rupture of chemical bonds in the chain or at crosslinks, and it is pertinent to inquire into the relative importance of chain motion and chain rupture in the fracture process.

For this purpose it is first necessary to associate the elastic component of mechanical polymer behavior with the elasticity of the molecule chains and the viscous response with the slipping of the entangled chains past each other during the process of reaching a new equilibrium state. The forces which act on a chain segment are therefore due to the forces transmitted along the chain as well as from the viscous interaction with the chains moving past it.

It is clear that bond rupture occurs only as the result of the forces which act on the bonded atoms. Because the time dependent motion of adjacent molecules contributes to these forces a part of the time dependence in viscoelastic fracture is due to the interaction of moving molecule chains. The remaining part of the time dependence arises from the bond rupture process which will be discussed later.

In terms of energy partition this understanding implies that the relative motion of the molecule chains contributes only to the dissipation of energy and influences rupture by raising the temperature, while only the elastically stored energy takes part

directly in the rupture process. If, e.g., rupture progresses at a constant temperature then only a part of the total work done on a polymer sample contributes to fracture.

In an earlier investigation of polymer fracture F. Bueche (10) used the concept of elastic energy. But while he attempted to calculate this quantity from molecular parameters we shall here take an alternate approach and use the phenomenologically determined material properties to express the elastic energy. As pointed out in section 1.1 this requires only the identification of the chain elasticity with the elastic spring elements in the mechanical model chosen to represent the mechanical behavior; this method obviates the uncertainties associated with the calculation of molecular parameters.

In order to examine the rupture resistance of the chain building blocks we proceed now to consider the effects which influence and determine the rupture of polymeric chain bonds.

c. The chemical bond. The nature of the chemical bond has been treated extensively by Pauling (26). Since we are interested primarily in the statistical aspects of bond strength we need be concerned here only with the concept that the bond strength is ultimately measured in terms of energy and is the result of the minimum energy states which the two atoms and their electrons have with respect to each other. Bond rupture can thus be caused by various effects which disturb the local energy state sufficiently.

Such a disturbance can be achieved, for instance, through a relative displacement of the three dimensionally conceived atoms corresponding to the macro-mechanical notions of tension, shear, bending and twist, and it is always involved in the fracture of rubbers under the influence of mechanical forces and deformations.

On the other hand, the local energy balance can be disturbed from its minimum state by an electronically active radical contained in the polymer as an impurity, which may result in a weakening of the bond. In this case, for instance, the tension required to break the bond would be less than that necessary for bond rupture in the absence of the radical.

If molecular bonds break in a polymer chain the newly created chain ends will also act as radicals which may combine with other free chain ends to produce temporarily relaxed chains' or, like the aforementioned impurities, weaken neighboring chains. Of course gross rupture occurs only if the rate of bond rupture exceeds the rate of bond re-formation.

Finally we note that on a macroscopically observable level the evidence of the bond interchange and re-formation process is manifested in the tackiness of new rupture surfaces. It is surprising at times to find that even after exposure of the newly created surfaces to the contaminations of a normal laboratory atmosphere, the fracture can heal partially so that the sample

* This type of bond interchange is responsible for the phenomenon of chemical stress relaxation (13).

regains a substantial part of its original strength*.

d. Atmospheric effects. In addition to the sensitivity of the polymer chain to the presence of electronically active components in the interior of a rubber the reaction of radicals with the unruptured molecule chain is of import on the promotion of rupture at surfaces exposed to atmospheric conditions.

It will be seen in section 1.7 that long time failure and slow crack propagation is in some polymers associated with the formation of a fibrous structure. Under such conditions a relatively large amount of area of the polymer under stress is exposed to the surrounding atmosphere and hence the influence of the reaction of chemical radicals with the strained polymer can significantly further the propagation of rupture.

The practical consequences of such a reaction are numerous, but suffice it to name only a few. In the Los Angeles area where the air contains appreciable amounts of ozone, it is a commonly known fact that the oxidative smog atmosphere has a detrimental effect on the life of automobile tires. Indeed, Braden and Gent (27) have studied the effect of ozone in an ionized oxygen atmosphere and found a strong increase in crack propagation velocities with increasing ozone concentration. In a related experiment Tobolsky, Prettyman and Dillon (28) demonstrated that the diffusion of molecular oxygen into a rubber sample caused complete

* In preliminary tests completely broken tensile specimens of an H-C rubber regained about 15% of their original strength after being rejoined at the fracture surfaces for only three minutes at room temperature.

stress relaxation as a result of polymer chain scission.

It is of interest to note that the fracture of metals involves similar phenomena as, for example, stress corrosion (29), hydrogen embrittlement (30) and the atmospheric effects on the fatigue strength (31). Although the elimination of any atmosphere eliminates also the oxidation problems for both metals and polymers one finds that the usual polymers are not stable in a hard vacuum. From the standpoint of fracture resistance an inert gaseous atmosphere at reasonable pressures is therefore most desirable for the protection of these organic materials from atmospheric influences.

1.6 Microscopic Aspects

While in the last section we have considered rupture from a molecular viewpoint we shall now concern ourselves with a larger collection of polymer chains and consider the susceptibility of amorphous* polymers to rupture at the level of molecular aggregates.

One of the phenomena observed in the fracture of materials is that the measured strength of bulk material is several orders of magnitude smaller than calculated from molecular strength considerations. This fact has led to the postulate that microscopic defects weaken the material and that the molecular

* If a polymer contains regions in which the polymer chains have formed a regular array resembling ionic crystal structures it is called crystalline; if such crystal-like regions are absent, the polymer is termed non-crystalline or amorphous.

bond strengths are realized only in the stress concentrations associated with such defects. It has been proposed in the past that these defects exist in materials in the form of microscopic cracks or other material discontinuities. However, the study of fracture initiation in metals revealed that such defects can develop under stress through the coalescence of dislocations (32, 33) which are not sufficiently large by themselves to account for the comparatively low bulk strength. By analogy it appears similarly reasonable that defects need not exist in polymers in the form of microscopic cracks or holes but can develop under stress from initially small weaknesses in the molecular structure. This concept does not, of course, preclude the importance of impurities and submicroscopic inclusions from the rupture process, but merely restricts them to the role of possible initiators of defect growth.

In contrast to the metals and crystalline polymers the structure of molecular aggregates in amorphous polymers has not been studied to any significant extent. The most important reason for this deficiency is probably the fact that the unordered structure of the amorphous polymers does not lend itself readily to an analysis under an electron microscope. As a consequence there exists no information which might aid us here in identifying certain regions in a polymer with defect sites where molecular configurations would promote the initiation and growth of rupture. We are therefore forced to hypothesize the nature of such regions

in order to proceed with the analysis of fracture in amorphous polymers.

a. The nature of polymer defects. Since the molecular structure is developed during the polymerization process the potential weak regions are presumably also formed in this stage.

When polymerization starts at isolated points due to local temperature fluctuations polymer chain complexes grow and eventually meet with neighboring chain aggregates. Because of the lack of steric hindrances during the initial growth stage the core of the polymer aggregate contains strong molecular bonds while the bonds formed at a later stage of polymerization are weak. This follows because the newly added chain building blocks must accommodate themselves into an already existing and increasingly dense chain structure. For the same reason the molecular weight of the polymer molecules is likely to be smaller than at the core of the growth complexes. Consequently the cross-link density in such regions is low or even non-existent. Inasmuch as it has been demonstrated that a small fraction of low molecular weight material in polymer blends has a disproportionately large harmful effect upon the ultimate properties (34) it appears logical that such regions are the sites of rupture initiation and microscopic growth. Furthermore, since the growing chain complexes solidify at different rates they cause non-uniform shrinkage and the intermediate and less solid regions provide the spatial adjustment at the expense of their own cohesive strength.

We envisage thus a polymeric structure of preferred strength regions which resembles the granular structure of metals without, however, exhibiting distinct grain boundaries. In principle this variation in molecular structure is similar to the difference between the morphological character of the spherulites and non-spherulitic material in a crystalline polymer as shown in fig. 7* and is also indirectly apparent in the formation of holes in the rubber sample of fig. 8. We shall see later that the weak region hypothesis forms an important part of the theory for calculating viscoelastic failure properties.

b. Effect of volume size upon rupture properties. Since this dissertation is concerned with fracture as a local phenomenon, it is appropriate to comment on the influence of the test volume size on the ultimate properties.

In view of the statistical nature of the polymerization process and the formation of weak regions as discussed in the last section it is evident that the bulk rupture behavior of polymers is also governed by statistical laws. An example in point is the distribution of tensile strengths about a most probable mean value. But in addition the statistical character of the weak domain makes the rupture strength also dependent upon the size of the test specimen (36).

This dependence on the size of the test volume is illustrated

* In this context the work of Hsiao and Sauer (35) on the structure of crystalline polymers is noteworthy.

by the simple observation that a larger test specimen is more likely to contain severe defects than a smaller one and will, therefore, be weaker on the average. Although Weibull (37) and Gumbel (38) have provided the mathematical analysis of this size dependence in fracture the inclusion of this effect in the present fracture calculations presents some practical problems. Foremost among these is the time consuming experimentation required to establish conclusively the dependence of the rupture properties upon the test volume and the appropriate distribution functions for a particular material. Another difficulty arises from the fact that for meaningful results specimen dimensions are required which are on the order of fractions of millimeters. While the latter requirement can be simulated in principle by means of stress concentrations, as for example demonstrated in section 1.11, it is not believed that the size effect is of such critical importance in this examination of the time dependence in viscoelastic fracture to warrant these special efforts. This belief is supported by experimental experience which suggests that the contribution of the size effect to viscoelastic rupture behavior at stress concentrations is no more important than those of the molecular mechanisms which are not included in this analysis. The statistical aspects of rupture which give rise to the volume effect will thus be excluded in the following development.

It should be noted, however, that this exclusion implies that we deal henceforth with an idealized micro-structure. In terms of the regional strength concept of this section the

simplification implies also the absence of statistical strength variations. In other words, the postulated weak regions are essentially identical and are distributed throughout the body in a regular manner. The exclusion of the statistical aspects of rupture--excepting those which relate to the molecular mechanisms of bond rupture--leads therefore to a conveniently simple model of the polymer microstructure which is amenable to a relatively uncomplicated mathematical treatment.

1.7 Macroscopic Considerations

While the initiation of rupture at the molecular level involves the material as a discontinuum, macroscopic phenomena admit the use of continuum mechanics concepts in a fracture analysis. Although the observed phenomena accompanying gross fracture are numerous and far from being all understood, it is possible to single out particularly prominent effects and consider them alone while disregarding further details. As an example of this simplification we cite the aforementioned energy balance concept of Griffith which determines in principle the relation between the size of a defect in a structural component and the maximum load which the member can support. In practice, however, the analytic formulation of this concept is limited by the mathematical difficulties of continuum theory so that one is often content with qualitative results derived from an approximate analysis.

Because of these analytic difficulties in describing the fracture process the experimental investigation of rupture phenomena continues to play a leading role in fracture mechanics. The various methods which are used in this exploration are too numerous to be considered in this place and only reference is made to some representative work reported elsewhere (39, 40). Here we shall only consider those aspects which relate directly to our later work.

a. Fracture markings. A primary source of information on fracture processes has been the inspection of fracture surfaces. For example, Kies, Sullivan and Irwin (41) have deduced from such observations on specimens broken in uniaxial tension that the fracture propagates discontinuously in all the metallic and non-metallic materials tested. Similarly Mason (42) established that the high speed propagation of cracks (~ 100 ft/sec) in a non-crystallizing rubber (SB-R) involves essentially the same processes of surface formation as in metals. Also, Andrews (43) has pointed out on the basis of fracture surface appearance that hysteresis effects are very important in the propagation of cracks through crystallizing rubbers under conditions of cyclic stress application. Here we shall add to these findings the results obtained from studying the motion of a slowly propagating crack ($\sim 10^{-4}$ - 1 ft/sec).

While the post mortem examination of fracture surfaces can produce conclusive results as indicated by the above examples, additional information can be gained by observing the motion of the material at the tip of a moving crack. For instance, one

notices with the aid of a low power microscope that material rupture occurs in an extended domain around the perimeter of the crack tip* where the material deteriorates through the formation of polymer ligaments and their subsequent severance. The ruptured polymer ligaments then retract while interacting in a viscous manner with the more solid crack boundary. When the crack propagates at a higher velocity the extent of volume participating in the ligament formation decreases and the ligaments become smaller. The corresponding change in the fracture surface appearance is shown in fig. 10 which demonstrates the decrease of surface roughness associated with the decrease of ligament size at higher speeds. Incidentally the formation of a rupture surface at slow crack speeds involves much more surface area than is visible by mere inspection of the final surface. Since the fibrous polymer bundles all possess surfaces in the extended state the resultant crack surface consists of many undercuts and partially rehealed surfaces.

The production of a fibrous structure at the crack tip and its velocity dependence can be explained in terms of the defect hypothesis discussed in section 1.6. At low speeds the material around the crack tip is under an elevated stress for a long time. Defects grow in the microscopic weak regions and eventually join, leaving only the ligaments which then break and thus effectively advance the position of the crack tip. According to calcu-

* See for instance fig. 9. The same phenomenon is evident in reference 8.

lations based on the energy concept of Griffith a higher stress at the crack tip requires only smaller defects to let the material rupture locally. At higher velocities and higher stresses at the crack tip the defects need to develop only to a smaller size and hence the fibrous polymer bundles decrease in size, also. Furthermore, as the rate of defect growth is not simply proportional to the stress and since the stress decays away from the crack tip it turns out that the defects at a distance from the tip do not develop to a visible size at higher crack speeds and higher stress around the crack tip; thus the volume involved in the ligament formation apparently decreases with increasing speed.

The same type of rupture phenomenon can be observed in fig. 8 which shows the fiber formation in a commercial rubber band after subjecting it to a constant uniaxial strain of 50% for approximately 3 months at room temperature.

Besides the two materials represented in figs. 8-10 the same effect was observed on a Butarez rubber* which possesses approximately the same glass transition temperature as the H-C rubber used in the crack propagation studies. In comparison, a polyurethane rubber develops a very smooth, glass-like surface when observed at the same temperature (22°C) and comparable speeds of crack propagation. However, at room temperature the polyurethane rubber is much closer to its glass transition temperature (-40°C) than the H-C rubber ($T_g \sim -85^\circ\text{C}$). Hence a more

* A carboxy terminated poly butadiene resin.

glass-like behavior should be expected as well as similar ligament rupture at temperatures about 60°-70°C, or at equivalently lower velocities ($v \sim 10^{-6}$ in/min). This expectation is, of course, in agreement with the previously stated observation that the behavior of different polymers is usually comparable only when the polymers are at the same temperature with respect to their glass transition temperature.

In a paper on viscoelastic fracture Williams (44) has pointed out the importance of energy dissipation as a controlling factor in the propagation of cracks. Whereas he was primarily concerned with the effect on the velocity of slowly moving cracks under isothermal conditions it is interesting to consider also the effect of the attendant temperature rise. In this context the earlier discussion on the isothermal and adiabatic rupture properties should be recalled. Depending upon the speed of crack propagation the heat generated in the stress concentration at the crack tip may contribute to lowering the material strength locally.

An increase in crack speed affects the temperature at the crack tip in two ways. Since the dissipation increases with the velocity* the temperature increases also. Secondly, the rate of heat flow away from the crack tip is reduced at higher crack speeds so that the heat remains more concentrated at the crack tip. One would therefore assume that the generation of heat at the crack tip plays a significant part in the propagation of cracks at high

* For low velocities the dissipation is proportional to the square of the velocity (45).

speeds ($v > 1000$ in/min).

b. Effect of the multiaxial stress state. Besides the pronounced time effect in the viscoelastic rupture process the fracture behavior is influenced by the stress distribution. Most work in polymer rupture has centered on the convenient uniaxial tensile test although attempts to delineate multiaxial failure conditions are rapidly increasing (15, 46, 47, 48). For example, Ko (49) has recently presented some quantitative results on the elastic rupture of rubber under various combinations of multiaxial tensile stresses. An exhaustive examination of the stress state dependence of polymer failure is too complicated and far-reaching to be attempted here. However it suffices for the present purposes to comment only upon the rate and temperature effects.

Near the glass temperature, typical uniaxial polymer specimens exhibit yield characteristics similar to those of a mild steel. It is tempting to assume therefore that yielding prior to rupture will also exist in a multiaxial stress state. But to conclude on this basis that the onset of such yielding in a glassy polymer is also governed by the von Mises yield criterion of a critical octahedral shear stress which applies to metals is somewhat premature. The caution is prompted by two observations: When a uniaxial polymer tensile specimen yields the yield boundary is almost invariably a line of constant principal stress and is perpendicular to the line of tension whereas in metals it appears along lines of constant shear stress which are at 45° with the tensile force.

Secondly, yield in metals is associated with the motion of dislocations under the action of shear stress; but no similar mechanism or molecular configuration in amorphous polymers has been associated with the preferred response to a shear stress. On the contrary, since polymer chains possess an essentially filamentous structure they should presumably respond more naturally to tensile forces.

The latter statement does not lose its validity at higher temperatures or correspondingly low strain rates where the material does not exhibit the yield phenomenon: Thus the general extrapolation of metal yield criteria to polymer rupture does not appear to be well founded. Nevertheless it has been suggested in the past that such criteria may prove useful in correlating polymer rupture. Instead, it seems more reasonable to expect a rupture criterion based on a linear combination of the principal stresses or on a constant value of the dilatational or total elastic energy*. For instance Williams, Schapery, Zak and Lindsey (48) have recently suggested on the basis of failure data in uniaxial and equal triaxial stress fields that the criterion of a constant dilatational energy at rupture may be quite reasonable.

Intimately connected with the stress state criterion is the orientation of the gross fracture surface. While in an elastic material the formation of a new surface seems to occur always

* The total elastic energy is equal to the sum of the energy of distortion and dilatation. It will be recalled that the von Mises yield criterion is equivalent to a constant value of the distortional strain energy density at yield.

in a manner so as to relieve as much energy in the system as possible, this is not necessarily true in a viscoelastic material. For example, it has been shown (50) in diametral compression tests on circular disks of highly filled rubber that the orientation of the fracture surface (and presumably the sensitivity to shear or normal stress) with respect to the axis of compression changes in tests at different temperatures from alignment to 45° and to alignment again as the temperature is increased from the glass transition temperature.

In regard to the orientation of fracture surfaces a fracture phenomenon in the poker-chip test* is of interest. Although the phenomenon does not appear to be of immediate and practical significance it illustrates nevertheless a deviation from usual engineering expectations that are based on the behavior of metals. While in this test configuration a metal specimen should rupture in a plane parallel to the specimen midplane the fracture surface in a rubber specimen cuts across the disk thickness and aligns itself parallel to the direction of pull. This behavior is connected with the fact that for these nearly incompressible materials and the close proximity of the rigid bond surfaces, more energy can be released by the load parallel orientation. This phenomenon vanishes rapidly (48) as Poisson's Ratio changes from values

* This test consists of pulling a thin disk (thickness to diameter ratio $\lesssim 1/20$) normal to its plane surfaces which are bonded to rigid supports. Since rubbers above their glass temperature are nearly incompressible (the ratio of tensile modulus to bulk modulus is very small) this tension produces stresses near the center of the disk which approximate conditions of equal triaxial tension.

near 0.5 to 0.47 and can therefore not be observed in the engineering metals which have a still smaller value of Poisson's Ratio.

It is evident from the past comments that the interaction of time, temperature and stress state play an important part in the fracture of viscoelastic materials. However, before exploring the interaction of the time-temperature and stress-state effects it is prudent to investigate the contribution of the individual effects to viscoelastic fracture. As it is possible on the one hand to study the rupture of polymers in multiaxial stress states while minimizing the dependence on time and temperature on the other hand this division permits the investigation of time-temperature effects in a very simple stress state. We shall therefore restrict ourselves in our further work conceptually to time and temperature dependent fracture in uniaxial tension while awaiting new developments in the understanding of rupture in multiaxial stress fields (47, 48, 49).

c. Energetics of crack growth. In the last paragraphs we have already encountered the influence of elastic energy on the fracture process. We shall now demonstrate the usefulness of energy considerations in the definition of a rupture criterion by considering as an example the behavior of brittle materials, and subsequently indicate under what conditions a similar criterion can be applied to viscoelastic materials.

In the absence of effects other than mechanical or thermal the law of conservation of energy can be expressed on a per unit time basis as

$$\dot{K} + \dot{F} = \dot{W}_B - D \quad (1.12)$$

where K = rate of change of kinetic energy in the system

F = rate of change of free energy

W_B = rate of energy input at the boundary and

D = rate of energy dissipation.

Although the calculation of individual terms in equation 1.12 may present considerable difficulties in general, useful information can be obtained in certain special cases. This has been demonstrated by Rivlin and Thomas (1), and by Schapery (45) on the problem of crack propagation in a geometry also used in this dissertation. The earliest application of this energy principle in fracture mechanics was made by Griffith in his work on brittle materials (51).

For a brittle solid the dissipation consists mainly of the energy spent in creating a new surface and the free energy is equal to the elastic strain energy in the structure. Thus the kinetic energy change can be expressed readily in terms of the remaining quantities for a particular boundary loading. At gross rupture the kinetic energy increases markedly due to the motion of the newly cracked surfaces. It appears therefore logical in terms of equation 1.12 to define fracture as imminent when the initially small kinetic energy increases to a significantly larger value. As a special case the criterion of Griffith is equivalent to stating that catastrophic rupture occurs when the kinetic energy increases from zero by only an infinitesimal amount.

Since cracks in brittle materials are observed to accelerate from rest to a speed of approximately 5000 ft/sec within a fraction of a second (36, 69) the simple Griffith criterion can predict the occurrence of gross fracture for those materials within the time scale of normal engineering interest. This is not necessarily true, however, when viscoelastic effects are present. Fig. 11 for example shows the acceleration stage of a crack in a rubber sheet:::. In this case rapid failure growth did not occur until three minutes after load application although the crack propagated slowly from the beginning of the test. In contrast to the case of brittle fracture a satisfactory description of the viscoelastic rupture process would therefore include a more detailed consideration of rate effects and the associated dissipation of energy,

In many situations of incipient viscoelastic rupture it turns out, however, that the time scale of the final fracture stage is relatively unimportant so that a simple criterion of the Griffith type serves a useful purpose. Such is the case, for instance, if it is necessary to know only whether or not a material will ever fail by gross rupture or, alternately, if the time span of the final fracture phenomena is small compared to the total life of the fracturing part. With the exception of the above example the latter case applies approximately to the rupture behavior considered in this work and will therefore permit the qualitative application of the simple fracture criterion in the subsequent fracture calculations.

* The experimental details are described in section 1. 12.

C. THE RUPTURE MODEL

In sections 1.5 -1.7 we have outlined some material characteristics and basic concepts which are fundamental in understanding polymer rupture. In order to concentrate on the overall rupture behavior of polymers without consideration of special chemical formulations it will only be necessary to incorporate the most dominant contributions from each of the molecular, microscopic and macroscopic effects. Indeed, the inclusion of more detailed information in a first quantitative analysis of rupture prediction would seem incompatible with the semi-qualitative methods available for the mathematical formulation of the problem. Consequently, the resulting theoretical relations will not fully describe all aspects of observed fracture behavior; but they will permit an examination of the agreement with experiment and thus a quantitative assessment of the relative importance of the effects included in or excluded from the analysis. For clarity of presentation we shall now describe a model for the simplified rupture process, deferring an explicit statement of assumptions until needed in the context,

First, in the absence of a more precise description of the initial flaw character, we hypothesize the existence of weak regions, as outlined in section 1.6, at which rupture always starts. Although the physical situation would entail a statistical distribution of weak regions we consider them to be of equal and definite size, uniformly distributed throughout the material.

Second, each weak region contains a large number of

breakable molecular bonds which possess a distribution of bond strengths, representative of the deviation from the possible maximum strength due to interaction with neighboring polymer chains. In addition each bond is of a statistical nature as prescribed by quantum mechanical considerations. When a bond breaks it may recombine with another broken bond but will not cause any unbroken bonds to rupture prematurely. The recombination is assumed to produce a chain which is indistinguishable from originally unbroken ones and contributes to the overall strength accordingly.

Third, bond rupture occurs at random locations in each weak region but the number of broken bonds is assumed to be proportional to the effective surface area of the growing defect.

Finally, since the rupture stress depends on the size of the defects the prediction of gross fracture requires the definition of when the ensemble of defects leads to catastrophic rupture.

As the defect size is by assumption related to the number of broken bonds, the problem of rupture prediction separates into two parts; first, the calculation of the number of broken bonds as a function of time and stress-strain history, and second the definition of the load criticality condition. We proceed therefore to determine now the rate of bond rupture. This will be accomplished by assuming a rate process for determining the defect growth. Following this development the energy balance for fracture instability, as discussed in section 1.7, will be presented.

1.8 Defect Growth

In predicting bond rupture in a molecular aggregate one is obviously faced with the difficulty of how to treat the spatial connectivity between molecule chains. We have chosen here to assume that bond rupture within a weak region takes place spatially at random. Since the weak region is conceived as having a definite size there must be a finite, though large number of bonds present; whether all of them take part in the rupture process is immaterial as long as the number of breakable bonds is large enough to permit the consideration of the bond rupture process on an average basis.

Since the formation and rupture of chemical bonds under mechanical stresses on the polymer sample involves in principle the same processes as the formation and dissolution of compounds in a chemical reaction we shall now use the theory of chemical reaction rates to estimate the rate of bond rupture in a weak region.

Let N_1 and N_2 denote, respectively, the number of unbroken and broken bonds in a weak region. The linear rate law

$$\frac{dN_1}{dt} = -\overline{\omega}_{12} N_1 + \overline{\omega}_{21} N_2 \quad (1.13)$$

predicts then the rate at which the number of unbroken bonds decreases or increases on the average; $\overline{\omega}_{12}$ and $\overline{\omega}_{21}$ are coefficients which determine the average rate of bond rupture ($\overline{\omega}_{12}$) and bond re-formation ($\overline{\omega}_{21}$). Similarly the rate of increase of broken bonds is governed by

$$\frac{dN_2}{dt} = \overline{\omega}_{12} N_1 - \overline{\omega}_{21} N_2 \quad (1.14)$$

Addition of equations 1.13 and 1.14 shows readily that the sum of broken and unbroken bonds is constant at all times which is consistent with the notion of a definite weak region size. Subtraction of these equations leads to the Debye equation

$$\frac{d}{dt} \left\{ \frac{N_2 - N_1}{N_0} \right\} = - (\bar{\omega}_{12} + \bar{\omega}_{21}) \left\{ \frac{N_2 - N_1}{N_0} \right\} + (\bar{\omega}_{21} - \bar{\omega}_{12}) \quad (1.15)$$

where $N_0 = N_1 + N_2$. For our purposes it suffices to consider only the particular solution of this first order differential equation*.

The solution is

$$\frac{N_2 - N_1}{N_0} = \exp \left\{ - \int_0^t (\bar{\omega}_{12} + \bar{\omega}_{21}) dt \right\} * \int_0^t \left\{ (\bar{\omega}_{21} - \bar{\omega}_{12}) \cdot \exp \left[\int_0^{\tau} (\bar{\omega}_{12} + \bar{\omega}_{21}) d\theta \right] \right\} d\tau \quad (1.16)$$

In order to relate the left hand side to the defect area we write the number of broken bonds as the sum of those already broken in the equilibrium state, N_2^0 , and the increase of broken bonds due to the application of a stress, ΔN_2 . Noting that $N_1 = N_0 - N_2$ and $N_0 = 2N_2^0$, we have

$$\frac{N_2 - N_1}{N_0} = \frac{\Delta N_2}{N_2^0} \quad (1.17a)$$

The second ratio is equal to the fractional increase of broken bonds under the application of a stress. In accordance with our earlier

* The number of broken bonds in the equilibrium state (zero stress) depends upon the relative magnitude of the rate functions $\bar{\omega}_{12}$ and $\bar{\omega}_{21}$ at equilibrium which are then more appropriately called equilibrium constants. Although the equilibrium constants must be determined by experiment it is more convenient to choose them equal in magnitude. This implies (cf. equation 1.15) that the number of broken bonds is equal to the number of unbroken bonds in the equilibrium state. Inasmuch as we are interested only in a deviation from the reference state this assumption is not very critical; the general character of the solution is not changed.

assumption we replace it by the area ratio A/A_m so that

$$\frac{N_2 - N_1}{N_0} = \frac{A}{A_m} . \quad (1.17b)$$

Here A is the instantaneous, effective area of the defect and A_m is the maximum area which the defect can attain. This choice follows from the fact that the right hand side of equation 1.16 has a maximum value of unity.

In order to obtain the rate functions $\overline{\omega}_{12}$ and $\overline{\omega}_{21}$ consider a large number of identical polymer chain links under equal loads. If an amount of energy h is required to break a single bond then the theory of rate processes (52) predicts, for example, the rate of bond rupture to be

$$\omega_{12} = a \frac{kT}{h} e^{-\frac{h-E}{kT}} \quad (1.18)$$

where a = proportionality constant

k = Boltzmann's constant

h = Planck's constant

T = absolute temperature

E = elastic energy in each bond due to the applied loads.

If on the other hand each bond does not have the same strength, but follows a distribution of bond strengths $q(h)$ as assumed for the defect model, the average rate of bond rupture $\overline{\omega}_{12}$ can be expressed as

$$\begin{aligned} \overline{\omega}_{12} &= \frac{\int_0^{\infty} q(h) \omega_{12}(h) dh}{\int_0^{\infty} q(h) dh} \\ &= a \left\{ \frac{kT}{h} \frac{\int_0^{\infty} q(h) e^{-\frac{h}{kT}} dh}{\int_0^{\infty} q(h) dh} \right\} e^{-\frac{E}{kT}} \end{aligned} \quad (1.19)$$

along with a similar expression for the average rate of bond re-formation

$$\overline{\omega}_{21} = a \left\{ \frac{kT}{h} \frac{\int_0^{\infty} q(h) e^{-\frac{h}{kT}} dh}{\int_0^{\infty} q(h) dh} \right\} e^{-\frac{E}{kT}}. \quad (1.20)$$

The quantity in brackets is a function of the temperature only and will be denoted by $\Theta(T)$, so that the average rate functions become

$$\begin{aligned} \overline{\omega}_{12} &= a \Theta(T) e^{-\frac{E}{kT}} \\ \overline{\omega}_{21} &= a \Theta(T) e^{-\frac{E}{kT}}. \end{aligned} \quad (1.21)$$

Upon substituting these expressions into the rate equation 1.15 and by using the definition of the area ratio 1.17 we obtain a relation for the rate of increase of the defect area

$$\frac{d A/A_m}{\Theta(T) dt} = -\lambda \left\{ \cosh \frac{E}{kT} \frac{A}{A_m} - \sinh \frac{E}{kT} \right\} \quad (1.22)$$

* The coefficient "a" is chosen equal in the expressions 1.19 and 1.20 to permit $\overline{\omega}_{12} = \overline{\omega}_{21}$ in the case that $E = 0$. This guarantees that A/A_m is zero in the absence of external forces.

where $\lambda = a/2$, and the solution 1.16 may be written in the same terms as

$$\frac{A}{A_m} = \exp\left\{-\lambda \int_0^t \Theta(\tau) \cosh \frac{E}{kT} dt\right\} * \int_0^t \left\{ \Theta(\tau) \sinh \frac{E}{kT} \cdot \left[\exp\left(\lambda \int_0^\tau \Theta(\tau) \cosh \frac{E}{kT} d\tau\right) \right] \right\} d\tau \quad (1.23)$$

From these equations it is obvious that the time dependence of both the temperature and the elastic energy per bond determines the growth history of the defect. While we shall consider in the following calculations only isothermal rupture processes the elastic energy will vary according to the stress-strain history imposed on the material before rupture. As pointed out previously the elastic energy per bond can be calculated approximately with the help of the phenomenological stress-strain law for any desired stress-strain history by dividing the elastic strain energy density by the number of bonds per unit volume, N . Since the resulting expressions are not a simple function of time, the integration of equation 1.22 or 1.23 must be accomplished in general by numerical means.

In this context it should be recalled from the discussion in section 1.5 that a part of the time dependence in viscoelastic rupture arises from the relaxation effects associated with the motion of polymer molecules relative to each other. This effect has been included in the defect growth analysis by considering only the elastic energy which is a function of the amount of relaxation occurring in any specific loading history. But even in the absence of relaxation when the elastic energy does not change with time the fracture process is time dependent as can be readily

seen from either equation 1.22 or 1.23.

We have thus identified the two major contributions to the time dependence in viscoelastic fracture, namely the relaxation effects as exemplified primarily in the stress-strain behavior and secondly the time dependence of the molecular bond rupture process.

1.9 A Condition of Critical Loading

In order to complete the prediction of gross rupture we determine now a relation between the defect size as calculated in the previous section and the critical stress at which a sample will break.

The different time scales of gross rupture propagation in the metals and viscoelastic materials were already pointed out in the last chapter. Because the gross propagation of rupture may not occur, by usual engineering standards, in a sudden or catastrophic manner after the first evidence of rupture initiation the definition of a critical instant in the progression of rupture is a somewhat arbitrary matter. One might, for instance, define the critical moment at the time of maximum acceleration of fracture propagation or alternately as the instant when rupture progresses at a particular rate. While the maximum acceleration can be calculated in principle from the concepts proposed by Williams (44) it proves to be more convenient to define the critical condition in terms of a rate dependent tearing energy as defined by Greensmith and Thomas (3). Briefly, this energy concept states that the amount

of energy spent in forming a new surface area in a material depends on the rate of area formation. Although this tearing energy includes the energy dissipated in the viscoelastic deformation of the material during surface formation in addition to the energy needed to form the visible surface the analogy to the surface energy of brittle materials or liquids is obvious. Since the surface energy plays an important role in the fracture of brittle materials it would follow that the rate sensitive tearing energy performs a similar function in the fracture of rubbers. We shall therefore deduce now how the tearing energy can be used to obtain a rupture criterion for visco-elastic rupture of the type first established by Griffith (51).

To begin with let us review briefly the salient arguments that lead to a criterion for the fracture of brittle solids. We shall do this by using the power equation 1.12 of section 1.7c. Note that for a brittle solid the energy dissipation consists primarily of the energy spent in forming the new surface, A , so that the rate of energy dissipation is equal to

$$\mathcal{D} = \gamma \frac{dA}{dt} \quad (1.25)$$

with γ as the surface energy per unit area formed. If we define rupture to be imminent when the kinetic energy increases from zero to a small value the power equation 1.12 predicts rupture when

$$\dot{F} - \dot{W}_B \geq - \gamma \frac{dA}{dt}. \quad (1.26)$$

For the case of a centrally cracked plate of unit thickness under a

uniform peripheral stress σ Griffith showed* that the inequality 1.26 predicts catastrophic failure when

$$\pi \cdot c \cdot \frac{\sigma^2}{2E} \geq \gamma \quad (1.27)$$

where c is the half crack length,

The derivation of an equivalent relation for the prediction of fracture in viscoelastic rubbers as relates to the concepts of this dissertation hinges on the two facts that 1) the shape of defects is not known and 2) the necessary stress analysis is intractable when large strains are encountered**. Nevertheless a detailed qualitative analysis involving various arguments on the above two points can lead to the result below, its derivation resting ultimately on arguments of dimensional analysis. In the interest of brevity and clarity we present therefore on dimensional grounds the analog of relation 1.27 for a viscoelastic solid as

$$W_{el} \sqrt{A} \geq \alpha T \quad (1.28)$$

Here A = surface area of the enlarging defect,

W_{el} = elastically stored energy density far away from the defect,

T = rate dependent tearing energy and

α = a proportionality constant.

* It is interesting to note in passing that Griffith predicted that the failure stress is independent of the biaxial nature of the stress field applied. Contrary to this common understanding Swedlow (53) has recently shown on analytic grounds that the applied stress system does indeed influence the ultimate stress.

** A notable exception is the analysis of fracture initiation from a spherical void in a uniform hydrostatic tensile stress field (48).

Since the energy T can be chosen to define rupture in accordance with experimental requirements we shall defer its evaluation at this time. Introducing the area ratio notation of the previous section the critical condition can be written as

$$W_{\alpha} \sqrt{\frac{A}{A_m}} \geq \Gamma \quad (1.29)$$

where $\alpha T / \sqrt{A_m}$ is a constant to be determined later by experiment.

So far we have considered only the criticality of a single defect in a viscoelastic solid and we must comment on the effect of many defects on the criticality condition 1.29. In this respect it suffices to say that the nature of the criticality relation is not changed if the defects are so far apart that their stress fields do not influence each other significantly. Koiter (54) has shown, for example, that the energy of interaction of two small parallel cracks in a large sheet under tensile loading is small compared to the energy due to the individual cracks if their separation is larger than their crack length. One would estimate therefore that the problem of defect interaction is not severe when the defect separation in a uniform stress field is larger than their largest lateral dimension. If the defect spacing is closer, however, the interaction effect has to be accounted for. In this case the left hand side of the inequality 1.29 may be estimated either by engineering intuition as for instance in reference 55 or from Westergaard's solution for an infinite array of colinear cracks (56).

Such considerations would lead to equivalent criticality conditions in the form

$$W_{el} \frac{\sqrt{A/e^2}}{1 - A/e^2} \geq \Gamma \quad (\text{ref. 55}) \quad (1.30)$$

or

$$W_{el} \frac{\ell}{\pi} \tan \frac{\pi \sigma_r}{\ell} > \Gamma \quad (\text{Westergaard's solution, ref. 56}) \quad (1.31)$$

where ℓ is the separation of the defects and A is again the defect surface. The numerical computations in the following chapter are based on the simple relation 1.29 and it appears from the results that the inequalities 1.30 or 1.31 are not necessary to calculate gross rupture.

Having determined now both the defect size as a function of time and the criticality relation for the defect size and the applied stress we can proceed to calculate rupture for some stress or strain histories.

D. APPLICATION TO RUPTURE PREDICTION

We shall now use the rupture equations 1.22 and 1.29 to calculate values of the ultimate stresses and strains for some specific situations which lead to rupture. Besides evaluating the three experimental quantities $\Theta(\tau)\lambda$, N and Γ these computations serve the triple purpose of 1) demonstrating the use of the rupture equations, 2) testing the applicability of the rupture model and 3) obtaining a quantitative understanding of failure accumulation prior to gross rupture,

Implicit in these calculations is the important idea that fracture may be sensitive to the stress or strain history prior to rupture and is not simply a function of the ultimate stress or strain state. (Note that in the time-differential formulation of the defect growth in equation 1.22 the failure model accommodates in principle any stress or strain and temperature history to which the material might be subjected.)

In order to relate this differential failure accumulation to more familiar concepts in viscoelasticity recall that in a linearly viscoelastic solid the stress at a certain time is a function of the entire strain history prior to that time and that the stress accumulation is governed by the relaxation modulus and the Boltzmann superposition integral*. Similarly the accumulation of failure is a function of the history dependent elastic energy and secondly, in analogy to the superposition integral, by the

* For historic reasons this is the common name for Duhamel's integral in linear viscoelasticity theory.

defect integral relation 1.23. In contrast to the Boltzmann integral, however, the relation 1.23 represents a non-linear accumulation with respect to the stress or strain history; this is unfortunate inasmuch as the simple mathematical properties of the linear superposition integral cannot be applied to failure accumulation.

Nevertheless, it would be extremely valuable from a practical standpoint if this analogy could be exploited in an approximate manner so as to permit rupture prediction in various situations on the basis of failure data procured in simple test configurations. However, an examination of this possibility leads beyond the scope of this dissertation and must therefore be left as a subject for future investigations.

Because the convenient constant strain rate test is at present the most commonly employed means of characterizing viscoelastic failure properties it will be useful to apply the failure calculations to this test. But in order to examine the concept of localized fracture it will be necessary to apply the analysis to rupture in stress concentrations; this will be done by calculating the initiation time for crack propagation and the propagation velocities of cracks in viscoelastic sheet material.

The failure equations 1.22 and 1.29 contain three experimental constants, namely the number of bonds per unit volume of weak region (N or NkT), the rate constant λ and the quantity Γ which contains the tearing energy. These constants have been chosen to fit the calculated failure behavior to the experimental data with the result that $NkT = 400$ psi, $\Gamma = 2$ psi and $\lambda = 1$. The

same constants are used in all calculations.

Besides considering the accumulation of failure in monotonic stress or strain histories a cursory examination of the effect of stress cycling is given in a section devoted to the exploration of rupture accumulation. Finally the extension or applicability of the failure model to filled polymers is discussed in section 1.14.

In the interest of a unified evaluation of the failure model based on these calculations only detailed observations relating directly to the particular computations are presented in the following sections, the comprehensive analysis being deferred to the final chapter of this part.

1.10 The Constant Strain Rate Test

The procurement of the ultimate uniaxial tensile data for the rubber employed in this work is given in detail elsewhere (16). As mentioned earlier this data represents the isothermal rupture properties and accordingly we shall consider the temperature constant for the following calculation*.

To determine the elastic energy stored in a tensile specimen under constant rate of extension consider the generalized Maxwell model shown in fig. 1B. The elastic response of the polymer chains is represented by the linear springs and the

* We assume in the following calculations that the time-temperature shift function $\Theta(T)$ is equal to the inverse of the shift factor a_T in fig. 5. Although there is no obvious reason for this choice on molecular grounds it would seem that the superposability of ultimate tensile data by the conventional shift factor scheme justifies the assumption. Since $a_T = 1$ for the reference temperature employed in the calculations (22.5°C) we have also $\Theta(295.8^\circ\text{K}) = 1$.

elastic energy by the energy stored in the springs.

Let the applied strain ϵ be given by

$$\epsilon = R \cdot t \quad (1.32)$$

with R denoting the constant strain rate and t the time. As each element experiences the same strain the stress σ_i in the i^{th} element can be calculated from the element stress strain law

$$\frac{d\sigma_i}{dt} + \frac{m_i}{\eta_i} \sigma_i = m_i \frac{d\epsilon}{dt} = m_i R \quad (1.33)$$

to be

$$\sigma_i = m_i \tau_i R \{1 - e^{-t/\tau_i}\} \quad (1.34)$$

where $\tau_i = \eta_i/m_i$ is the relaxation time of the i^{th} element. The energy W_i in the i^{th} spring is therefore

$$W_i = \frac{\sigma_i^2}{2m_i} = \frac{1}{2} m_i (\tau_i R)^2 \{1 - e^{-t/\tau_i}\}^2. \quad (1.35)$$

If m_e denotes the spring constant of the viscosity degenerate Maxwell element representing the equilibrium modulus then the total elastic energy is obtained by summing the energy in all the springs of the viscoelastic model:

$$W_{el} = \frac{1}{2} m_e (Rt)^2 + \frac{1}{2} \sum_{i=0}^N m_i (\tau_i R)^2 \{1 - e^{-t/\tau_i}\}^2 \quad (1.36)$$

Recall that this represents the elastic energy for small strains.

In order to take into account the non-linear stress-strain behavior at large strains we multiply the expression with a constant

correction factor in accordance with the discussion of section 1.4. For our present work a reasonable value of this constant is $1/2$; this corresponds to replacing the spring constants of the visco-elastic model by one half of their values measured at infinitesimal strains. Utilization of the expression 1.36 permits then the evaluation of the defect integral 1.23. Because the integration has to be performed numerically the differential equation 1.22 is more conveniently used. Upon satisfying the critical load condition 1.29 one obtains the failure curves shown in fig. 12 together with the experimental data.

1.11 Rupture Initiation Time

Having demonstrated the application of the failure calculation to the rupture of a uniaxial tensile specimen, we turn now to a consideration of fracture initiation at a stress concentration, and in particular the incubation time between loading and fracture.

In a practical example consider a solid propellant rocket grain containing a crack near the internal surface. Since the structural integrity of the rocket may depend on the rate of crack propagation after ignition, it will be important to compare its growth rate to the burning rate of the solid fuel. Obviously if the latter exceeds the former, this particular type of fracture would not concern the designer.

Williams, Blatz and Schapery (15) have calculated the initiation time for crack propagation by using a constant critical strain as a rupture criterion. The time dependence of the

fracture phenomenon is thus entirely controlled by the time effects in the stress-strain behavior*. In contrast the rupture calculations presented here contain the time dependence of both the stress-strain behavior and the bond rupture process. It turns out therefore that the present theory can predict time dependent rupture if the viscoelastic material is in the relaxed state. This is, however, not true for the calculations based on the critical strain criterion.

Because the geometrical conditions at the tip of a naturally formed crack in a rubbery material are subject to wide variations it was necessary in the experimental analog of the crack initiation studies to provide a crack tip of consistent dimensions. This was achieved by drilling a 1/64 inch diameter hole through the test sheet shown in fig. 15.A while the rubber was held at dry ice temperature (-78°C)**. The drilling operation was standardized in drill speed and drill feed in order to minimize variations arising from the mechanical formation of the crack tip. Under a magnification of about 20 diameters the drilled surface was found to be smooth although not as free of imperfections as, for example, a surface cast against a polished mandrel. Therefore

* These authors have also proposed the extension of their computations to include a time or rate dependent critical strain in the form of experimental data. While this suggestion leads in the right direction it does not treat the effect of strain history on rupture in an adequate manner. The consequence of this will become evident in the following discussion.

** As a reference, the dilatometrically determined glass transition temperature is -87°C .

a part of the experimental scatter must be attributed to surface imperfection. Upon loading the specimen across its width to the desired constant strain magnitude in less than 1/4 sec, the motion of the material at the crack tip could be observed. The rupture initiation, or incubation, time was defined as the time lapsed between load application and the first evidence of local tearing as observed with a low power microscope.

A characteristic feature of viscoelastic fracture is the relatively large scatter in the experimental data. This phenomenon is a consequence of the statistical nature of the molecular polymer structure which was discussed in section 1.6. As an example the variation in the crack initiation time has been obtained in 37 tests at the same load condition and the results are shown ordered by magnitude in fig. 13. Note that the time values vary over three orders of magnitude from 2 seconds to 1 3/4 hours. Nevertheless, it is obvious from the inset histogram in the same figure that there exists a most probable value of the initiation time at about 7 seconds for this particular loading condition.

Because of the time consuming nature of this test only a limited amount of initiation time data was obtained at different stress levels. The results presented in fig. 14 are sufficient, however, to define a scatter band which covers the time values in the vicinity of the most probable value.

The calculation of the initiation time requires the knowledge of the stresses at the crack tip, $\bar{\sigma}_c$. As the deformed

boundary of the crack tip is free of normal and shear stresses the stress field is locally uniaxial and the magnitude of the stress is approximately proportional to the gross stress σ_{∞} in the uncut region of the specimen, i. e., $\sigma_t \approx \beta \sigma_{\infty}$. If the failure times are sufficiently long (longer than about one second for this H-C rubber) most of the rupture process takes place while the material is in the relaxed condition and the local, elastically stored energy density is given by

$$W_{el} = c \frac{(\beta \sigma_{\infty})^2}{2 m_e} \quad (1.37)$$

with m_e denoting again the rubbery modulus and the constant c accounting for the adjustment due to the non-linear nature of the material stress-strain law as pointed out previously. Under these conditions the failure time is obtained from equation 1.29 as

$$c \frac{(\beta \sigma_{\infty})^2}{2 m_e} \sqrt{\frac{A}{A_m}} = \Gamma \quad (1.38)$$

where the area ratio can now be obtained explicitly from the defect integral 1.23 as

$$\frac{A}{A_m} = \tanh \left[c \frac{(\beta \sigma_{\infty})^2}{2 m_e N k T} \right] \left\{ 1 - \exp \left[-\lambda t \cdot \cosh \frac{c (\beta \sigma_{\infty})^2}{2 m_e N k T} \right] \right\}. \quad (1.39)$$

Solving for the time t by combining equations 1.38 and 1.39 one obtains the rupture time

$$\lambda t_R = - \frac{1}{\cosh \frac{c(\beta \sigma_{\infty})^2}{2 m_e N k T}} \ln \left\{ 1 - \frac{\Gamma^2}{\left[\frac{c(\beta \sigma_{\infty})^2}{2 m_e} \right]^2 \tanh \frac{c(\beta \sigma_{\infty})^2}{2 m_e N k T}} \right\} \quad (1.40)$$

Using the previous values of λ , N and Γ the result of equation 1.40 is compared with the experimental data in fig. 14 for a stress-concentration factor of 1.75* and c was chosen equal to 1.5**, to replace the modulus by two thirds of its initial tangent value.

While the stress range covered in the experimental study is hardly sufficient to prove or disprove a theory the importance of the comparison lies in demonstrating that the same experimental parameters can be used to predict rupture for different types of tests.

1.12 Crack Propagation at Constant Velocity

In their experimental investigation of rupture propagation in rubbers Greensmith and Thomas (3, 4, 5, 6) have studied the tear behavior at constant rates of tear and found an experimental relationship between the aforementioned tearing energy and the steady rate of tearing. But while these authors used primarily a test configuration as shown in fig. 15B we shall employ here another test configuration which was also used by them, the cracked strip geometry shown in fig. 22. Although the tear

* Stress-optically, the concentration factor could not be determined better than between 1.5 and 2.5 due to the poor optical quality of the material,

** It should be noted that the strains encountered in this study were smaller than in the constant strain rate tests where the strain values ranged over 400%.

specimen of fig. 15B is more convenient from an experimental standpoint it turns out that an approximate stress analysis is more easily performed for the cracked strip specimen. The latter configuration lends itself therefore more readily to a failure analysis of the type outlined below.

a. Analytical considerations. The cracked strip geometry lends itself readily to studying the behavior of self-propagating cracks in steady motion. If, for instance, the strip boundaries are displaced parallel to each other so that the material far ahead of the crack is under a uniform tensile strain ϵ_{∞} , and if further enough time has passed since strain application to allow the stress σ_{∞} to be at its equilibrium value, then the crack will propagate at a constant velocity:::

Schapery (45) has considered this problem from the standpoint of thermodynamics by using the power equation 1.12. By assuming a simplified form of the strain field in the crack tip vicinity he related the applied stress σ_{∞} to small velocities of crack propagation. Although this concept can be applied to the calculation of higher velocities through a refined stress analysis we shall here treat the same problem from the standpoint of local and time dependent failure.

* In terms of the Rivlin-Thomas tear energy T the inequality $\mathcal{W}(\sigma_{\infty}) > T$ guarantees crack propagation if $\mathcal{W}(\sigma_{\infty})$ is the energy per unit length and thickness of the strip far ahead of the crack. In practice the velocity will be constant only on the average. Incidentally, some stress relaxation during crack propagation is still obvious in the velocity curve of fig. 11,

In terms of the present failure model we envisage the process of crack propagation to occur in the following manner: As a point on the line of crack propagation is approached by the steadily advancing crack tip it experiences a time dependent strain rate arising from the stress concentration at the crack tip; accordingly defect growth occurs at that point with a rate determined by the differential failure equation 1.22. But when the point is just reached by the crack tip the combination of local defect size and elastic energy must satisfy the critical condition 1.28. The analytic determination of the crack velocity v which satisfies this condition for a given applied stress leads to an integral equation with the velocity as an implicit function of the applied stress σ_{∞} through their joint effect on the elastic energy $W_{el}(v, \sigma_{\infty})$. Rather than solving the integral equation it will be easier, however, to determine the velocity-stress relation by a trial and error method.

For reasons of mathematical simplicity we limit the occurrence of rupture to a narrow band along the line of crack propagation across which the stress conditions are essentially uniform. Neglecting inertia effects for slowly moving cracks* one can deduce from the stress analysis in

* Based on the equilibrium shear modulus of the H-C rubber studied here the equivoluminal wave speed is 10^5 in/min (-150 ft/sec). Speeds below 10^3 in/min should therefore be admissible for this analysis; the maximum velocity measured in the experimental studies was approximately 50 in/min.

part II of this dissertation that the stress across the narrow band, σ_y , is approximately equal to

$$\sigma_y = \sigma_\infty \left\{ \frac{0.5 \sqrt{b}}{\sqrt{x + \rho}} + 1 - \frac{1}{2} \left[e^{-\frac{x}{3b}} + e^{-\frac{5x}{2b}} \right] \right\} \quad (1.41)$$

where x is the distance from the crack tip, b is the half width of the test strip and ρ has the meaning of a crack tip radius. A complication arises from the presence of the σ_x stress parallel to the direction of crack propagation. In order to remain consistent with the idea of a uniaxial stress field we will, however, neglect this stress* and reduce the problem of crack propagation to a problem in uniaxial tensile failure under a special stress history.

Making the steady state velocity transformation $\xi = x - vt$ where v is the (unknown) crack velocity we consider therefore a small uniaxial tensile specimen as located at $x = x_0$ far ahead of the crack and subject it to the stress history

$$\frac{\sigma}{\sigma_\infty} = \frac{\sigma(t)}{\sigma_\infty} = \frac{0.5 \sqrt{b}}{\sqrt{\xi + \rho}} + 1 - \frac{1}{2} \left\{ e^{-\frac{\xi}{3b}} + e^{-\frac{5\xi}{2b}} \right\} \quad (1.42)$$

* Although the σ_x stress is by definition zero at the crack boundary it is not zero ahead of the crack where its value is a fraction of the σ_x stress. (It is also a tensile stress.) Note, however, that as the shear stress is zero on the crack axis the energy density there is for an incompressible solid $w_d = \frac{1}{2} [\sigma_y^2 + \sigma_x^2 - \sigma_x \sigma_y]$; this has a minimum for $\sigma_x = \sigma_y/2$ which is, however, only 25% smaller than when $\sigma_x = 0$. Neglecting the σ_x stress should therefore not influence the results seriously but may lead to higher crack speeds than would probably be obtained if it were not neglected.

with $\xi = x_0 - vt$. The problem of crack speed determination consists thus of finding the value of the velocity for a given value of the applied stress σ_∞ such that the criticality equation 1.29 is satisfied when $\xi = 0$.

The time dependent elastic energy at a point undergoing eventual rupture can be calculated again with the help of a viscoelastic material model by summing the energy stored in the springs of the model. But because the stress is now prescribed we employ the generalized Voigt model in fig. 2B. The strain in the i^{th} element is determined from Duhamel's Integral as

$$\epsilon_i(t) = \int_0^t \frac{\sigma(t-\theta)}{m_i \tau_i} e^{-\theta/\tau_i} d\theta \quad (1.43)$$

and upon using the stress 1.42 there results

$$\epsilon_i(t) = \frac{\sigma_\infty}{m_i \tau_i} \left\{ \frac{0.5\sqrt{b}}{\sqrt{v\tau_i}} e^{\frac{\xi+p}{v\tau_i}} \Gamma\left(\frac{1}{2}, \frac{\xi+p}{v\tau_i}\right) + 1 - \frac{b}{2} \left[\frac{3e^{-\frac{\xi}{3b}}}{\sqrt{\tau_i} + 3b} - \frac{2e^{-\frac{5\xi}{2b}}}{5\sqrt{\tau_i} + 2b} \right] \right\} \quad (1.44)$$

where $\Gamma(u, \alpha)$ is the incomplete gamma function of order $1/2$. By summation of the energy in the springs of the generalized Voigt model the total time dependent energy is obtained as

$$W_{el} = \frac{1}{2} \frac{\sigma_y(t)^2}{m_{ge}} + \frac{1}{2} \sum_{i=0}^N m_i \epsilon_i^2 \quad (1.45)$$

with r_{ng} representing the short time response modulus of the material. The use of the energy and strain relations 1.44 and 1.45 permits again the numerical integration of the defect rate equation 1.22. Since for $\xi > 1$ the stress is approximately constant and equal to σ_{∞} and by assumption at its equilibrium value the integration extends over the range $0 \leq \xi \leq 1$ with the initial value of A/A_m being given again by the analog of equation 1.39 for long times as

$$\frac{A}{A_m} = \tanh \left\{ \frac{c}{NkT} \frac{\sigma_{\infty}^2}{2m_e} \right\} \quad (1.46)$$

From the standpoint of numerical evaluation it was found convenient to calculate values of

$$g(v) = W_{el} \sqrt{\frac{A}{A_m}} \quad (1.47)$$

in the integration interval for a given stress σ_{∞} and several crack velocities v ; the velocity corresponding to that stress was then found by interpolation of the function $g(v)$ at $g(v) = \Gamma$.

Greensmith (4, 7) has related the effective radius of curvature to the roughness of the fracture surface. According to the discussion in section 1.7 the surface roughness and thus the tip radius decreases with increasing crack speed. It turns out however, that a velocity dependent radius of curvature does not lead to a significantly different result, so that a constant radius was used in the calculations. A particular value of $\rho = 0.01$ inches was chosen to make the theoretical results at slow velocities

coincident with experiment.

Since the radius of curvature is an unknown parameter in these calculations the computation of crack velocities actually amounts to a determination of this quantity, A reasonable value for the crack radius constitutes therefore a test of the failure theory in addition to the comparison of the calculated and the experimental relation between the applied stress and the velocity. The value of $r \approx 0.01$ inches is consistent with the findings of Greensmith (7) who measured effective radii between 0.01 and 0.02 inches. The calculated velocity values are shown as the solid curve in fig. 16 for the previous values of NkT , λ and Γ .

b. Experimental Analysis. Figure 16 shows also the experimental points determined with the sheet geometry of fig. 22. The load was applied to the specimen through displacing the clamped long boundaries in an arrangement which produced a uniform strain along the specimen length. Approximately 3-4 minutes after load application when the material was at the equilibrium condition a 1/8 inch cut was introduced through the sheet as shown in fig. 15C. The subsequent motion of the crack was photographed through an accurate Lucite scale with an automatic Beattie Varitron camera synchronized to a Xenon flashtube and triggered by a variable speed timing mechanism. This test equipment is shown in fig. 17. By using the scale markings on the film record* as a reference, the crack tip position was

* These markings are barely visible in fig. 9.

determined on a comparator for each exposure frame, which then permitted the calculation of the velocity from the knowledge of the time lapse between frames. As an example the plot of the crack position and velocity as a function of time is given in fig. 11; the uncertainty in the velocity is the result of the difficulty encountered in defining the location of the crack tip, which was often diffuse as exemplified by the extreme case shown in fig. 9. Note however that in spite of this uncertainty the velocity deviates considerably from the average value. It is believed that this behavior indicates the statistical nature of the material strength properties as experienced in the earlier initiation time study. The velocities plotted in fig. 16 are the mean velocities as determined from the average slope of the displacement time curve under exclusion of the acceleration stage, and the bars on the symbols indicate the measure of local velocity deviation from the mean. The open square symbols represent data on material of the same formulation but prepared separately from the material represented by the open circles.

1.13 Suggested Applications of the Failure Theory

It was pointed out at the beginning of this chapter that rupture is a process which involves the whole stress history of the material. Since ultimate properties are usually obtained in simply conducted tests for a specific stress or strain history, the question arises whether such empirical data can be used to predict rupture under different loading histories.

This problem is not restricted solely to the fracture of polymeric materials but is equally important, for example, in the design of metallic structures subject to conditions favoring failure by fatigue. In this case experimental data are usually available only in the form of simple S-N diagrams. While a number of rules on the generalized application of S-N curves has been proposed it has been proven in equally many cases that they apply only in special situations and have no basic foundation. The problem of damage accumulation in metal fatigue has therefore been approached in a more fundamental way by Valluri (57, 58) in a theory which is analogous to the failure analysis presented in this dissertation. On the basis of this theory Valluri was able to explain and predict phenomena which the previously established rules could not, particularly the sensitivity of the fatigue crack growth to loading history.

Following the developments of Miner (59) on the damage accumulation in metal fatigue Williams (60) has suggested for viscoelastic solids a rule for estimating rupture in variable strain histories from constant strain rate failure data:*. Expressed in mathematical terms as

$$\int_0^{T_R} \frac{dt(\dot{\epsilon})}{t_R(\dot{\epsilon})} = 1 \quad (1.48)$$

* The concept of damage accumulation in polymeric materials was proposed earlier by Alfrey (11), but the proposition was mathematically not well defined.

this rule states simply that the strength attrition is proportional to the fraction of the time spent at a particular strain rate to the total life at that strain rate, and that the total life T_R is spent when the sum of the fractional attrition quotients equals unity. While this rule predicts rupture correctly in the limit case of a constant strain rate test (as $t_R(\dot{\epsilon})$ is measured in such a test) it is insensitive to the order in which high or low strain rates (or loads) are applied to the material. We shall show below that this is not in agreement with reality.

Although we have already demonstrated that the present rupture theory accommodates an arbitrary stress or strain history it is also recognized that the amount of computational work in its application is not small. It is therefore in the interest of engineering analysis to develop an intuitive understanding of the failure process which will aid in establishing simpler approximate formulas for rupture prediction. However, the development of rules which permit an extrapolation of simple test data to more complicated situations will not now be attempted, Rather, we shall consider the effect of damage accumulation by way of some specific examples to develop a qualitative appreciation of its significance with respect to more general problems of viscoelastic rupture.

We shall thus consider briefly the problem of accelerated crack propagation as a problem of cumulative damage against the background of the earlier steady crack propagation calculations

and explain why crack accelerations cannot in general be calculated from constant velocity data. Following an examination of damage accumulation in the previously discussed constant strain rate test we demonstrate the cumulative effect in a situation involving two different strain rates instead of a single one, Finally we present a cursory examination of rupture due to a cyclically varying stress.

a. Crack acceleration. In the last two sections we have calculated the time of initiation and the steady propagation rate of a crack. It seems appropriate for a complete description of macroscopic rupture progression to consider the problem of accelerated crack motion in viscoelastic materials.

Williams, Blatz and Schapery (15) have computed the accelerated growth of a crack in a viscoelastic material. We have already referred to this work in connection with the initiation time calculations. By representing the stress-strain properties by a simple Voigt model they found an exponential increase in crack velocity with time. Essentially the same result was reported by Williams (44) on the basis of thermodynamic considerations. While these calculations can be made for more realistic material properties than the simple representations used by the authors for demonstrative purposes the amount of computational work is large and the desired results by no means certain.

With respect to computational difficulties the present theory offers no advantage, Whereas the calculation of steady crack motion leads to an integral equation involving the (constant)

velocity implicitly, the acceleration problem requires the determination of a velocity-time history.

In order to circumvent the mathematical difficulties one would naturally inquire whether constant crack velocity data, as shown for example in fig. 16, could be used to estimate the acceleration behavior.

This problem is analogous for instance to that of predicting failure in an arbitrary strain history from constant strain rate failure data which was considered by Williams (44)*. Although acceleration calculations were carried out by following a similar line of reasoning they could not predict for example the acceleration behavior in fig. 11 and merely confirmed in a qualitative manner the results expected on intuitive grounds. It suffices therefore to present only the pertinent results of the analysis.

First recall that the velocity data in fig. 16 represents the propagation of a crack through a viscoelastic material which is in the state of long-time equilibrium. One would therefore expect that acceleration behavior can be predicted reasonably well if the stress or strain which causes the acceleration increases so slowly that the crack speed increases through successive steps of equilibrium growth. This would be the case for example if a slit strip specimen (cf. fig. 22) were strained slowly at a constant rate of strain.

On the other hand, if the same specimen were strained

* See the beginning of this section.

quickly to a fixed strain before the crack can propagate the strain history of the material at the crack tip would be very different. One should therefore not expect in this case that the use of the equilibrium data (fig. 16) would render an adequate description of the ensuing acceleration unless the effect of the strain history on damage accumulation is considered.

The acceleration of an initially stationary crack is primarily controlled by the defect growth in the crack tip vicinity, To illustrate this by way of example, it was observed in tests conducted with the geometry of fig. 15C* above gross strains of 30 % that the crack velocity initially attained a value which was higher than the steady velocity corresponding to equilibrium crack propagation in the slit strip geometry. This extra velocity increase had the appearance of an inertial overshoot but was observed at velocities where dynamic effects are entirely negligible. At gross strains above 30 % an extended region around the crack tip is under a high strain and damage accumulates there more rapidly than in the uniformly strained part of the specimen. At the time of initial crack propagation (incubation time) the crack progresses quickly through the highly damaged material at the crack tip, but at a slower rate through the less damaged uniform strain region, Indeed, it appears as if the acceleration of an initially stationary crack were more akin to the rupture of a tensile specimen at a

* The specimen was in a relaxed stress state before the cut was made into the sheet.

high constant strain than to the propagation of a crack under equilibrium conditions.

It is obvious that the problem of accelerated crack motion in viscoelastic materials involves the complete local stress or strain history of the rupturing material. Acceleration behavior might therefore be predicted from related velocity data only if the strain history of the material on the crack path is similar to that which gave rise to the velocity data.

b. Cumulative damage in the constant strain rate test.

Because the constant strain rate test is presently commonly employed in rupture studies it is useful to consider the accumulation of failure in this simple strain history. Although the time dependent defect size would be the appropriate measure of damage it does not by itself indicate how close the material is to failure. We have therefore chosen to represent the damage by a criticality function F_c which incorporates explicitly the defect size and the elastic energy, and is defined as

$$F_c \equiv W_{el} \sqrt{\frac{A}{A_m}} \quad (1.49)$$

This is of course recognized as the criticality condition 1.29 when $F_c = \text{constant} = \bar{\Gamma}$. The criticality function has been plotted against the strain in fig. 18 for various strain rates. Note in passing that a cross plot of the strains as a function of the strain rates at $F_c = \bar{\Gamma} = 2$ yields the ultimate strain curve of fig. 12.

Two observations are of primary interest. First observe

that for high strain rates ($R > 10^{10}$ in/in/min)* the function F_c rises relatively sharply near the fracture point thus indicating that significant damage occurs only at strains close to rupture strains. For example, at a strain rate of 10^{14} in/in/min virtually no damage occurs until after 200% strain while total rupture takes place at 240% strain ($F_c = 2$). Secondly note that although the strain rates 10^6 and 10^{12} in/in/min lead to about the same rupture strain ($F_c = 2$) the accumulation of failure is not the same. For instance at 250% strain the sample strained more slowly has suffered approximately 50% damage whereas the faster strained material has been barely damaged.

These observations illustrate in a tangible manner the fact that damage accumulation is not linear up to rupture but is more pronounced close to fracture. One would therefore conclude that the effect of variations in the stress or strain history are, in terms of the rupture strain curve of fig. 12, more seriously reflected in the rupture behavior the closer the rupture curve envelope is approached.

c. The dual strain rate test. In order to put the qualitative understanding of failure accumulation on a quantitative basis failure strains have been calculated for a strain history which involves two constant strain rates instead of a single one. This test may be considered as a simple model of a more general

* Recall that these are temperature reduced strain rates and not necessarily physically realizable values.

variable strain rate history and as such is important in the study of cumulative damage. Since the computations are in principle the same as those worked out for the constant strain rate test we omit them here and present only the result.

Consider therefore the strain rate history indicated by the arrow marked 1 in fig. 19: After straining the material at the higher of the two possible strain rates to a given strain the rate is changed to a lower value. By varying the strain at which the strain rate changes one can, for example, obtain an indication of how damage accumulates as a function of strain or time.

In view of the past comments on the importance of the stress or strain history on viscoelastic rupture one should not expect the same rupture strain if the sequence of the high and low strain rates is changed. This expectation is confirmed as fig. 19 shows. The upper dashed curve represents the rupture strain in a slow-fast dual strain rate test and the lower one the same quantity in a fast-slow test. The locus of rupture strains for intermediate single, constant strain rate tests falls in between the two curves; it has been omitted from the graph to avoid confusion.

Harstad (61) has verified these calculations qualitatively in an experiment on an H-C rubber of slightly different formulation than employed in this work. His results are shown in fig. 20. Although the scatter of experimental points is considerable it is

nevertheless clear that the order in which high and low strain rates are applied has a significant effect upon the ultimate properties*; this is similar to the conclusion Valluri found for metal fatigue. While the difference in the ultimate strains was in these examples only 100% a greater variation is possible depending upon the two strain rates chosen.

d. Stress cycling. The failure of polymers under a periodically varying stress is one of the least explored areas of viscoelastic failure, although presently new efforts are directed towards this problem.

A complication that arises in the stress cycling of viscoelastic solids is the dissipation of energy and the attendant temperature rise**. Whereas this difficulty can be accommodated by the proposed failure model it is expedient for the present purposes to consider only sufficiently high or low cycle rates where energy dissipation is low either because viscous flow does not occur to any large extent or because the material is always in the relaxed state. The same considerations would also apply at intermediate frequencies when one considers stress cycling in local stress concentration, at a temperature constant surface. At any rate, the inclusion of temperature

* Note that high strain rates correspond to high stresses and low strain rates to low stresses. One would therefore expect a similar behavior if the order of stress application in a dual load test to failure were interchanged. This sensitivity to the order of load application has its parallel in metal fracture under fatigue conditions as noted previously.

** An interesting account of this temperature effect in solid propellant materials has been given by Tormey and Britton (62).

effects is, in principle, not a difficult matter.

Under these conditions defect growth is again governed by the rate equation 1.22 which we rewrite here as

$$\frac{dA/A_m}{dt} = -\lambda \left\{ \cosh \frac{We}{NkT} \cdot \frac{A}{A_m} - \sinh \frac{We}{NkT} \right\}. \quad (1.50)$$

If the number of cycles to failure is small this equation must be integrated exactly. However if rupture is accumulated over many cycles so that A/A_m does not change markedly in any cycle, one may integrate equation 1.50 over the N^{th} cycle (between the time $(N-1)/\omega$ and N/ω , ω being the cycle frequency) to give

$$\omega \frac{dA/A_m}{dN} = - \left\{ C \frac{A}{A_m} - S \right\}$$

where

$$C = \int_{(N-1)/\omega}^{N/\omega} \cosh \frac{We}{NkT} dt \quad (1.51)$$

$$S = \int_{(N-1)/\omega}^{N/\omega} \sinh \frac{We}{NkT} dt .$$

The integration extends only over that part of the cycle where the stress is tensile rather than compressive; this restriction follows from the fact that damage accumulation is not expected from compressive stresses. Using again the particular solution of equation 1.23 one has

$$\frac{A}{A_m} = \frac{S}{C} \left\{ 1 - e^{-\lambda C \frac{N}{\omega}} \right\}. \quad (1.52)$$

The criticality condition 1.28 is unchanged except that the elastic energy is interpreted as the maximum value during each cycle.

Since the constants C and S represent only the average effect of the stress history during a cycle equation indicates that there may be several stress cycle shapes with the same frequency which can lead to rupture in the same number of cycles, provided the maximum elastic energy per cycle is also the same.

Finally it should be pointed out that we have not considered here a problem of polymer fatigue as the term is understood in relation to metal failure under cyclic stress. Whereas metal fatigue implies a failure stress below the static long time material strength, we have considered here merely another problem of time dependent damage accumulation. Due to the intermittent type of loading the material can indeed sustain a peak load longer than under static conditions.

The problem of fatigue in unfilled polymers has not been investigated in great detail* and there is a question as to whether it exists to any significant extent. The molecular mechanism that would be associated with it is probably of a different nature than those discussed previously and their experimental exploration appears to present even greater difficulties than the development of fatigue cracks in metals.

* Wintergerst (63) has obtained stress cycling data on unplasticized polyvinylchloride in the form of an S-N diagram. While the result is of the type predicted by equation 1.52 no correlation with the static strength was attempted. Similarly Lindsey (64) has tested a filled rubber under cyclic loading and found a very small breaking stress (2 psi) without, however, comparing it to the long time static strength.

1.14 Filled Polymer Systems.

In filled polymers additional problems arise due to the interaction of the polymer binder and the filler particles. It is safe to assume that, except under high compressive loads, the filler particles remain intact, so that there are basically two causes of failure: breaking of filler-to-polymer bonds, generally termed pull-away, and the breaking up of the polymer matrix. One might, therefore, consider the filler-to-binder bonds as one bond system and the matrix as another bond system. Failure may be primarily caused by pull-away effects through creating the necessary cavities or, in the case of very strong filler-to-binder bonds, by failure of the binder matrix. Each bond system should, of course, have its own rate laws. However, if one of the two bond systems is primarily responsible for failure then the present failure analysis may apply reasonably well.

Although we have not studied the rupture behavior of filled polymers in detail the rupture equations 1.22 and 1-29 were applied in an exploratory investigation to the tensile properties of a filled H-C rubber as reported by Kruse (65). While the limited amount of computation does not permit a conclusive evaluation it appears that the rupture theory is also applicable to filled polymers. As an example the calculated ultimate stress in a constant strain rate test is compared with experimental data in fig. 21.

E. EXAMINATION OF THE FRACTURE MODEL

Because many details of the fracture process were excluded from the fracture model it was already anticipated during its formulation that the theoretically predicted fracture behavior should not agree in all details with experimental evidence. This expectation is indeed confirmed when one compares theory and experiment in fig. 12, 14 and 16.

In spite of using a linear stress-strain law in the calculation of the elastic energy the gross agreement of experiment and theory is reasonably good for the constant strain rate test (cf. fig. 12). A relative estimate of the error attributable to either the non-linear material behavior or the limitation of the failure model is not possible without performing similar, but more detailed calculations. Nevertheless it appears that a substantial improvement can be obtained by using a more realistic stress-strain law. Note, for instance, that by employing a realistic material representation with respect to time rather than a simple viscoelastic model the time or rate dependence of the rupture behavior is very well predicted.

The deviation of the theory from experiment becomes more apparent in the crack velocity calculations, although a part of the discrepancy must be attributed to the simplified form of the local stress field used in the computations. Nevertheless, the theoretical curve exhibits the correct functional behavior and furthermore stays within the span of experimentally encountered stress values.

With regard to the initiation time calculations there are two items which invite particular attention: First, the relatively short initiation time at low stress levels and second the existence of a lower failure limit.

From a practical standpoint the prediction of failure at long times is one of the most desirable items of interest and it is unfortunate that the failure model appears incapable of representing this behavior in sufficient detail. A possible reason for this deficiency can be deduced by an analogy to the viscoelastic stress-strain behavior. Note that the expression for the defect size, equation 1.39,

$$\frac{A}{A_m} = \tanh \frac{Wd}{NkT} \left\{ 1 - e^{-\lambda \cdot t \cdot \cosh \frac{Wd}{NkT}} \right\} \quad (1.53)$$

resembles the expression for the creep compliance of a single Voigt element*. Recalling from the material properties discussion of section 1.1 that the simple Voigt model is usually incapable of representing the actual material behavior it appears that equation 1.53 is a similarly oversimplified expression of the material behavior. To be more specific it seems that a more precise description of the long time failure process should also include a more detailed

* It should be pointed out in this context that Williams, Blatz and Schapery (15) have used the Voigt mode! in their crack incubation time calculations and obtained the relation

$$\epsilon^* = \epsilon_0 (1 - e^{-t/\tau_0})$$

where ϵ_0 and τ_0 are experimental constants and t is the incubation time for a prescribed critical rupture strain ϵ^* .

consideration of molecular chain flow in the vicinity of ruptured chains in addition to the bond rupture process. Note in passing that the prediction of short rupture times is paralleled by the prediction of relatively large crack velocities at low stress values. Inasmuch as the failure model predicts rupture at higher stress levels and short times in better agreement with experiment than at long times, one concludes that besides chemical bond rupture other factors contribute significantly to the fracture process at low stress levels.

The existence of a lower failure limit is a consequence of admitting bond reformation in the fracture process. It is readily shown from the rate equations 1.13 and 1.14 that at elevated stress states an equilibrium can exist between broken and unbroken bonds, according to the relation

$$\frac{N_2}{N_1} = \frac{\overline{\omega}_{12}}{\overline{\omega}_{21}} \quad (1.54)$$

If the equilibrium number of broken bonds corresponds to a sub-critical defect size, rupture does not occur although the material has suffered some damage.

Although previous investigators of polymer fracture (9, 10) have discounted the importance of bond reformation in the fracture process there is no reason to omit it from a failure analysis since its effect has been demonstrated in chemical stress relaxation (28). Whereas bond reformation is unlikely to be important at high stress levels this is not necessarily true for low stress values. Because

the fraction of bonds broken in a molecule chain may be taken as a qualitative measure of the importance of bond reformation in fracture, we shall now calculate the number of bonds broken in a chain of the H-C rubber when the applied stress is equal to the lower strength limit.

Recall that the value of NkT used in the calculations was determined to be approximately equal to 400 psi. Since the temperature for these calculations was 396°K one finds for the number of bonds per unit volume

$$N \approx 6.5 \times 10^{20} \text{ bonds/cm}^3.$$

At the long time failure threshold of about 35 psi the average elastically stored energy is about 2.5 in lb/in^3 or $2 \times 10^5 \text{ erg/cm}^3$, which corresponds to 3×10^{-16} ergsibond. The energy contained in a carbon-carbon bond is approximately 4.2×10^{-12} erg which is four orders of magnitude larger than the energy available to each bond at rupture. It appears therefore that only one out of every 1.4×10^4 bonds experiences enough energy change to break. Since the number of bonds between chemical cross links is approximately equal to 8.5×10^3 (13) it appears further that only about one or two bonds break between cross links. This is indeed a small number and one would believe that under such conditions bond reformation plays an important part in controlling the molecular fracture process.

It is interesting to note in passing that this small number of bond ruptures per chain is just sufficient to locally reduce the rubber

network to an uncrosslinked polymer. Recalling that the uncross-linked polymers can exhibit permanent flow under low loads one would suspect again that the flow of molecule chains near bond rupture sites plays a significant role in the failure process at low stress levels.

Because the rupture model is only a crude approximation to the actual rupture process the above calculation is not expected to be accurate. But it is nevertheless encouraging that the calculated molecular parameters are of the order of magnitude one might normally expect.

F. CONCLUSION

The process of fracture in viscoelastic materials is influenced by many factors which relate to the molecular, microscopic and macroscopic material properties. While the various aspects of time dependent fracture are too numerous to include in a first analysis of the rupture process the judicious combination of the most dominant contributions to rupture from each of the three size categories leads to a simplified fracture theory.

Because only few important phenomena of the rupture process have been included in the analysis the theory cannot predict rupture in all the details observed experimentally. Nevertheless the agreement with experiment is reasonably good and further refinements of the theory are possible. These improvements should include the use of a non-linear stress-strain relation and a more precise description of molecule motion near molecular bond rupture sites. The latter addition to the theory is believed important primarily at long failure times and at high temperatures.

To demonstrate its use and to test its range of validity the theory has been applied to some selected test situations. While previous authors (9, 10, 15, 44) have considered the same test configurations their calculations were applicable only over small ranges of test conditions and included experimental fitting parameters for each type of test. In contrast, the present theory approaches the different situations from a unified point of view.

The most significant feature of the theory is that it accommodates in principle an arbitrary stress or strain history, the prime limitation being the mathematical complexity associated with the use of realistic mechanical properties of viscoelastic materials. Although the theory is thus not simply applied in common engineering design problems it is nevertheless believed to be a foundation on which engineering design rules can be based, However, the derivation of such rules must be left as a separate problem to continuing research.

PART II

STRESS ANALYSIS OF A SPECIAL CRACK GEOMETRY

The early investigations of crack problems by Inglis (66), Griffith (67) and Neuber (68) have been of fundamental importance in the studies relating to the fracture behavior of materials. Although these problems deal with cracks in an infinite medium there has been in general little difficulty in applying them in an approximate manner to sheet geometries of finite dimensions. However, there exist situations where these solutions are insufficient, particularly in those cases where the crack lies close to the boundary of a structural member. Although Westergaard (56), Willmore (70), Wigglesworth (71) and Isida (72) have considered geometries involving boundaries close to a crack, these problems are essentially variants of Inglis' elliptic perforation problem inasmuch as the loads are applied in the form of stresses far away from the crack and parallel to the boundaries. It seems therefore pertinent to investigate the stress field arising from the prescription of boundary displacements normal to the crack.

Lowengrub (73) and Koiter (74) have explored such configurations without, however, arriving at a general quantitative evaluation. It is therefore hoped that the following work will aid in elucidating further the effect of boundary conditions on the stress field near the crack tip, particularly for geometrical configurations which may occur in practical situations.

As a typical problem of this class we shall therefore investigate the stress distribution in a thin, infinite strip containing a semiinfinite crack parallel to the supporting boundaries and strained across its width. The assumptions of classical elasticity will be invoked even though infinitesimal strains and a linear stress-strain law will in general be violated when one deals with the strain magnitudes at the point of fracture. Before we can apply the results of the classical elasticity problem to the fracture propagation in rubbers we must therefore estimate the effect of finite deformations on the stress field in the vicinity of a crack. This will be done in an experimental study of essentially the same geometry. Inasmuch as the analysis of stresses at a crack tip represents a rather extreme case of finite deformations one would also hope that the experimental results provide an upper bound on the influence of finite deformations in stress analysis problems.

The following work is thus motivated by the interest in 1) the effect of a previously unexplored boundary condition upon the elastic stress field near a crack, 2) the application of this stress solution to the calculation of fracture propagation in rubber materials, and 3) the relation of solutions based upon infinitesimal elasticity theory to the behavior incorporating large deformations.

A. CLASSICAL ELASTICITY SOLUTION

The crack geometry to be considered consists of a thin, infinitely long strip containing a semi-infinite crack (cf. fig. 22). We wish to determine the stresses which arise from straining the strip across its width (perpendicular to the crack orientation) so that the infinite boundaries remain parallel.

From the standpoint of practical application to fracture work it would be desirable to formulate the problem so as to prescribe only the displacements along the parallel boundaries. The reason of course is that sheet material is more readily loaded by displacing relatively rigid clamping supports than by applying stress directly to the boundary, as for example by small tabs or hooks. It turns out, however, that the computational complexity of the problem can be reduced considerably if a slightly modified problem is considered. This situation corresponds to straining the strip uniformly across its width while leaving the displacement along the boundary free to adjust to a condition of zero shear stress at the same boundary. While this condition does not duplicate the convenient experimental arrangement used in the crack propagation studies it will be seen to give representative results.

The solution is obtained by using the Fourier transform and Wiener-Hopf techniques. Although the stresses are first obtained in the form of contour integrals in the Fourier transform plane they can be evaluated by the theory of residues. The stress

values are then calculated from the resulting series expressions and compared with those of some well known related crack geometries,

It is sometimes possible to obtain the stresses in crack geometries in the form of integral representations which are very hard to evaluate numerically for general conditions. Under such circumstances one often resorts to an asymptotic evaluation of the stress integrals in the region around the crack tip. Since our present calculations do permit the evaluation of the stresses by the series representation it will be useful to examine the range of validity of such an asymptotic expansion. While this comparison can also be performed for the better known crack solutions it turns out that such a comparison sheds further light on the nature of the stress field near the crack tip.

2. 1 Statement of the Mathematical Problem

The coordinate system appropriate for this geometry is shown in fig. 22. As in the case of a central crack in a large sheet there is only one characteristic length, namely the strip width. For convenience we take the half width therefore as unity.

Since we are considering a two dimensional elasticity problem, it proves convenient to make use of the Airy stress function $\phi(x,y)$, defined through the differential relations

$$\frac{\partial^2 \phi}{\partial x^2} = \sigma_y$$

$$\frac{\partial^2 \phi}{\partial y^2} = \sigma_x$$

(2.1)

$$\frac{\partial^2 \phi}{\partial x \partial y} = -\tau_{xy}.$$

The problem reduces then to that of integrating the partial differential equation

$$\nabla^4 \phi(x, y) = \frac{\partial^4 \phi}{\partial x^4} + 2 \frac{\partial^4 \phi}{\partial x^2 \partial y^2} + \frac{\partial^4 \phi}{\partial y^4} = 0 \quad (2.2)$$

subject to the appropriate boundary conditions; in the further investigation of this problem we shall restrict ourselves to conditions of plane stress.

Because of the symmetry of the geometry and boundary loads with respect to the x axis we need concern ourselves only with the domain $0 \leq y \leq 1$; in this case the boundary conditions are stated as: at $y = 0$

$$\tau_{xy}(x, 0) = 0 \quad -\infty \leq x \leq \infty$$

$$\sigma_y(x, 0) = 0 \quad x < 0 \quad (2.3a)$$

$$v(x, 0) = 0 \quad x \geq 0$$

and at the upper boundary where $y = 1$

$$v(x, 1) = 1 \quad (2.3b)$$

$$\tau_{xy}(x, 1) = 0$$

We shall use the superposition property of solutions in linear elasticity theory and regard the solution of the problem as resulting from the addition of the stress field

$$\begin{aligned}
 \sigma_y(x, y) &= E & \nu(x, y) &= y \\
 \sigma_x(x, y) &= 0 & u(x, y) &= -\nu x \\
 \tau_{xy}(x, y) &= 0
 \end{aligned}
 \tag{2.4}$$

where ν = Poisson's ratio, E = Young's modulus, and the stress field arising from the boundary conditions

$$\begin{aligned}
 \tau_{xy}(x, 0) &= 0 & -\infty < x < \infty & & \nu(x, 1) &= 0 & -\infty < x < \infty \\
 \sigma_y(x, 0) &= P = -E & x < 0 & & \tau_{xy}(x, 1) &= 0 & -\infty < x < \infty \\
 \nu(x, 0) &= 0 & x \geq 0 & & & &
 \end{aligned}
 \tag{2.5}$$

It is interesting to note in passing that the boundary conditions 2. 3 give also rise to the stress field in an infinite sheet containing an infinite number of parallel cracks (cf. fig. 23) which has been strained normal to the crack lines. This fact may be used to calculate the interaction energies of closely spaced parallel cracks as has been done approximately for the case of shear loading by Koiter (54).

2. 2 Solution

Assuming proper functional behavior for the Airy stress function $\phi(x, y)$ we shall perform a Fourier transformation on the stress function $\phi(x, y)$ with respect to x in the form

$$\bar{\phi}(\omega, \gamma) = \int_{-\infty}^{\infty} \phi(x, \gamma) e^{i\omega x} dx \quad (2.6)$$

the inverse being given by

$$\phi(x, \gamma) = \frac{1}{2\pi} \int_{\gamma} \bar{\phi}(\omega, \gamma) e^{-i\omega x} d\omega ; \quad (2.7)$$

ω is allowed to be complex valued and γ denotes a suitable contour for the inversion integral. Transforming the biharmonic field equation 2. 2 in this manner yields an ordinary fourth order differential equation

$$\frac{d^4 \bar{\phi}(\omega, \gamma)}{d\gamma^4} - 2\omega^2 \frac{d^2 \bar{\phi}(\omega, \gamma)}{d\gamma^2} + \omega^4 \bar{\phi}(\omega, \gamma) = 0 \quad (2.8)$$

with the solution

$$\begin{aligned} \bar{\phi}(\omega, \gamma) = & \alpha_1(\omega) \sinh \omega \gamma + \alpha_2(\omega) \cosh \omega \gamma \\ & + \alpha_3(\omega) \gamma \sinh \omega \gamma + \alpha_4(\omega) \gamma \cosh \omega \gamma . \end{aligned} \quad (2.9)$$

Similarly the transformed boundary conditions 2. 5, become

$$\overline{\tau}_{xy}(\omega, 1) = 0 \quad (2.10a)$$

$$\overline{v}(\omega, 1) = 0 \quad (2.10b)$$

$$\overline{\tau}_{xy}(\omega, 0) = 0 \quad (2.10c)$$

$$\sigma^- \equiv \int_{-\infty}^0 \sigma_y(x, y) e^{i\omega x} dx = \frac{P}{i\omega} \quad (2.10d)$$

$$\gamma^+ \equiv \int_0^{\infty} v(x, y) e^{i\omega x} dx = 0 \quad (2.10e)$$

Conditions 2.10d and 2.10e are the result of writing the appropriate functions in the form

$$f(x, 0) = f^-(x, 0) + f^+(x, 0)$$

where

$$\begin{aligned} f^{1-}(x, 0) &= f(x, 0) & x < 0 \\ &= 0 & x > 0 \\ f^{1+}(x, 0) &= f(x, 0) & x > 0 \\ &= 0 & x < 0 \end{aligned} \quad (2.11)$$

leading to the Fourier transform

$$\overline{f}(\omega, 0) = \int_{-\infty}^{\infty} f(x, 0) e^{i\omega x} dx = \int_{-\infty}^0 f^{1-}(x, 0) e^{i\omega x} dx + \int_0^{\infty} f^{1+}(x, 0) e^{i\omega x} dx \quad (2.12a)$$

or, with the definitions

$$f^-(\omega, 0) \equiv \int_{-\infty}^0 f^{1-}(x, 0) e^{i\omega x} dx \quad (2.12b)$$

$$f^+(\omega, 0) \equiv \int_0^{\infty} f^{1+}(x, 0) e^{i\omega x} dx$$

to

$$\bar{f}(\omega, 0) = f^-(\omega, 0) + f^+(\omega, 0). \quad (2.12c)$$

The constants of integration a_1 in the stress function ϕ , equation 2. 9, must be determined by the boundary conditions 2. 10; the relations 2. 10a-c readily determine three of them in terms of the fourth. One thus deduces that

$$\bar{v}(\omega, 0) = -2\omega a_1(\omega) \quad (2.13a)$$

$$\bar{\sigma}_y(\omega, 0) = 2\omega F(\omega) a_1(\omega) \quad (2.13b)$$

with

$$F(\omega) = \frac{\omega}{4} \frac{\sinh 2\omega + 2\omega}{\sinh^2 \omega}$$

Using the relations 2. 12a and 2. 12c this yields

$$v^+(\omega, 0) + v^-(\omega, 0) = -2\omega a_1(\omega) \quad (2.14a)$$

$$\sigma^+(\omega, 0) + \sigma^-(\omega, 0) = 2\omega F(\omega) a_1(\omega) \quad (2.14b)$$

which under consideration of the boundary conditions 2. 10d and 2. 10e results in

$$\sigma^+ + \frac{P}{i\omega} = -F(\omega) v^- \quad (2.15)$$

after elimination of $a_1(\omega)$.

The solution of the problem is given if \bar{v}^+ or v^- is determined, for then $a_1(\omega)$ is determined from equations 2. 13a or 2. 13b and the stresses can be derived purely mechanically from the stress function $\phi(x, y)$, equation 2. 7.

Since the Wiener-Hopf equation 2. 15 itself does not determine \bar{v}^- or v^- uniquely, auxiliary conditions must be found in the analytical properties of the transforms \bar{v}^+ and v^- and in the behavior of their inverses as $x \rightarrow +\infty$ or $x \rightarrow -\infty$.

In order to recall briefly the pertinent properties of the Fourier transform let $\bar{f}(\omega)$ be the Fourier transform of $f(x)$ where

$$\begin{aligned} f(x) &= g(x) & x > 0 \\ &= 0 & x < 0 \end{aligned} \quad (2.16)$$

such that

$$\begin{aligned} \bar{f}(\omega) &= \int_{-\infty}^{\infty} f(x) e^{i\omega x} dx \\ &= \int_0^{\infty} \{g(x) e^{-\tau x}\} e^{i\alpha x} dx \end{aligned} \quad (2.17)$$

with $\omega = \alpha + i\tau$. If $g(x) < e^{-\tau^+ x}$ then

- 1) $\bar{f}(\omega)$ is a regular function of ω (has no singularities) in the half plane $\text{Im}(\omega) = \tau > \tau^+$, and
- 2) $\bar{f}(\omega) \rightarrow 0$ as $|\omega| \rightarrow \infty$ in the half plane $\tau > \tau^+$.

Therefore if \bar{v}^+ is the transform of

$$\begin{aligned} \sigma_Y^+(x, 0) &= \sigma_Y(x, 0) & x > 0 \\ &= 0 & x < 0 \end{aligned} \quad (2.18)$$

then σ^+ 1) is regular in an upper half plane $\tau > \tau^+$

and

2) goes to zero as $|\omega| \rightarrow \infty$ there.

Similarly σ^-

1) is regular in a lower half plane $\tau < \tau^-$ and

2) goes to zero there as $|\omega| \rightarrow \infty$.

Returning now to the Wiener-Hopf equation 2. 15 it follows from the conditions on σ^+ that $i\omega F\sigma^-$ is regular in an upper half plane although σ^- itself is regular in a lower half plane. Suppose the function $F(\omega)$ can be written as the product of two functions F^+ and F^- , i. e.

$$F = F^+ F^- \quad (2.19)$$

where F^+ is regular and an entire⁴ function in an upper half plane

and F^- is a regular and entire function in a lower half plane.

Then equation 2. 15 can be written as

$$\frac{i\omega\sigma^+ + P}{F^+} = -i\omega F^- \sigma^- \quad (2.20)$$

* It will be seen that if, e. g. F^- has zeros in a lower half plane then σ^- will have singularities there; this is not permitted.

from which one deduces that the lower half plane, where the left hand side is regular, overlaps with the upper half plane where the right hand side is regular: the left and right hand side of equation 2. 20 continue each other analytically through the strip $\tau^- < \tau < \tau^+$. Assuming that σ^+ and ν^- behave algebraically* as $|\omega| \rightarrow \infty$ in respective half planes it can be shown by using Weierstrass' factorization theorem that (see Appendix A)

$$F^-(\omega) = \prod_{n=1}^{\infty} \frac{(1 - \frac{\omega}{\omega_n})(1 - \frac{\omega}{\bar{\omega}_n})}{(1 - \frac{i\omega}{n\pi})^2} = F^+(-\omega) \quad (2.21)$$

where ω_n are the solutions of $\sinh 2\omega_n + 2\omega_n = 0$ located in the complex plane as shown in fig. 24 and $\bar{\omega}_n$ are their complex conjugates, and that

$$F^-(\omega) \rightarrow 1 \quad \omega \rightarrow 0$$

$$\rightarrow \frac{\Gamma^2(\frac{3}{4}) \prod_{n=1}^{\infty} \left\{ \frac{(4n-1)\pi}{4|\omega_n|} \right\}^2}{\sqrt{\pi e}} e^{i\frac{\pi}{4} \sqrt{\omega}} \quad (2.22)$$

$\omega \rightarrow \omega$ in $\tau^- < \tau < \tau^+$.

It follows from Louiville's theorem that the left and right hand sides of equation 2.20 are equal to a constant \mathcal{P} , denoting the pressure, in the strip $\tau^- < \tau < \tau^+$ and by analytic continuation

* This assumption is inferred from the expected behavior of the physical stresses. Since there exists a uniqueness theorem for problems in classical elasticity the assumption is subject to verification through examination of the final solution. The details of the verification, however, are simple and have been omitted.

$$\begin{aligned} P &= -i\omega F^- v^- \quad \text{in } \tau < \tau^+ \\ P &= \frac{i\omega \sigma^+ + P}{F^+} \quad \text{in } \tau > \tau^- . \end{aligned} \quad (2.23)$$

Consequently one derives from equation 2. 14a that

$$a_1(\omega) = -\frac{v^-}{2\omega} \quad (2.24)$$

or

$$a_1(\omega) = P \frac{\varphi(\omega)}{2i\omega^2} , \quad \varphi \equiv \frac{1}{F^-}$$

Having now determined the last of the integration parameters $a_1(\omega)$ the stresses can be written as

$$\begin{aligned} \sigma_y(x,y) &= \frac{P}{4\pi i} \int_y \left\{ \frac{\cosh \omega(1-y)}{\sinh \omega} + \omega y \frac{\sinh \omega(1-y)}{\sinh \omega} + \omega \frac{\cosh \omega y}{\sinh^2 \omega} \right\} \varphi(\omega) e^{-i\omega x} d\omega \\ \sigma_x(x,y) &= \frac{P}{4\pi i} \int_y \left\{ \frac{\cosh \omega(1-y)}{\sinh \omega} - \omega y \frac{\sinh \omega(1-y)}{\sinh \omega} - \omega \frac{\cosh \omega y}{\sinh^2 \omega} \right\} \varphi(\omega) e^{-i\omega x} d\omega \quad (2.25) \\ \tau_{xy}(x,y) &= \frac{P}{4\pi} \int_y \left\{ -\omega y \frac{\cosh \omega(1-y)}{\sinh \omega} + \omega \frac{\sinh \omega y}{\sinh^2 \omega} \right\} \varphi(\omega) e^{-i\omega x} d\omega \end{aligned}$$

and the displacements as

$$\begin{aligned} E v(x,y) &= -\frac{P}{4\pi i} \int_y \left\{ (1-\nu) \frac{\cosh \omega(1-y)}{\omega \sinh \omega} - (1+\nu) \left[y \frac{\sinh \omega(1-y)}{\sinh \omega} + \frac{\cosh \omega y}{\sinh^2 \omega} \right] \right\} \varphi(\omega) e^{-i\omega x} d\omega \\ E u(x,y) &= \frac{P}{4\pi} \int_y \left\{ 2 \frac{\sinh \omega(1-y)}{\omega \sinh \omega} + (1+\nu) \left[y \frac{\cosh \omega(1-y)}{\sinh \omega} - \frac{\sinh \omega y}{\sinh^2 \omega} \right] \right\} \varphi(\omega) e^{-i\omega x} d\omega , \end{aligned} \quad (2.26)$$

the contour of integration γ being placed as shown in fig. 24 to assure that $\sigma_v(x, 0) = 1$ for $x < 0$.

2.3 Evaluation of Stress and Displacement Integrals

As the integrands in the stress and displacement expressions, equations 2.25 and 2.26, are single valued functions of ω the integrals can be evaluated by summation of residues: closing the contour in the conventional way by an arc $\omega = Re^{i\theta}$ in the upper half plane for $x < 0$ and in the lower half plane for $x > 0$ (cf. fig. 24) it can be shown that the contribution from these arcs vanishes as $R \rightarrow \infty$. The evaluated series representations for the stresses and displacements are given in Appendix B.

It will be noticed upon cursory inspection of the stress representations that the normal stresses increase without bound as x and y approach zero. The behavior of the stresses in the vicinity of the crack tip can be obtained by asymptotic expansion of the integrals for small values of x and y . Consider for example the integral I in the stress expressions 2.25

$$I = \int_{\gamma^*} \frac{\cosh \omega(1-y)}{\sinh \omega} \varphi(\omega) e^{-i\omega x} d\omega. \quad (2.27)$$

Choose the contour γ^* as in fig. 25 and divide the range of integration into sections such that (cf. fig. 25)

$$I = \int_{-\infty}^W + \int_W^\epsilon + \int_{C_\epsilon} + \int_\epsilon^W + \int_W^\infty \quad (2.28)$$

C_ϵ denoting the integral along the semi circle with radius ϵ around the origin which is equal to $i\pi$ for $\epsilon \rightarrow 0$. The second and fourth integrals are computed as the sum

$$\begin{aligned}
 I_{2,4} &= \lim_{\epsilon \rightarrow 0} \int_{-W}^{-\epsilon} \frac{\cosh \omega(1-\gamma)}{\sinh \omega} \varphi(\omega) e^{-i\omega x} d\omega + \int_{\epsilon}^W \frac{\cosh \omega(1-\gamma)}{\sinh \omega} \varphi(\omega) e^{-i\omega x} d\omega \\
 &= \lim_{\epsilon \rightarrow 0} i \int_{\epsilon}^W 2 \operatorname{Im} \frac{\cosh \omega(1-\gamma)}{\sinh \omega} \varphi(\omega) e^{-i\omega x} d\omega
 \end{aligned} \tag{2.29}$$

under consideration of $\varphi(-\bar{\omega}) = \overline{\varphi(\omega)}$. The integral is bounded as ω is finite and $\varphi(\omega)$ is continuously finite and approaches unity as $\omega \rightarrow 0$. Finally the sum of the first and fifth integral is

$$\begin{aligned}
 I_{1,5} &= 2i \int_W^{\infty} \operatorname{Im} \frac{\cosh \omega(1-\gamma)}{\sinh \omega} \varphi(\omega) e^{-i\omega x} d\omega \\
 &\doteq 2i \int_W^{\infty} \operatorname{Im} \varphi(\omega) e^{-\omega(\gamma+ix)} d\omega
 \end{aligned} \tag{2.30}$$

if W is sufficiently large. By making the substitution

$$u = \omega(\gamma + ix) \tag{2.31}$$

the integral transforms into

$$I_{1,5} = 2i \operatorname{Im} \int_{W(\gamma+ix)}^{\infty} \varphi\left(\frac{u}{\gamma+ix}\right) e^{-u} \frac{du}{\gamma+ix} \tag{2.32}$$

which becomes

$$I_{1,5} = 2i \operatorname{Im} \frac{\Gamma\left(\frac{1}{2}\right) \varphi_{\infty}}{\sqrt{y+ix}} \quad (2.33)$$

as x and y tend to zero, since $(\alpha) \sim \varphi_{\infty}/\sqrt{\alpha}$ for $|\alpha| \rightarrow \infty$ as shown in Appendix A. If the remaining terms of the integrand are expanded in the same manner the stress expansions in the crack tip vicinity are given as functions of the radial variable $r = \sqrt{x^2+y^2}$ and the angular variable $\Theta = \arctan(x/y)$ by the relations

$$\sigma_y \sim E \frac{A}{\sqrt{r}} \left\{ \frac{1}{\sqrt{2}} \left[\sin \frac{\Theta}{2} + \cos \frac{\Theta}{2} \right] + \frac{\cos \Theta}{2\sqrt{2}} \left[\sin \frac{3\Theta}{2} + \cos \frac{3\Theta}{2} \right] \right\} + \dots$$

$$\sigma_x \sim E \frac{A}{\sqrt{r}} \left\{ \frac{1}{\sqrt{2}} \left[\sin \frac{\Theta}{2} + \cos \frac{\Theta}{2} \right] - \frac{\cos \Theta}{2\sqrt{2}} \left[\sin \frac{3\Theta}{2} + \cos \frac{3\Theta}{2} \right] \right\} + \dots \quad (2.34)$$

$$\tau_{xy} \sim E \frac{A}{\sqrt{r}} \left\{ \frac{\cos \Theta}{2\sqrt{2}} \left[\sin \frac{3\Theta}{2} - \cos \frac{3\Theta}{2} \right] \right\} + \dots$$

which agree with the functional variation given by Ang, Folias and Williams (74). The stress intensity factor is given by

$$A = \frac{\sqrt{e}}{2 \Gamma^2\left(\frac{3}{4}\right)} \prod_{n=1}^{\infty} \left\{ \frac{4|\omega_n|}{(4n-1)\pi} \right\}^2 = 0.650, \quad (2.35)$$

e being the base of the natural logarithm and $\Gamma(3/4)$ is the gamma function. Note that since ω_n is independent of the material properties the stress intensity factor and therefore the stress expansions are independent of the material properties.

For later reference it is convenient to deduce an expression for the radius of curvature of the deformed crack boundary at the origin. Using the expansions 2.34 the stress-strain equations can be integrated to yield the displacements. In particular, the displacement of the crack boundary normal to the crack axis is given by

$$v = 6(1-\nu) A V_{\infty} \sqrt{\frac{r}{b}} \quad (2.36)$$

where b is now the strip half width and V_{∞} the boundary displacement. From this relation the deformed radius of curvature ρ on the crack axis is readily determined as

$$\rho = \frac{1}{2} [6(1-\nu)A]^2 \frac{V_{\infty}^2}{b} . \quad (2.37)$$

2.4 Numerical Evaluation

Using the series expressions in Appendix B the stresses were calculated and are represented in fig. 26. The normalizing strain ϵ_{∞} is the uniform strain across the strip width far ahead of the crack. In fig. 27 a map of the maximum shear stress is compared with the map obtained stress optically, the qualitative agreement being very good. The dark areas around the crack tip are due to the

* See also reference 75.

interaction of the parallel light rays of the optical system and the surface deformation of the stress optic material, Thiokol Solithane rubber.

There are two features of the stress field which distinguish it from that in a large sheet with either a central or external double crack. First, the stresses approach the uniform conditions at the right and left of $x = 0$ faster than one might estimate from the stress field in the infinite sheet geometries (76). Second, close to the crack tip the maximum principal stress, the octahedral and maximum shear stress assume values near the crack axis which are smaller than their uniform values far ahead of the crack. This is not observed in the previously mentioned crack geometries and is a consequence of prescribing a constant displacement at the boundary rather than a constant stress.

While we are mainly interested in the application of this solution to elastomeric materials one should recall that for metallic materials the octahedral shear stress is associated with the phenomenon of yielding. One is therefore tempted to conjecture from the above observation that the amount of yield near the crack tip is smaller in a strip geometry than, for example, at the tip of a central crack in a large plate, provided crack length is equal to the strip width and the stress far away from the cracks is the same. This is of course only a possibility and depends actually on other geometric details as for example the thickness of the sheet material (77).

For the cracked strip the relatively fast decay of the stresses away from the crack tip should lead to a larger discrepancy between the exact stresses and the values calculated from the asymptotic expansion than for the central crack. This is indeed the case as demonstrated by the following calculations.

Singling out a point on the crack axis $y = 0$ at $x = 0.01$ for the purpose of comparison one finds from the series representations^{2.34} that

$$\begin{aligned}\sigma_y(0.01, 0) &= 4.11 \sigma_\infty \\ \sigma_x(0.01, 0) &= 3.49 \sigma_\infty\end{aligned}\tag{2.38}$$

where σ_∞ is the uniform stress far ahead of the crack. For the same point, represented by the cylindrical coordinates $\theta = \pi$ and $r = 0.01$, one obtains from the asymptotic expansions 2.34

$$\sigma_y(0.01, \pi/2) = \sigma_x(0.01, \pi/2) = 6.50 \sigma_\infty\tag{2.39}$$

which is on the order of 50 per cent larger than the values above. A more complete comparison for the normal stresses on the crack axis with the asymptotic expansion values is shown in fig. 28.

A similar calculation for the corresponding point near a central crack in a large plate gives the exact values

In order to permit a meaningful comparison of the asymptotic stress expansions 2.34 the stresses were calculated from the series expressions of Appendix B with an upper bound on the error of one per cent. Due to the crude method of bound estimation the error is probably better than prescribed.

$$\begin{aligned}\bar{\sigma}_y(0.01, 0) &= 7.11 \bar{\sigma}_\infty \\ \bar{\sigma}_x(0.01, 0) &= 6.11 \bar{\sigma}_\infty\end{aligned}\tag{2.40}$$

and the asymptotic approximations

$$\begin{aligned}\bar{\sigma}_y(0.01, 0) &= 8.05 \bar{\sigma}_\infty \\ \bar{\sigma}_x(0.01, 0) &= 7.05 \bar{\sigma}_\infty\end{aligned}\tag{2.41}$$

In this case the difference is therefore only of the order of 15 per cent. Because the stress intensity factors are not particularly different for the two geometries^{*} it appears that the main effect of the displacement boundary condition on the stress field near a large crack is felt in an increased localization of the stress concentration at the crack tip.

^{*} The intensity factor is equal to $\frac{1}{\sqrt{2}} = 0.707$ for the central crack in a plate.

B. EXPERIMENTAL ANALYSIS OF THE STRESSES IN A SLIT RUBBER SHEET

Problems in large deformation analysis are as yet restricted to a limited number of geometries and are soluble only for some simple boundary conditions. In most cases solutions obtain only when the displacements are known or known to be functions of one variable such as to permit easy satisfaction of the equilibrium equations. Unfortunately the problem of determining the stresses in the vicinity of a crack tip does not fall into this category and other means must be employed to determine the stress field.

Andrews (78) has performed a stress optic study of this problem. By employing an energy parameter for normalization of the coordinate along the crack axis he deduced the engineering stresses along that line to be of a form commensurate with infinitesimal elasticity. This energy parameter is predicted from infinitesimal theory to be proportional to the deformed crack tip radius, which is the locally governing characteristic length, near the crack tip. It is therefore natural to inquire whether the energy parameter merely accounts for the deformation of the coordinate system. In other words, if the stresses are related to the undeformed coordinates the special manipulation with a generally not easily defined parameter may be eliminated. The treatment of non-linear and large deformation analysis of cracks may thus be tied closer yet to classical elasticity analysis than was demonstrated by Andrews.

Because the propagation of cracks through viscoelastic rubbers requires the knowledge of the stress field on the path of crack propagation we are interested primarily in that domain. But because the method of data reduction involves the strain field measurements away from the crack axis we present the principal stresses in a strip parallel to the axis and ahead of the crack. The principal stresses are determined by measuring the strain field and by relating the strains to the stresses by means of a non-linear stress-strain relation.

2. 5 Large Deformation Stress Analysis

Unlike classical elasticity theory, large deformation analysis requires that the dependent quantities be related explicitly to either the undeformed or to the deformed coordinates. We shall use here the undeformed coordinates. This means that if a point $P(x, y)$ is carried by material deformation into a new point $\bar{P}(x, y)$ with respect to a stationary coordinate system then we shall relate the stresses at $\bar{P}(x, y)$ to the original point $P(x, y)$.

While the following calculations can be performed with equal ease for true stresses or engineering type stresses it turns out that the use of engineering stresses reduces the results to a form which is more readily identified with that obtained in an analysis of crack geometries by infinitesimal elasticity methods. We shall therefore employ engineering stresses in the following work.

We assume that the material stress-strain behavior is embodied in the neo-Hookean strain energy function W^* which we list again for reference as

$$W = \frac{E}{6} [\lambda_1^2 + \lambda_2^2 + \lambda_3^2 - 3] \quad (2.42)$$

along with the side condition (incompressibility)

$$\lambda_1 \lambda_2 \lambda_3 = 1. \quad (2.43)$$

The λ_i are the extension ratios in the directions of principal strains.

The principal engineering stresses are obtained from the strain energy density function 2.42 by performing a virtual variation of the energy function with respect to the extension ratios λ_i , subject to the incompressibility restriction 2.43. The details of this operation are given elsewhere (79). We list here simply the result as

$$\tau^i = \frac{E}{3} \left\{ \lambda_i - \frac{k}{\lambda_i} \right\}. \quad (2.44)$$

Here k is an unknown function of the coordinates which must be determined in general from the equilibrium equations and the boundary conditions. However, by using the thin sheet assumption that the stress through the thickness, τ^3 , is zero, k can be determined from equation 2.44 to be equal to $\frac{2}{\lambda_3}$ and we obtain thus for the principal engineering stresses

* For rubbers this strain energy function is reasonable up to extension ratios of $\lambda \approx 6$. For these tests the largest value of λ measured was 5.7.

$$\begin{aligned}
 \tau^1 &= \frac{E}{3} \left[\lambda_1 - \frac{\lambda_3^2}{\lambda_1} \right] \\
 \tau^2 &= \frac{E}{3} \left[\lambda_2 - \frac{\lambda_3^2}{\lambda_2} \right] \\
 \tau^3 &= 0.
 \end{aligned}
 \tag{2.45}$$

The stresses can thus be calculated if the stretch ratios λ_1 and λ_2 are known (λ_3 is then determined by the incompressibility condition 2.43). These we proceed to compute now from the measured displacement field.

A rectangular coordinate system inscribed upon the undeformed body deforms with it upon load application into a contoured network (cf fig. 29). Consider a small section of the deformed grid $A'D'C'D'$ as shown in fig. 30; if one assumes the displacements which produce this form expressible as a power series in the undeformed coordinates, in particular to be of the simple form

$$\begin{aligned}
 u(x,y) &= ax + bxy + cy \\
 v(x,y) &= \alpha x + \beta xy + \gamma y
 \end{aligned}
 \tag{2.46}$$

then the transformations for the deformed coordinates X , Y , and Z become

$$\begin{aligned}
 X &= (1+a)x + bxy + cy \\
 Y &= \alpha x + \beta xy + (1+\gamma)y \\
 Z &= \lambda(x,y) \cdot z.
 \end{aligned}
 \tag{2.47}$$

The following analysis is approximate inasmuch as the displacements 2.46 do not necessarily satisfy the equilibrium equations. However the reason for choosing this form is that the six constants are easily determined from the dimensions of the deformed quadrilateral, and neglecting satisfaction of the equilibrium equations amounts only to neglecting the curvature of the line segments bounding the element.

The components of the metric deformation tensor G^{ij} are defined as

$$G^{ij} = \frac{\partial X_i}{\partial x_k} \frac{\partial X_j}{\partial x_k} \quad (2.48)$$

with X_i and x_i denoting the three deformed and undeformed coordinates respectively, double subscripts implying summation; they are now readily calculated to be

$$\begin{aligned} G^{11} &= (1+a+b'y)^2 + (b'x+c)^2 \\ G^{12} &= (1+a+b'y)(\alpha+\beta'y) + (b'x+c)(\beta'x+1+\gamma) = G^{21} \\ G^{22} &= (\alpha+\beta'y)^2 + (\beta'x+1+\gamma)^2 \\ G^{33} &= \lambda^2(x,y) \\ G^{i3} &= G^{3i} = 0, \quad i = 1,2 \end{aligned} \quad (2.49)$$

where

$$\begin{aligned} b' &= b-a-c-1 \\ \beta' &= \beta-\alpha-\gamma-1. \end{aligned}$$

Upon rotation of coordinate axis to the principal strain axes the tensor G^{ij} becomes diagonal and is of the form

$$\text{Diagonal } G^{ij} = [\lambda_i^2] = \begin{bmatrix} \lambda_1^2 & 0 & 0 \\ 0 & \lambda_2^2 & 0 \\ 0 & 0 & \lambda_3^2 \end{bmatrix} \quad (2.50)$$

the stretch ratios λ_i being defined as

$$\begin{aligned} \lambda_1^2 &= G^{11} \cos^2 \theta + G^{22} \sin^2 \theta - G^{12} \sin 2\theta \\ \lambda_2^2 &= G^{11} \sin^2 \theta + G^{22} \cos^2 \theta + G^{12} \sin 2\theta \\ \lambda_3^2 &= \lambda^2(x, y) \end{aligned} \quad (2.51)$$

with $\tan 2\theta = 2G^{12} / (G^{11} - G^{22})$.

These stretch ratios are easily calculated once the displacement coefficients a, b, etc. have been determined experimentally.

2.6 Experimental Procedure

The geometry used for this study is shown in fig. 31. Loads were applied to the rubber sheet by displacing the clamped boundaries opposite to each other while keeping them parallel.

The grid shown in fig. 29 was imprinted onto a 0.01 inch thick natural rubber, commercially available Dental Dam rubber. The printing pattern consisted of a network of 0.003 inch wide grooves inscribed 0.005 inches deep into a smooth Lucite block. Upon filling the grooves with printer's ink the rubber could be

pressed against the Lucite pattern with a soft backing, causing the rubber to deform into the ink filled grooves^{*}. The printing was performed while the rubber was in a state of equi-biaxial stretch, the equi-biaxiality being controlled by deforming a square with sides of 1 inch into a larger square; the grid pattern was imprinted in the center of the large square. The grid spacing thus obtained was measured with a traveling microscope to be 0.006 inches.

After cutting the crack with a razor blade into the grid area the sheet was strained and the grid photographed under five diameter magnification. The resulting negative was further enlarged by projection onto a poster board where lines were drawn as best as possible through the somewhat diffuse grid lines. Any apparent unevenness in the grid map was removed by careful rechecking. The location of the grid points in the deformed state were then measured and the pertinent coefficients in the transformation equation 2.47 could be calculated.

In order to reduce the error incurred in producing the enlarged grid chart and in reading the grid point locations the data was subjected to a data smoothing operation which is described in reference 80.

2.7 Numerical Evaluation

The maximum and minimum principal engineering stresses were calculated from expressions 2.47 and 2.51 with the help of a

* This is the standard method of printing etchings and engravings.

digital computer and are shown in fig. 32 as functions of the undeformed coordinates; the strain in the relatively uniformly stressed section of the sheet specimen was $\epsilon_{\infty} = 19\%$ and the corresponding maximum principal stress was used for normalization in the figures.

As mentioned previously the behavior of the principal stresses on the crack axis is of special interest. Figure 33 shows a logarithmic plot of the maximum principal stress. Two observations are pertinent: Note first that due to the data smoothing process the experimental scatter is very limited; second, most of the points follow a straight line with slope $-1/2$. Expressed mathematically this relation states that the engineering stress, based on the undeformed cross-section, behaves as

$$\sigma_y(x, y=0) = \frac{0.5 \sigma_{\infty}}{\sqrt{\frac{x}{b} + 0.0025}} \quad (2.54)$$

b being the half width of the tensile specimen.

The small number 0.0025 appearing with x/b under the square root in equation 2.54 is of the form of an initial radius of curvature as already noted by Andrews. Although the initial radius of curvature as obtained with the razor blade was smaller than $0.0025 b = 0.0065$ inches, Andrews has noted the variation of this quantity with applied strain and attributed the change to local tearing. Apart from this small quantity the σ_y stress exhibits near the crack axis

essentially the same dependence on the x-coordinate as the asymptotic expansion of the infinitesimal elasticity solution 2. 34

$$\sigma_y \sim \frac{A \sqrt{\epsilon_\infty}}{\sqrt{x}} \quad (2. 55)$$

Note that the values of σ_y for $A = 0. 5$ are bounded by those of the asymptotic expansion and the values calculated from the series expressions of the infinitesimal elasticity analysis (cf. fig. 34). This close agreement of the classical elasticity calculation experimental results from a large deformation strain field is indeed surprising. Whereas classical elasticity theory is normally applied to strains on the order of at most one per cent the strains involved in the large deformation study were in excess of 500 per cent!

In order to demonstrate that this result is not accidental for the particular gross strain employed in the test measurements it would be necessary to repeat the same experimental procedure for different gross strains. In view of the laborious data reduction method we shall demonstrate only that the stress intensity factor A is approximately independent of the gross strain. This will be done by relating the intensity factor A and the gross strain to the radius of curvature of the crack boundary at the crack origin.

Recall that in the last chapter the deformed radius of curvature was obtained from classical elasticity considerations as, (2. 37),

$$\rho = \frac{1}{2} [6(1-\nu) A]^2 b \epsilon_\infty^2 \quad (2. 56)$$

where the strain ϵ_{∞} replaces the displacement of the strip boundary and b is the strip-half width. For a value of Poisson's ratio of $1/2$ (incompressible materials) the stress intensity factor is given in terms of measurable quantities as

$$A = \frac{1}{3} \sqrt{\frac{2P}{b \epsilon_{\infty}^2}} \quad (2.57)$$

The experimentally determined relation between p , A and ϵ_{∞} are shown in figs. 35 and 36. Due to the difficulty in measuring the radius of curvature at small strains the experimental scatter in fig. 36 is approximately ± 12 per cent. Nevertheless, it appears that the stress intensity factor is reasonably independent of the applied strain.

Although the agreement of infinitesimal elasticity and large deformation analysis is surprisingly good with respect to the maximum principal stress on the crack axis the classical elasticity solution is completely in error when one considers the minimum principal stress. As a result of applying the boundary conditions in the undeformed state the infinitesimal elasticity analysis predicts large values (mathematically infinite) for this stress at the tip of a sharp crack; but during the deformation process that boundary condition changes completely and requires that the minimum principal stress (the stress normal to the boundary) be zero. This fact is evident in the plot of the minimum principal stress in fig. 32.

Because the boundary conditions along the displaced edges of the strip geometry are not identical for the previous infinitesimal elasticity solution and the experimental test geometry a more detailed comparison between the results of the two analyses is not too meaningful. Nevertheless, it appears from the evidence presented here that the stresses not precisely at the crack tip in a rubber sheet under large strain can be calculated by using infinitesimal elasticity theory, within reasonable engineering error. Yet the inaccuracy is probably no larger than that encountered in using an asymptotic expansion instead of an exact representation within the framework of classical elasticity theory. Such an estimate applies of course only to stresses and related quantities which are not markedly influenced by a change in the boundary conditions during the deformation process.

C. CONCLUSION

The classical elasticity analysis of the cracked strip geometry has been found to apply approximately to a finite length crack in a strip if the crack length is larger than the strip width, While in the case of a crack far from a neighboring boundary the stresses at the crack tip are proportional to the square root of the crack length they are proportional to the square root of the distance from the boundary (parallel to it) if the distance to the boundary is smaller than the crack length (81). The present solution affords therefore an estimate of the boundary effect on the stresses near the crack tip.

The effect is primarily evident in an increased localization of the high stress values in the crack tip vicinity. Because this condition reduces the amount of energy stored near the crack tip, the possibility of initiating crack propagation should also be reduced the closer the crack lies to a rigid parallel boundary. The corresponding phenomenon for a crack perpendicular to a boundary can be inferred from the reduction of the stress intensity factors presented by Isida and Itagaki (82).

The effect of finite deformations on the stresses in the crack tip vicinity is surprisingly moderate. This result is attributed to the fact that the finite deformation analysis was formulated in terms of undeformed coordinates and engineering stresses which are germane to classical elasticity analysis.

Inasmuch as the stress field near the tip of a crack represents a rather extreme case in non-linear and finite deformation analysis, one would believe that other, less extreme deformation problems have solutions which are correspondingly similar to their classical elasticity counterparts. For instance, Blatz (83) has considered the problem of bending a rectangle into an annulus; even for the case of a square the stresses calculated from infinitesimal elasticity theory differed by only 30 per cent from those obtained by large deformation analysis.

This result should thus be of value in the development of approximate methods for the solution of problems within the scope of finite deformation theory.

REFERENCES

1. Rivlin, R. S. , Thomas, A. G. : Rupture of Rubber. I. Characteristic Energy for Tearing. *J. Pol. Sci. , Vol. 10, (1952), pp. 291-318.*
2. Thomas, A. G. : Rupture of Rubber. II. The Strain Concentration at an Incision, *J. Pol. Sci. , Vol. 18, (1955), pp. 177-188.*
3. Greensmith, H. W. , Thomas, A. G. : Rupture of Rubber. III. Determination of Tear Properties. *J. Pol. Sci. , Vol. 18, (1955), pp. 189-200.*
4. Greensmith, H. W. : Rupture of Rubber. IV. Tear Properties of Vulcanizates Containing Carbon Black. *J. Pol. Sci. , Vol. 21, (1956), pp. 175-187.*
5. Thomas, A. G. : Rupture of Rubber. V. Cut Growth in Natural Rubber Vulcanizates. *J. Pol. Sci. , Vol. 31, (1958), pp. 467-480.*
6. Thomas, A. G. : Rupture of Rubber. VI. Further Experiments on the Tear Criterion. *J. Appl. Pol. Sci. , Vol. 3, (1960), pp. 168-174.*
7. Greensmith, H. W. : Rupture of Rubber. VII. Effect of Rate of Extension in Tensile Tests. *J. Appl. Pol. Sci. , Vol. 3, (1960), pp. 175-182.*
8. Greensmith, H. W. : Rupture of Rubber. VIII. Comparison of Tear and Tensile Rupture Measurements. *J. Appl. Pol. Sci. , Vol. 3, (1960), pp. 183-193.*
9. Tobolsky, A. V. , Eyring, H. : Mechanical Properties of Polymeric Materials. *J. Chem. Phys. , Vol. 11, (1943), pp. 125-134.*
10. Bueche, F. : (1) Tensile Strength of Plastics above the Glass Temperature. *J. Appl. Phys. , Vol. 26, (1955), pp. 1133-1140.*
(2) Tensile Strength of Plastics below the Glass Temperature. *J. Appl. Phys. , Vol. 28, (1957), pp. 784-787.*
11. Alfrey, T. : Mechanical Behavior of High Polymers. Interscience Publishers, Inc. , New York (1948).
12. Ferry, J. D. : Viscoelastic Properties of Polymers, John Wiley and Sons, Inc., New York, (1961).

13. Tobolsky, A. V. : Properties and Structure of Polymers. John Wiley and Sons, Inc. , New York, (1960).
14. Bueche, F. : Physical Properties of Polymers. Interscience Publishers, New York, (1962).
15. Williams, M. L. , Blatz, P. J., Schapery, R. A. : Fundamental Studies Relating to Systems Analysis of Solid Propellants. GALCIT SM 61-5, California Institute of Technology, ASTIA No, AD 256 905 (February 1961).
16. Knauss, W. G. : On the Mechanical Properties of an H-C Rubber. GALCIT SM 63-1, California Institute of Technology, (January 1963).
17. Williams, M. L., Landel, R. F., Ferry, J. D.: The Temperature Dependence of Relaxation Mechanisms in Amorphous Polymers and Other Glassforming Liquids. J. Am. Chem. Soc. , Vol. 77, (1955), pp. 3701-3707.
18. Landel, R. F. , Stedry, P. J.: Stress as a Reduced Variable: Stress Relaxation of SB-R Rubber at Large Strains. J. Appl. Phys., Vol. 31 (1960), pp. 1885-1891.
19. Becker, G. W., Radernacher, H. J.,: Mechanical Behavior of High Polymers under Deformations of Different Time Function, Type and Magnitude. J. Pol. Sci. , Vol. 58, (1962), pp. 621-631.
20. Smith, T. L. : Stress-Strain-Time-Temperature Relationships for Polymers. Symposium on Stress-Strain-Time-Temperature Relationships in Materials. Published by the American Society for Testing and Materials, (1962), pp. 60-89.
21. Jones, J. W. : Personal Communications; See also: Fracture Mechanics of Solid Propellants, E. I, DuPont de Nemours and Co. Report No. E Lab. A-20, (1960), (Confidential Report).
22. Taylor, G. I. : The Mechanism of Plastic Deformation of Crystals. Proc. Roy. Soc, Series A, Vol. 145, (1934), pp. 362-404.
23. Orowan, E. : Zur Kristall Plastizitat. Teile I, II und III. Z. Phys., Vol. 89, (1934), pp. 605-659.
24. Polanyi, M. : Uber eine Art Gitterstörung, die einen Kristall plastisch machen konnte. Z. Phys. , Vol. 89, (1934), pp. 605-659.

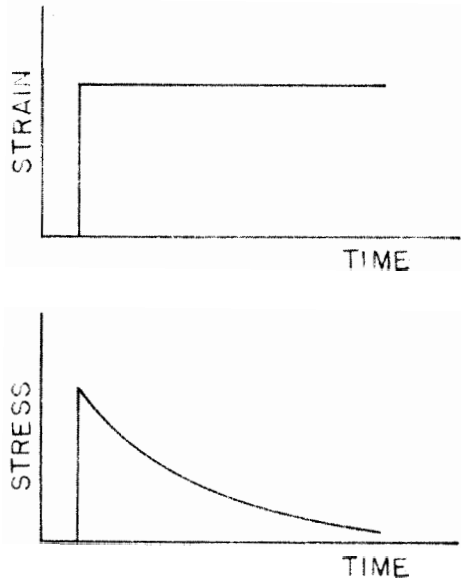
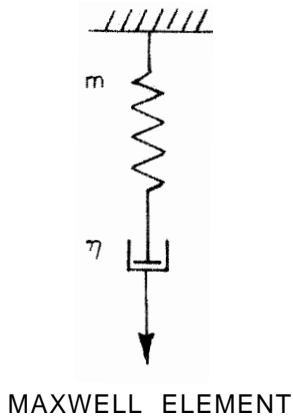
25. Flory, P. J. : Principles of Polymer Chemistry. Cornell University Press, Ithaca, New York, (1953).
26. Pauling, L. : The Nature of the Chemical Bond, Cornell University Press, Ithaca, New York, (1948).
27. Braden, M. , Gent, A. N. : The Attack of Ozone on Stretched Rubber Vulcanizates. I. The Rate of Cut Growth. II. Conditions for Cut Growth. *J. Appl. Pol. Sci.* , Vol. 3, (1960), pp. 90-106.
28. Tobolsky, A. V., Prettyman, I. B., Dillon, J. H. : Stress Relaxation of Natural and Synthetic Rubber Stocks. *J. Appl. Phys.*, Vol. 15, (1944), pp. 380-395.
29. Anthony, H. L. : Stress Corrosion of High Strength Steels and Alloys; Artificial Environment. Mellon Institute, Project 389-1, (1961).
30. Cup, C. R. : Gases in Metals. Progress in Metal Physics. Vol. 4. Edited by B. Chalmers, Pergamon Press, London, (1953).
31. Fujita, F. E. : Oxidation and Dislocation Mechanics in Fatigue Crack Formation. *Fracture of Solids*. Edited by D. C. Drucker and J. J. Gilman. John Wiley and Sons, (1963). (Proceedings of an International Conference of Fracture, August 1962).
32. Zener, C. : The Micro-Mechanism of Fracture. Fracturing of Metals. A Seminar on the Fracturing of Metals, Chicago (1947). American Society for Metals, (1948).
33. Stroh, A. N. : Crack Nucleation in Body-Centered Cubic Metals. *Fracture*. Edited by Averbach, Felbeck, Hahn and Thomas. The Technology Press of the Massachusetts Institute of Technology and John Wiley and Sons, New York, (1959).
34. Sookne, A. M. , and Harris, M. : (1) Controlled Molecular Length, *Textile Research*, Vol. 8, (1943), pp. 17-31. (2) Polymolecularity and Mechanical Properties of Cellulose Acetate. *Ind. Eng. Chem.*, Vol. 37, (1945), pp. 478-482.
35. Hsiao, C. C. , and Sauer, J. A. : On Crazeing of Linear High Polymers. *J. Appl. Phys.*, Vol. 21, (1950), pp. 1071-1083.
36. Schwarzl, F. , and Staverman, A. J. : Bruchspannung und Festigkeit von Hochpolymeren. *Die Physik der Hochpolymeren*. Edited by H. A. Stuart, Vol. IV, Springer Verlag, Berlin, (1956), pp. 165-214.

37. Weibull, W. : A Statistical Theory of the Strength of Materials. Proc. Roy. Swed. Inst. Engng. Res., (1939), No. 151.
38. Gumbel, E. J. : Statistical Theory of Extreme Values and Some Applications. U. S. Bureau of Standards, (1954), Applied Mathematics Series 33.
39. Proceedings of the Crack Propagation Symposium. College of Aeronautics, Cranfield, England, Vols. I and II, (September 1961).
40. Winne, D. H. , Wundt, B. M. : Application of the Griffith-Irwin Theory of Crack Propagation to the Bursting Behavior of Disks, Including Analytical and Experimental Studies. Trans. ASME, Vol. 80, (1958), pp. A 1643-1658.
41. Kies, J. A. , Sullivan, A. M. , Irwin, G. R. : Interpretation of Fracture Markings. J. Appl. Phys., (1950), Vol. 21, pp. 716-720.
42. Mason, D. : High Speed Fracture in Rubber. J. Appl. Phys. , Vol. 29, (1958), pp. 1146-1150.
43. Andrews, E. H. : Crack Propagation in a Strain-Crystallizing Elastomer. J. Appl. Phys., Vol, 33, (1961), pp. 542-548.
44. Williams, M. L. : The Fracture of Viscoelastic Material. Fracture of Solids. Edited by D. C. Drucker and J. J. Gilman, John Wiley and Sons, (1963).
45. Schapery, R. A. : Irreversible Thermodynamics and Variational Principles with Application to Viscoelasticity, Ph. D. Thesis, California Institute of Technology, (June 1962), ARL 62-418.
46. Fitzgerald, J. E. : A Biaxial Test for Solid Propellants. Bulletin of the 19th Meeting of JANAF Physical Properties Panel, (September 1960).
47. Scharma, M, G., Lim, C. K., and Sabrosky, R. : Mechanical Properties of Solid Propellants for Combined States of Stress at Various Temperatures. Annual Report (1962), Pennsylvania State University, Department of Engineering Mechanics.
48. Williams, M. L., Schapery, R. A., Zak, A. R., and Lindsey, G. H. : The Triaxial Tension Failure of Viscoelastic Materials. GALCIT SM 63-6, California Institute of Technology, (February 1963).

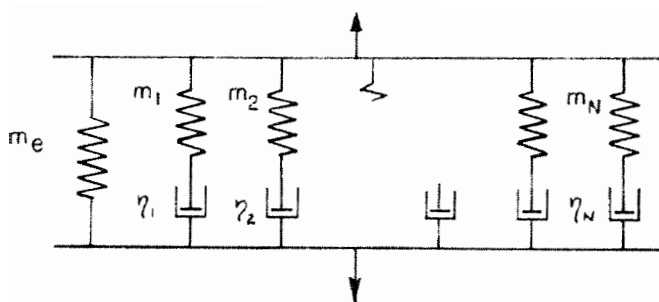
49. Ko, W. L. : Application of Finite Elastic Theory to the Behavior of Rubber-Like Materials. Ph, D. Thesis, California Institute of Technology, (June 1963).
50. Francis, E. C. , and Cantey, D. : Structural Integrity of Propellant Grains. Lockheed Propulsion Company Report No. 556-F, (January 1963), p. 3-43,
51. Griffith, A. A. : The Phenomena of Rupture and Flow in Solids. Phil. Trans. Roy, Soc. (London), Series A, Vol. 221, (1920), pp. 163-198.
52. Glasstone, S. , Laidler, K. J. , and Eyring, H. : The Theory of Rate Processes. McGraw-Hill, New York, (1941).
53. Swedlow, J. L. : Generalization of Griffith's Theory of Brittle Fracture. GALCIT SM 62-16, California Institute of Technology, (February 1962).
54. Koiter, W. T. : An Infinite Row of Parallel Cracks in an Infinite Elastic Sheet. Problems of Continuum Mechanics. Published by the Society for Industrial and Applied Mathematics, Philadelphia, Pennsylvania, (1961).
55. Knauss, W. G. : Failure of Polymeric Continua. GALCIT SM 62-28, California Institute of Technology, (July 1962).
56. Westergaard, H. M. : Bearing Pressures and Cracks. J. Appl. Mech. , Series A, Vol. 6, (1939), pp A 49-53.
57. Valluri, S. R. : A Unified Engineering Theory of High Stress Level Fatigue. Aerospace Engineering, Vol. 20, (1961), p. 18.
58. Valluri, S. R. : Some Recent Developments at GALCIT Concerning a Theory of Fatigue. To be published in Acta Metallurgica.
59. Miner, M. A. : Curnulative Damage in Fatigue, J. Appl. Mech. , Series A, Vol. 12, (1945), pp. 159-164.
60. Williams, M. L. : Mechanical Properties and the Design of Solid Propellant Motors. Progress in Astronautics and Rocketry. Vol. 1. Edited by M. Summerfield, Academic Press, New York, (1960).
61. Harstad, K. : An Experiment on the Curnulative Damage in a Viscoelastic Material. GALCIT CP 63-2, California Institute of Technology, (May 1963).

62. Tormey, J. F., and Britton, S. C. : Effect of Cyclic Loading on Solid Propellant Grain Structures. Presented at the Solid Propellant Rocket Society, Philadelphia, Pennsylvania, (January 1963). American Rocket Society.
63. Wintergerst, S.: Dynamisches Verhalten von Hart-PVC. Kunststoffe, Vol, 50, (1960), pp. 277-280.
64. Lindsey, G. H. : Rotating Beam Fatigue Test for Filled Elastomers, GALCIT CP 62-10, California Institute of Technology, (May 1962).
65. Kruse, R. B. : The Role of Broad-spectrum Mechanical Response Studies in Propellant Evaluation. 20th Meeting Bulletin of the JANAFAN Panel on Physical Properties of Solid Propellants, Vol. I, (November 1961).
66. Inglis, C. E.: Stresses in a Plate Due to the Presence of Cracks and Sharp Corners. Transactions of the Institute of Naval Architects (London), Vol. 60, (1913), pp. 219-230.
67. Griffith, A. A. : Stresses in a Plate Bounded by a Hyperbolic Cylinder. Reports and Memoranda, No. 1152 (M 55) Aeronautical Research Committee, Air Ministry, London, (January 1928).
68. Neuber, H. : Kerbspannungslehre. Springer Verlag, Berlin, (1937).
69. Schardin, H. : Velocity Effects in Fracture. Fracture. Edited by Averbach, Felbeck, Hahn and Thomas. The Technology Press of the Massachusetts Institute of Technology and John Wiley and Sons, New York, (1959).
70. Willmore, T. J. : The Distribution of Stress in the Neighborhood of a Crack. Quart. J. of Mech. and Appl. Math, , Vol. 2, (1949), pp. 53-63.
71. Wigglesworth, L. A. : Stress Distribution in a Notched Plate. Mathematika, Vol. 4, Part 1, (1957), pp. 76-96.
72. Isida, M. : On the Tension of a Semi-Infinite Plate with an Elliptic Hole. Report of the Faculty of Engineering. Tokushirna University, Vol. 5, No. 1, (1955).

73. Lowengrub, H. : Penny Shaped Crack in a Thick Plate. Crack Problems in the Mathematical Theory of Elasticity. I. Sneddon, North Carolina State College, Departments of Mathematics and Engineering Research, (1961).
74. Ang, D. D., Folias, E. S., and Williams, M. L. : The Effect of Initial Spherical Curvature on the Stresses Near a Crack Point. ARL Report 62-356, (May 1962).
75. Williams, M. L. : On the Stress Distribution at the Base of a Stationary Crack. *J. Appl. Mech.*, Vol. 24, (1957), pp. 109-114.
76. Swedlow, J. L. : On the Elastostatic Stresses in Cracked Plates. GALCIT SM 62-9, California Institute of Technology, (August 1962).
77. Liu, H. W. : Size Effects on Fatigue Crack Propagation. GALCIT SM 63-7, California Institute of Technology, (March 1963).
78. Andrews, E. H. : Stresses at a Crack in an Elastomer. *Proc. Phys. Soc.*, Vol. 77, (1961), pp. 483-499.
79. Green, A. E. , and Zerna, W. : Theoretical Elasticity. Clarendon Press, Oxford, (1960).
80. Milne, W. E. : Numerical Calculus. Princeton University Press, Princeton, New Jersey, (1949).
81. Knauss, W. G. : On the Effect of a Boundary on the Stresses in the Vicinity of a Crack. GALCIT SM 62-46, California Institute of Technology, (November 1962).
82. Isida, M. , and Itagaki, Y. : The Effect of Longitudinal Stiffeners in a Cracked Plate under Tension. The National Aeronautical Laboratory, Tokyo, Japan.
83. Blatz, P. J. : Personal Communication, California Institute of Technology, Pasadena, California (1962).
84. Noble, B. : Methods Based on the Wiener-Hopf Technique for the Solution of Partial Differential Equations. Pergamon Press, New York, (1958).

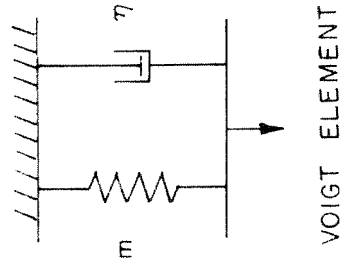
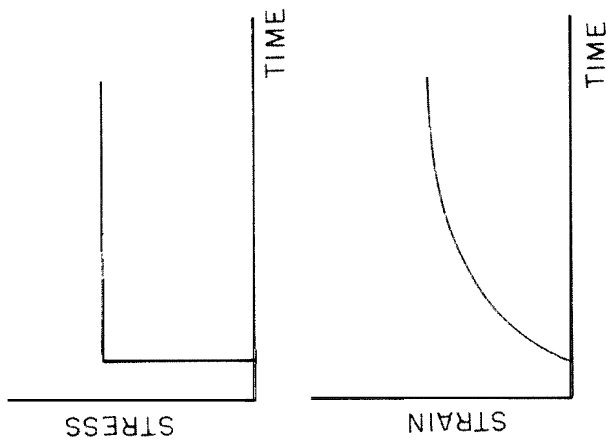
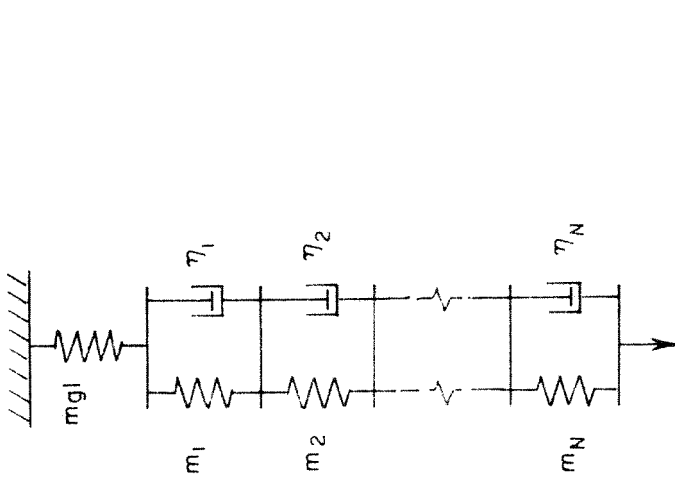


A. STRESS RESPONSE OF MAXWELL ELEMENT TO STEP STRAIN



B. GENERALIZED MAXWELL OR WIECHERT MODEL

FIG. 1 MAXWELL ELEMENT AND WIECHERT MODEL FOR REPRESENTATION OF VISCOELASTIC STRESS RELAXATION BEHAVIOR



a STRAIN RESPONSE OF VOIGT ELEMENT TO STEP STRESS b. GENERALIZED VOIGT OR KELVIN MODEL

FIG. 2 VOIGT ELEMENT AND KELVIN MODEL FOR REPRESENTATION OF VISCOELASTIC CREEP BEHAVIOR

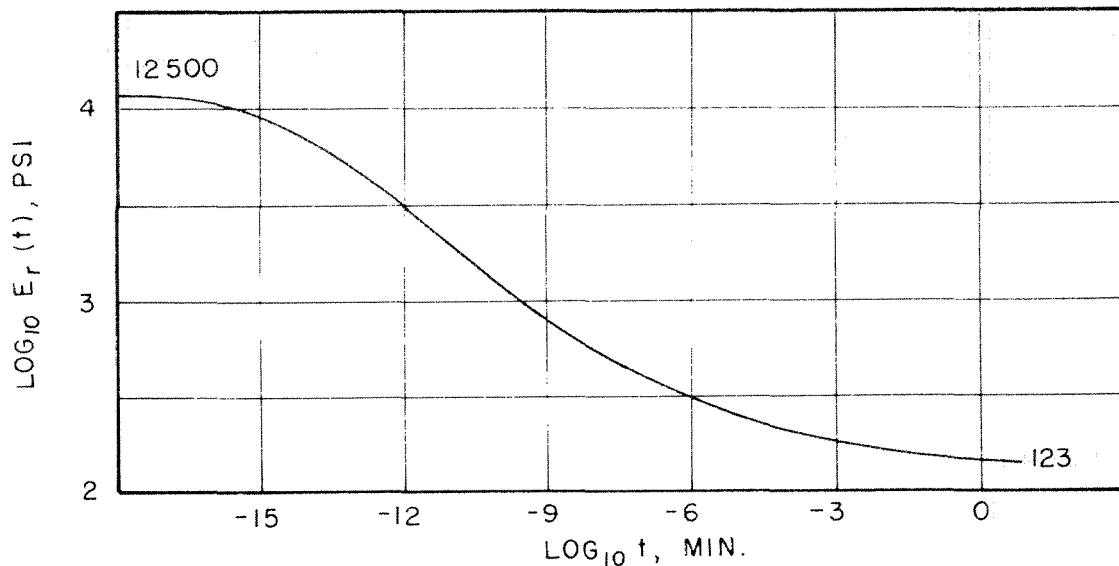


FIG. 3 RELAXATION MODULUS E_r AS A FUNCTION OF TIME FOR H-C RUBBER , TEMPERATURE = 22.5 ° C

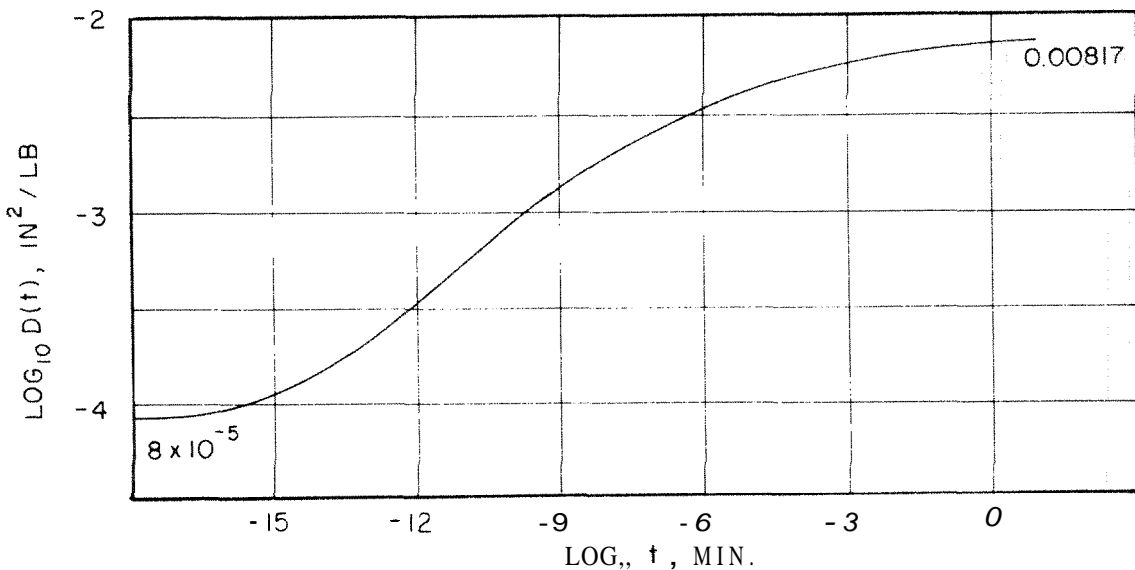


FIG 4 CREEP COMPLIANCE $G(t)$ AS A FUNCTION OF TIME FOR H - C RUBBER , TEMPERATURE = 22.5 ° C

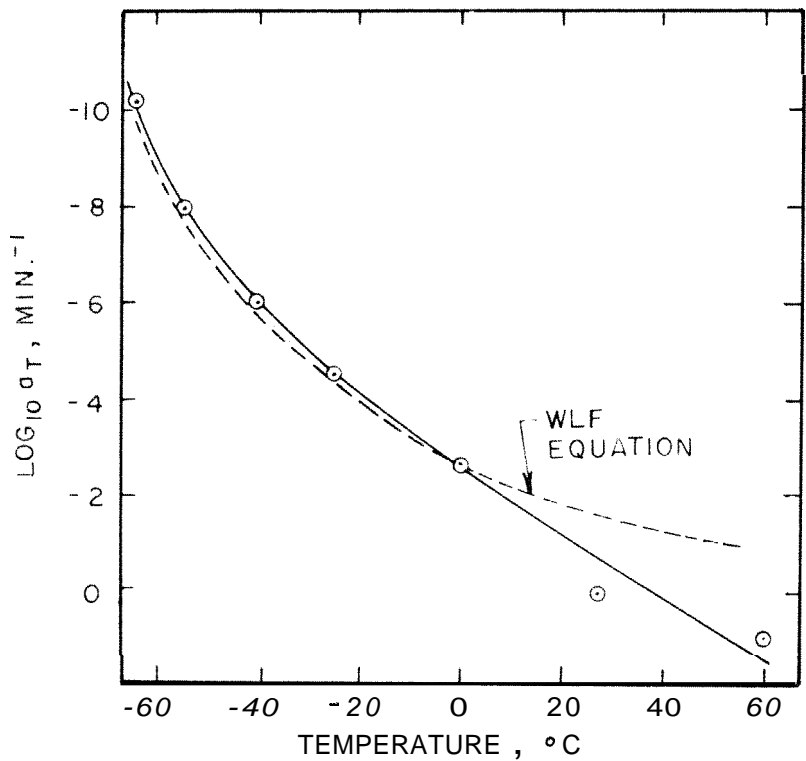


FIG. 5 TIME - TEMPERATURE SHIFT FACTOR FOR H-C RUBBER

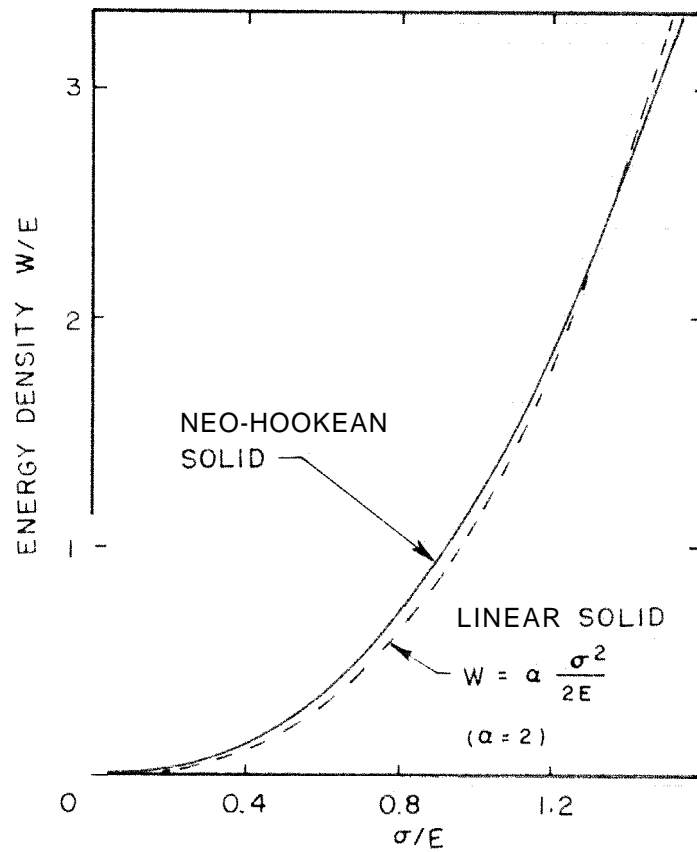


FIG 6 COMPARISON OF ENERGY DENSITY FUNCTION FOR NEO-HOOKEAN SOLID AND EQUIVALENT HOOKEAN SOLID

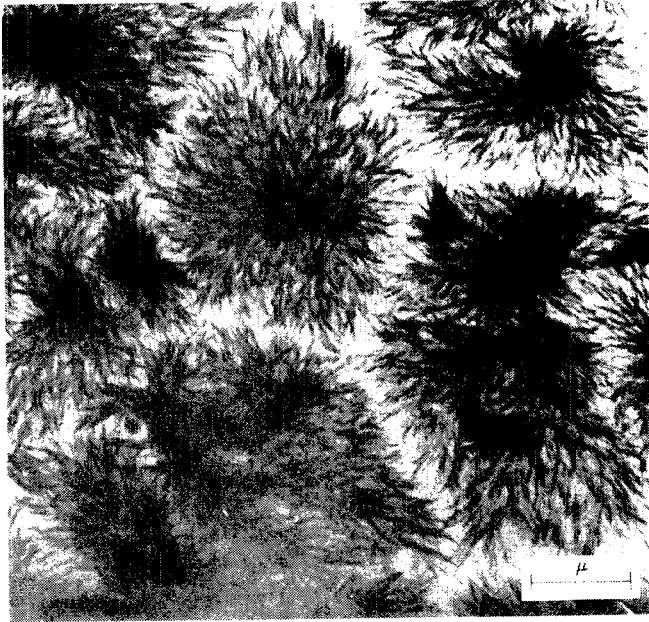


FIG.7 ELECTRON MICROGRAPH OF
A THIN FILM OF POLYETHYLENE
SHOWING FINE STRUCTURE
OF SPHERULITES

(REPRODUCED FROM REF. 13
WITH PERMISSION OF THE
AUTHOR)

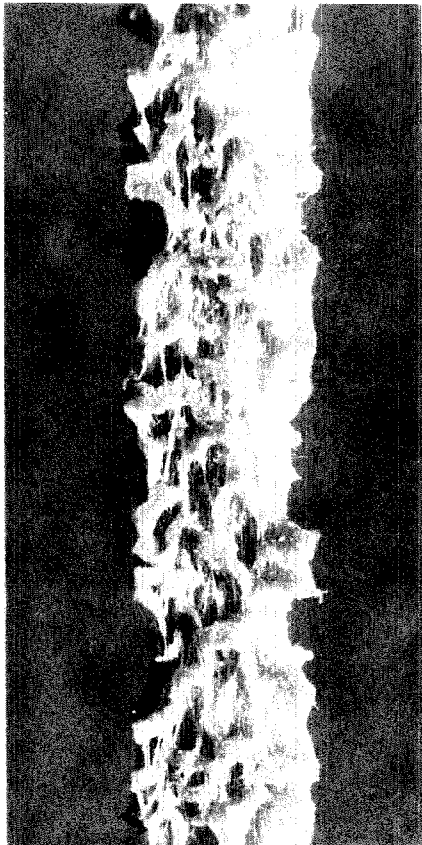
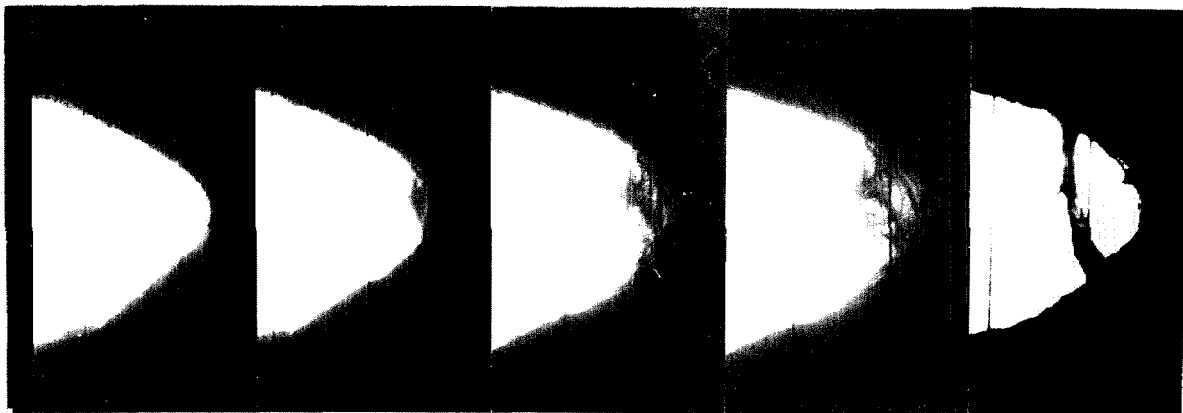


FIG.8 RUPTURE OF COMMERCIAL
RUBBER BAND.
THE BAND WAS UNDER 50%
CONSTANT STRAIN FOR THREE
MONTHS IN UNCONTROLLED
ROOM ATMOSPHERE



(5 X)

FIG. 9 CRACK TIP SEQUENCE SHOWING FIBROUS MATERIAL DETERIORATION IN H-C RUBBER. (TIME INTERVAL ~ 15 SEC, VELOCITY ~ 0.1 IN./MIN.)

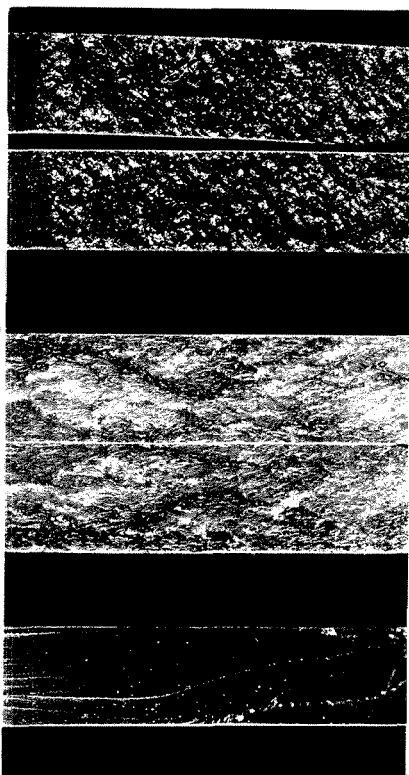


FIG. 10 FRACTURE SURFACES RESULTING FROM VARIOUS SPEEDS OF CRACK PROPAGATION. APPROXIMATE SPEEDS ARE, FROM TOP TO BOTTOM 10^{-3} IN./MIN. 1 IN./MIN. 10^3 IN./MIN.

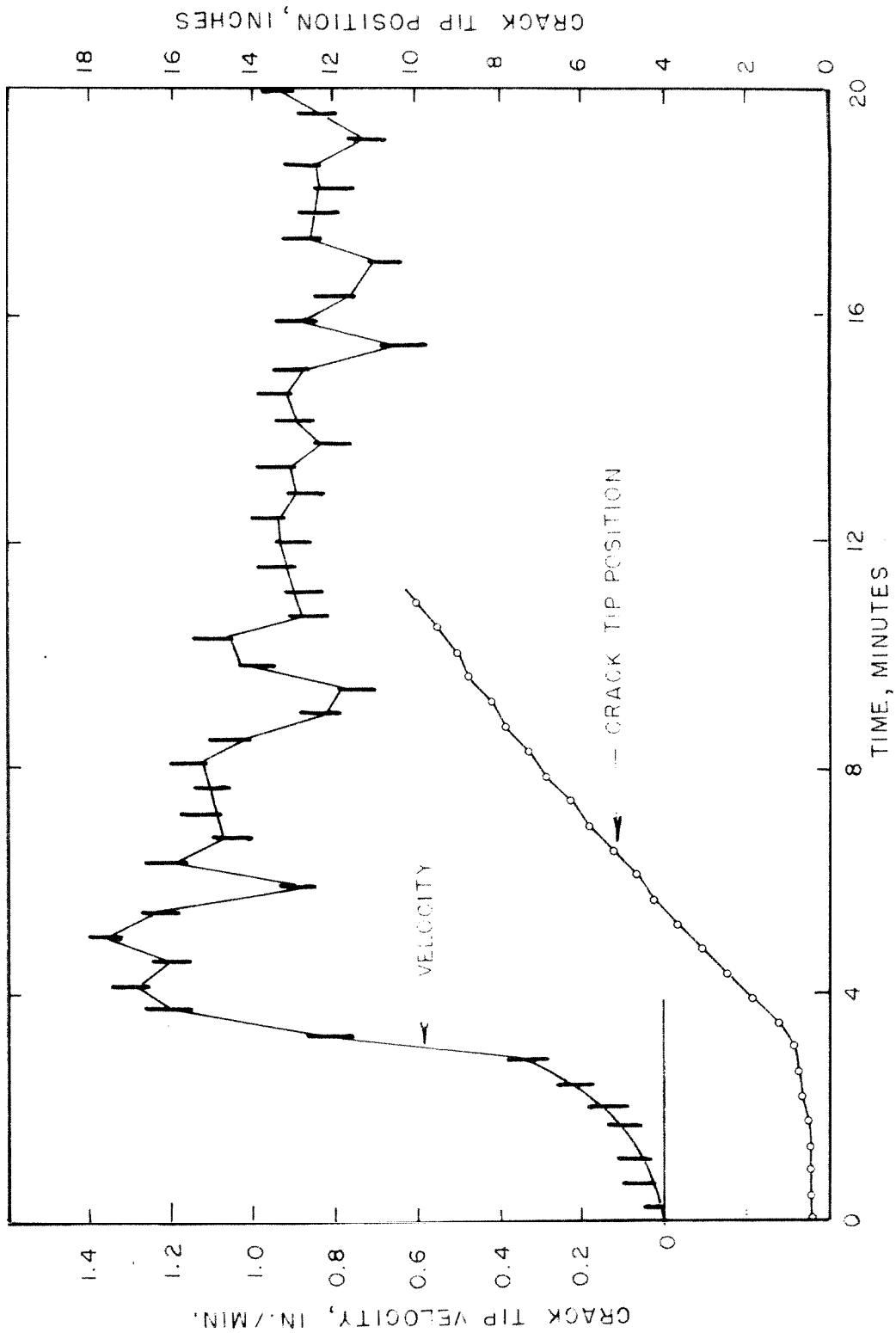


FIG. II EXPERIMENTAL HISTORY OF CRACK TIP POSITION AND VELOCITY. INSTANTANEOUS VELOCITY IS TAKEN AS AVERAGE VELOCITY BETWEEN NEIGHBORING CRACK TIP POSITIONS

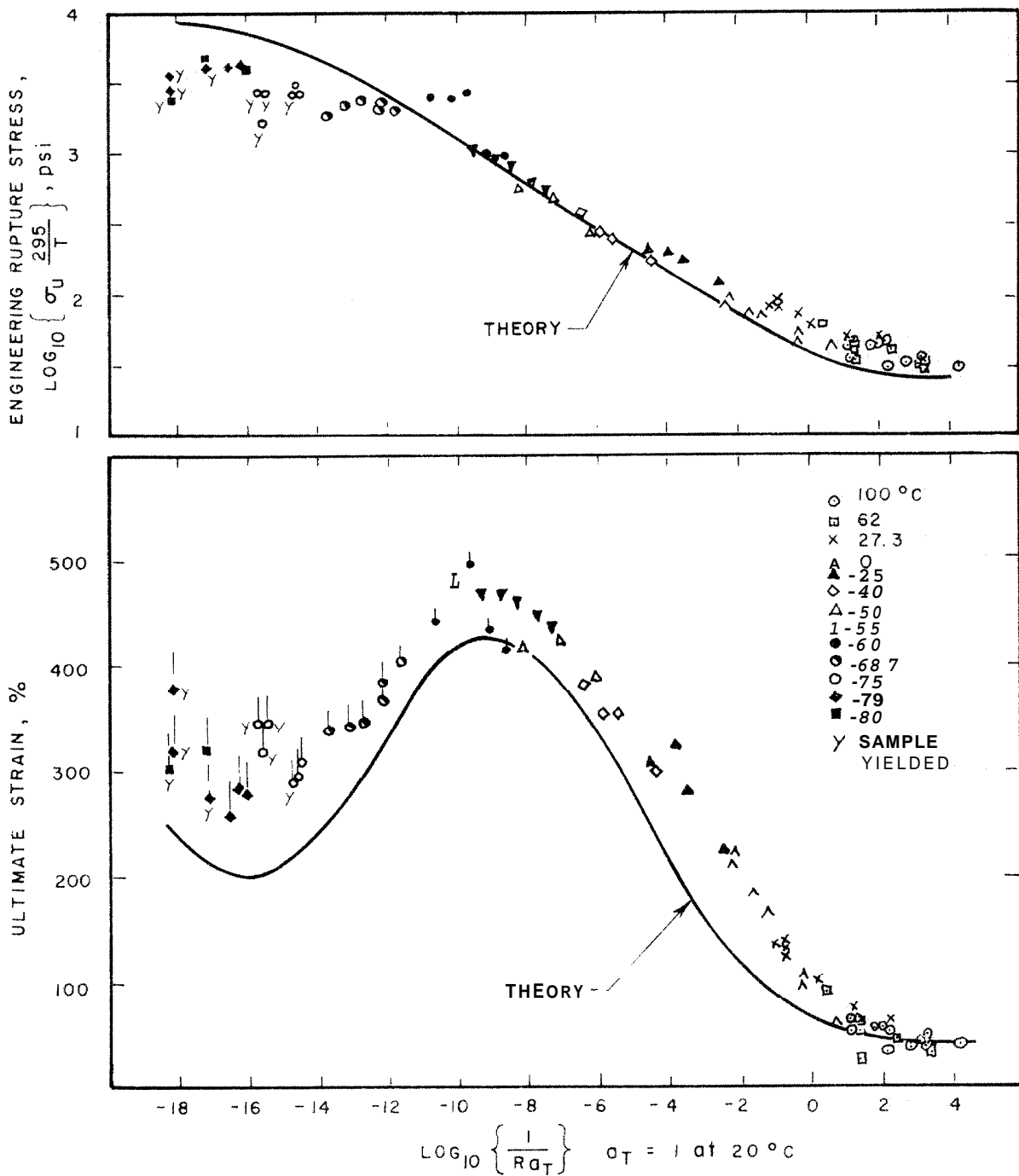


FIG 12 ULTIMATE STRESS AND STRAIN IN AN ISOTHERMAL, UNIAXIAL CONSTANT STRAIN RATE TEST AS A FUNCTION OF TEMPERATURE REDUCED STRAIN RATE

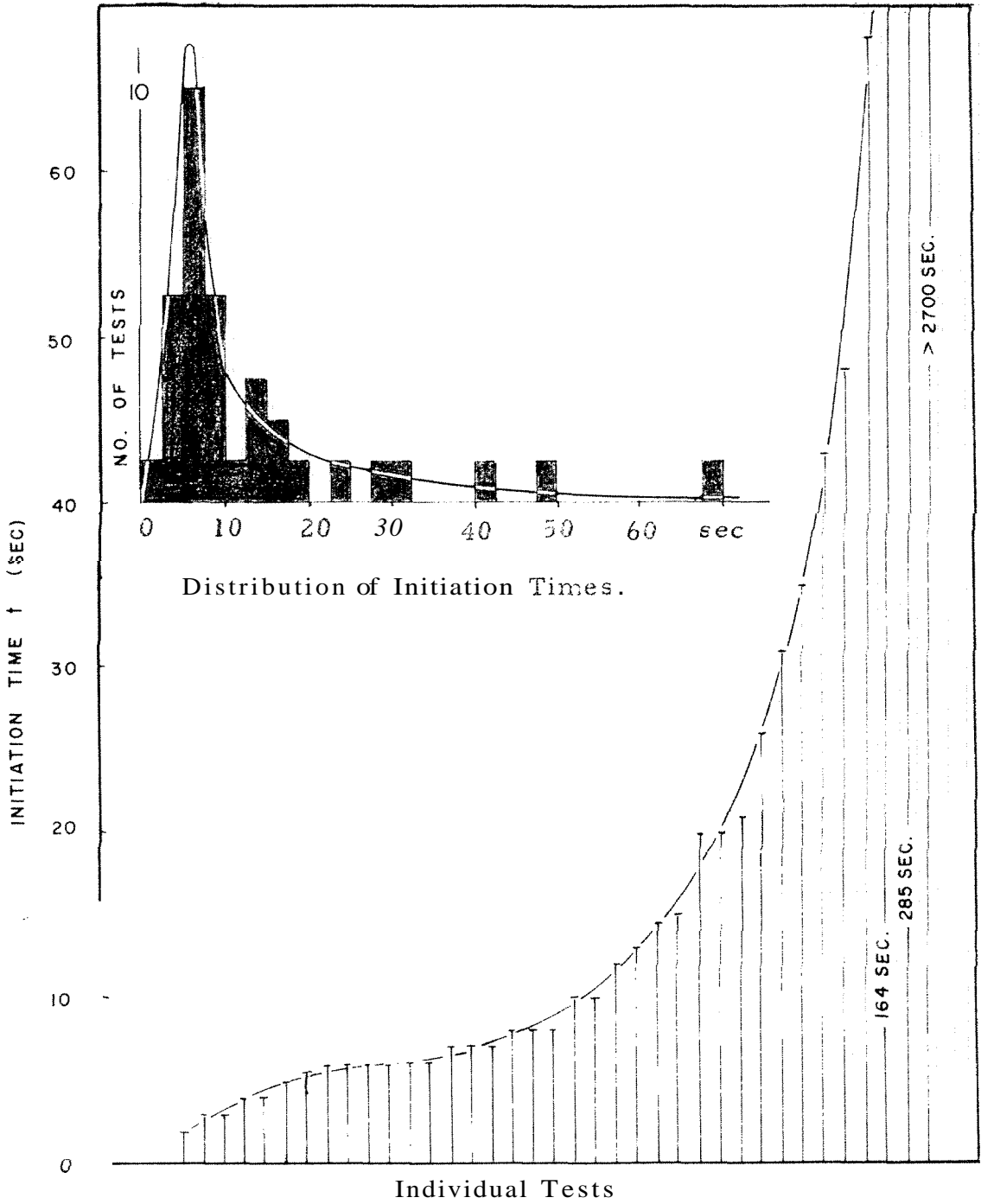


FIG. 13 EXPERIMENTAL CRACK INITIATION TIME AT A GROSS STRAIN OF 38%, INDICATING STATISTICAL NATURE OF FAILURE PROPERTIES

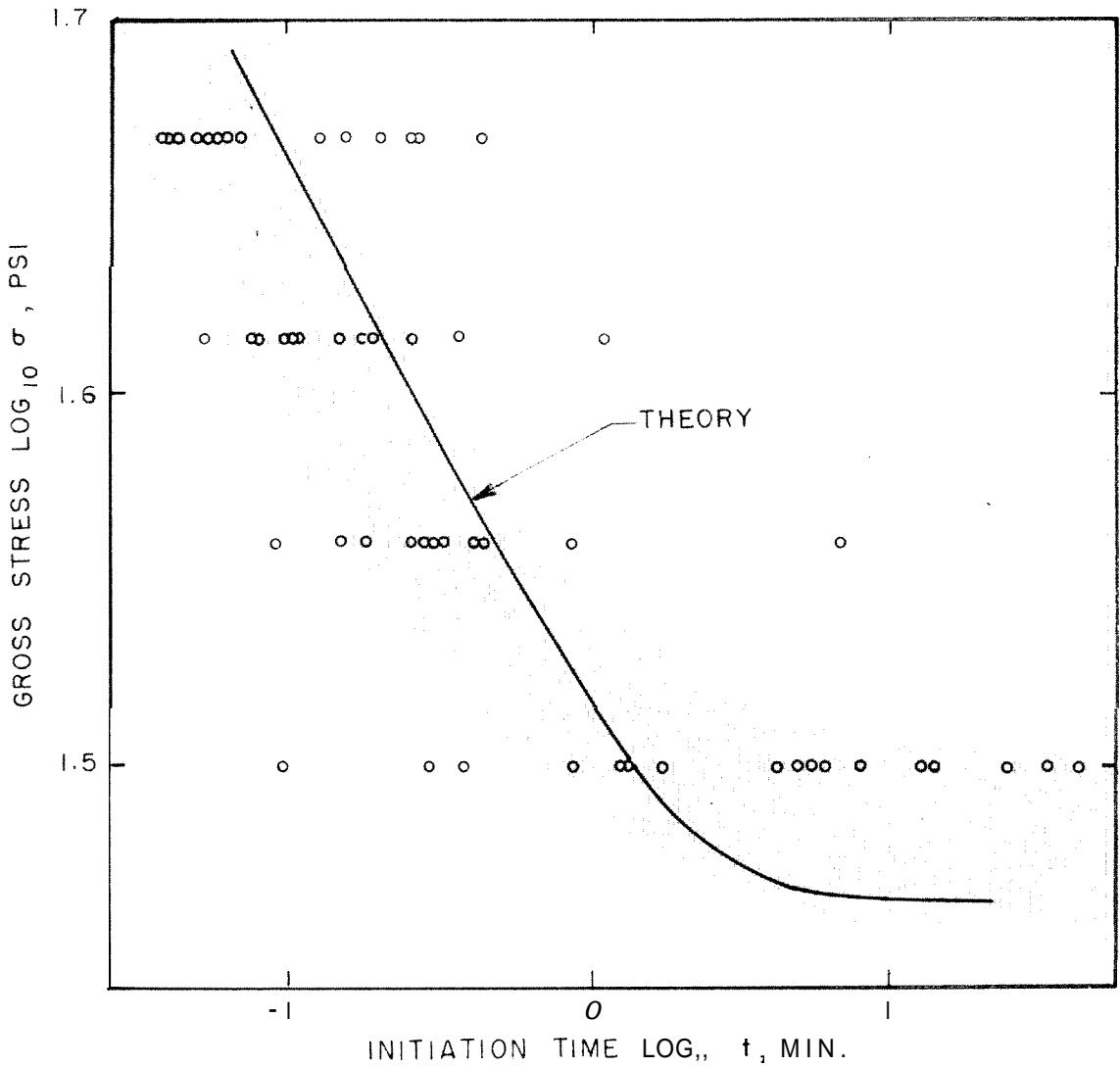
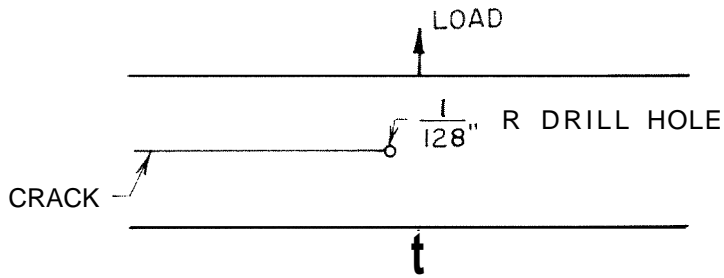
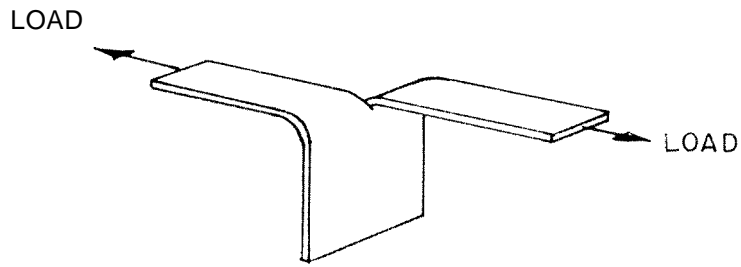


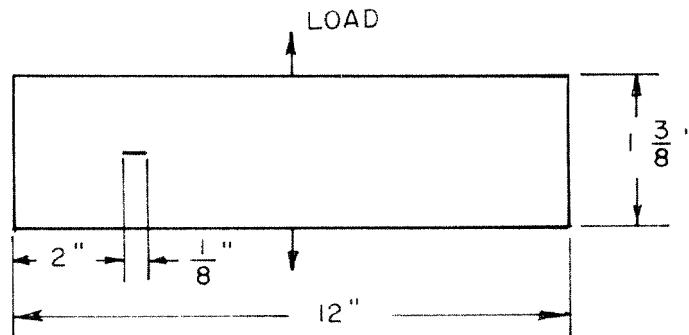
FIG 14 COMPARISON OF EXPERIMENTAL AND THEORETICAL RELATION BETWEEN CRACK INITIATION TIME AND GROSS STRESS ON TEST SPECIMEN



A. GEOMETRY OF CRACK INITIATION TIME TEST



B. TEAR TEST SPECIMEN



C. INITIAL GEOMETRY IN CRACK ACCELERATION STUDY

FIG. 15 TEST GEOMETRIES USED IN RUPTURE STUDIES

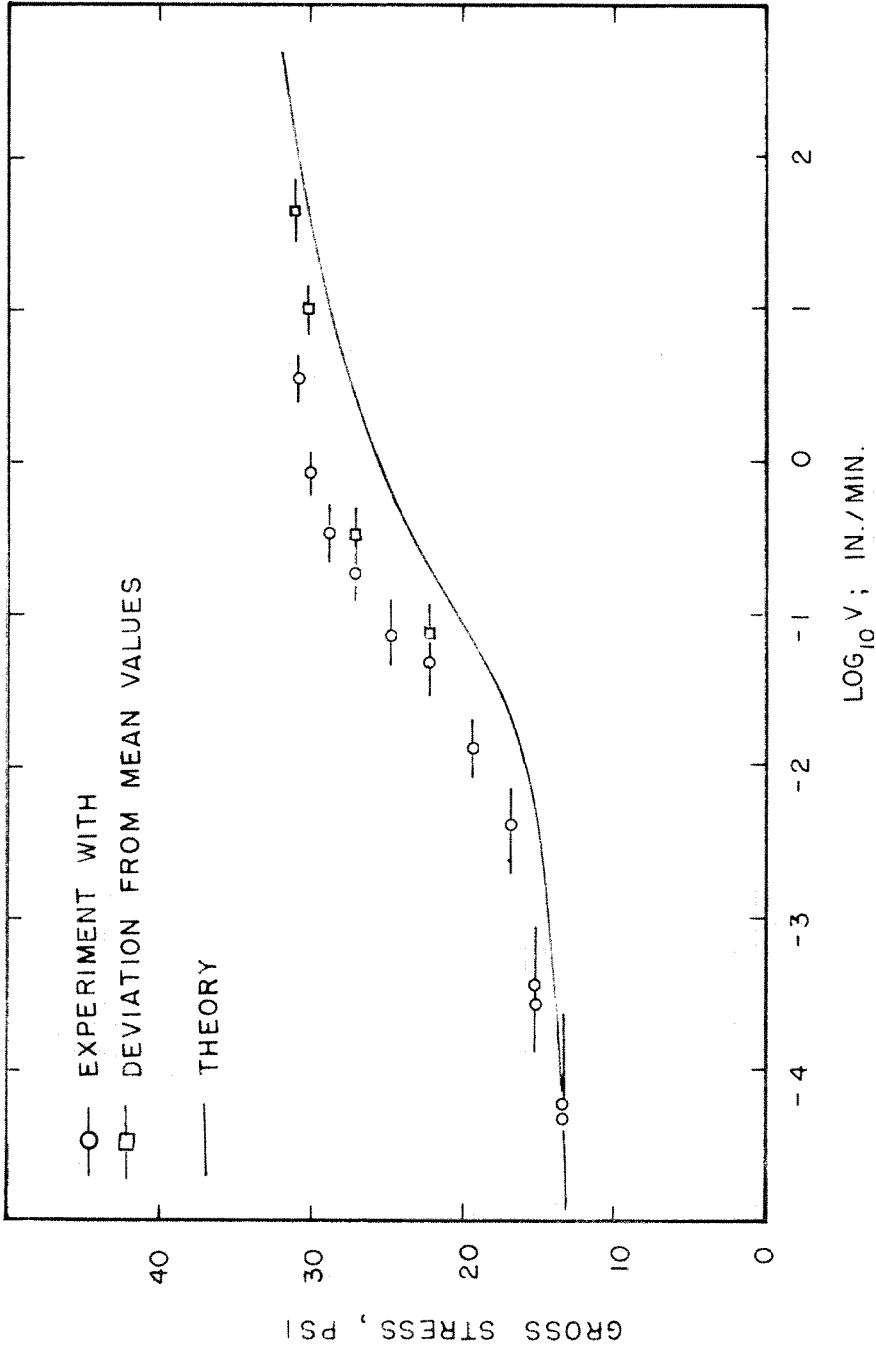


FIG 16 CRACK PROPAGATION SPEEDS VS. GROSS STRESS IN BIAXIAL STRIP.
CIRCLES AND SQUARES DENOTE MATERIAL OF SAME FORMULATION
BUT PREPARED SEPARATELY

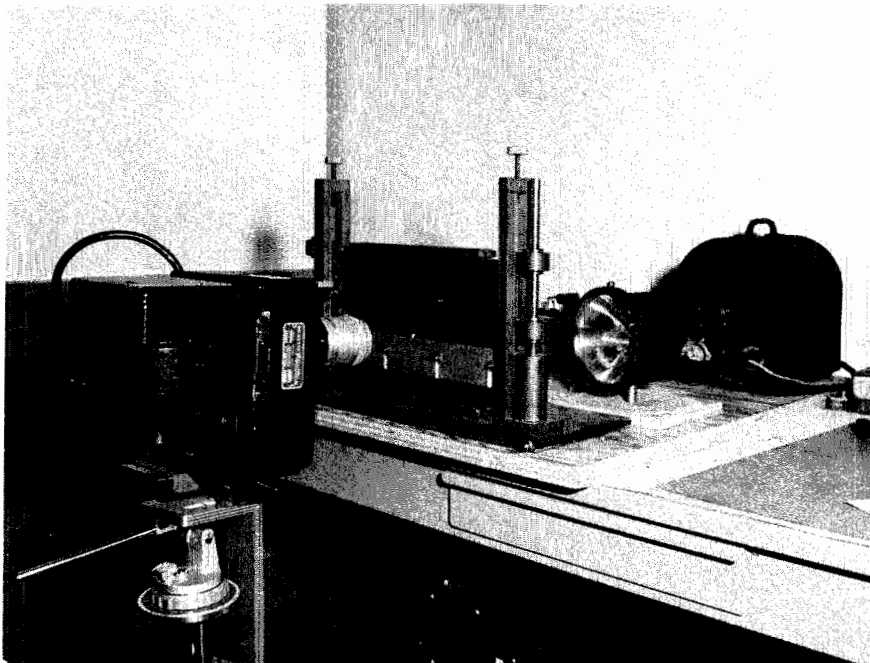
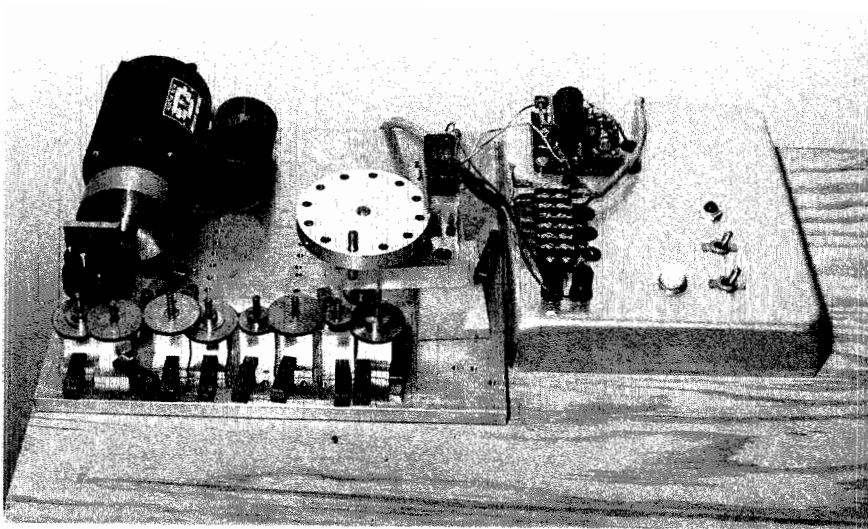


FIG. 17 EQUIPMENT USED IN CRACK PROPAGATION STUDIES

ABOVE : VARIABLE SPEED TIMING DEVICE
BELOW: STRAINING MECHANISM WITH SLIT STRIP SPECIMEN IN PLACE AND AUTOMATED CAMERA -FLASH COMBINATION

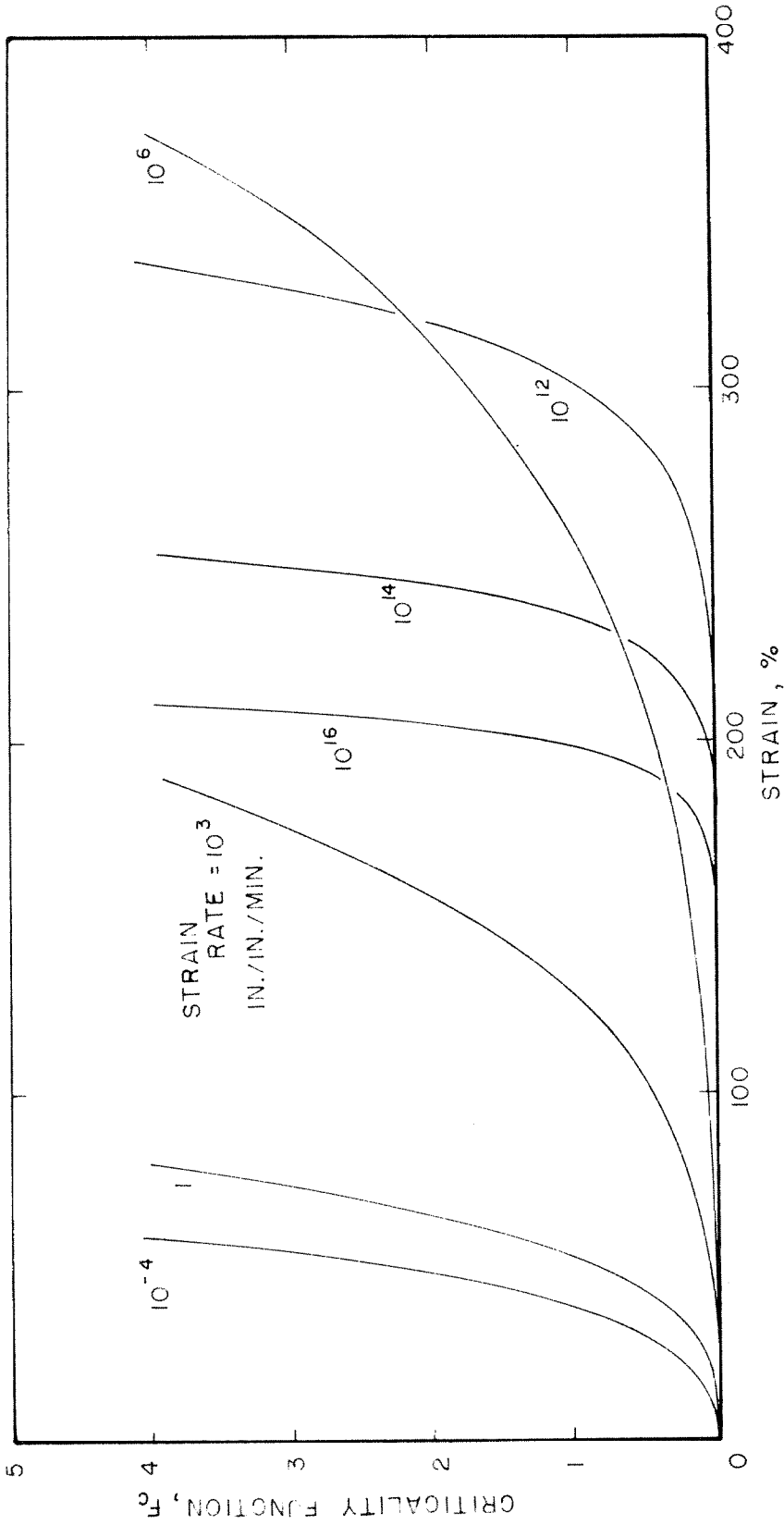


FIG. 18 CRITICALITY FUNCTION F_c VS. STRAIN IN CONSTANT STRAIN RATE TESTS, INDICATING RATE OF DAMAGE ACCUMULATION AS A FUNCTION OF STRAIN RATE

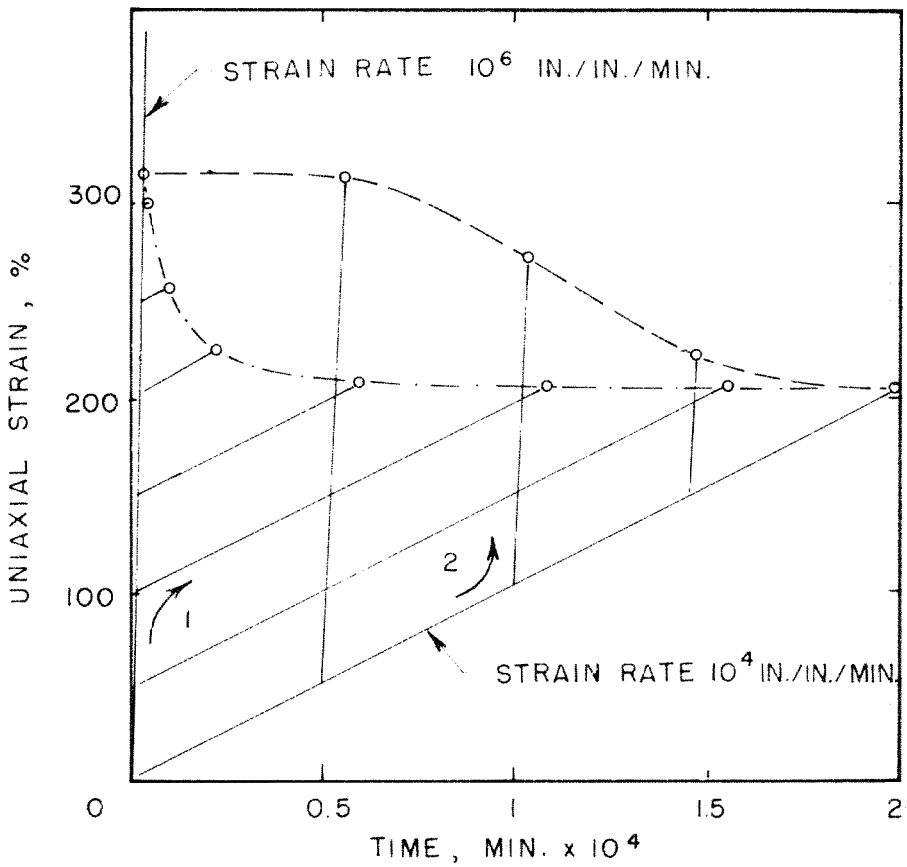


FIG 19 THEORETICALLY PREDICTED EFFECT OF LOADING HISTORY UPON ULTIMATE STRAIN IN A DUAL STRAIN RATE TEST

LINES DENOTE VARIOUS TRACES OF STRAIN. EXAMPLE ;
ARROW ① INDICATES SEQUENCE OF HIGH STRAIN RATE TO STRAIN OF 100 % , THEN LOW STRAIN RATE TO RUPTURE.
ARROW ② INDICATES REVERSED SEQUENCE. CIRCLES DENOTE CALCULATED RUPTURE POINTS

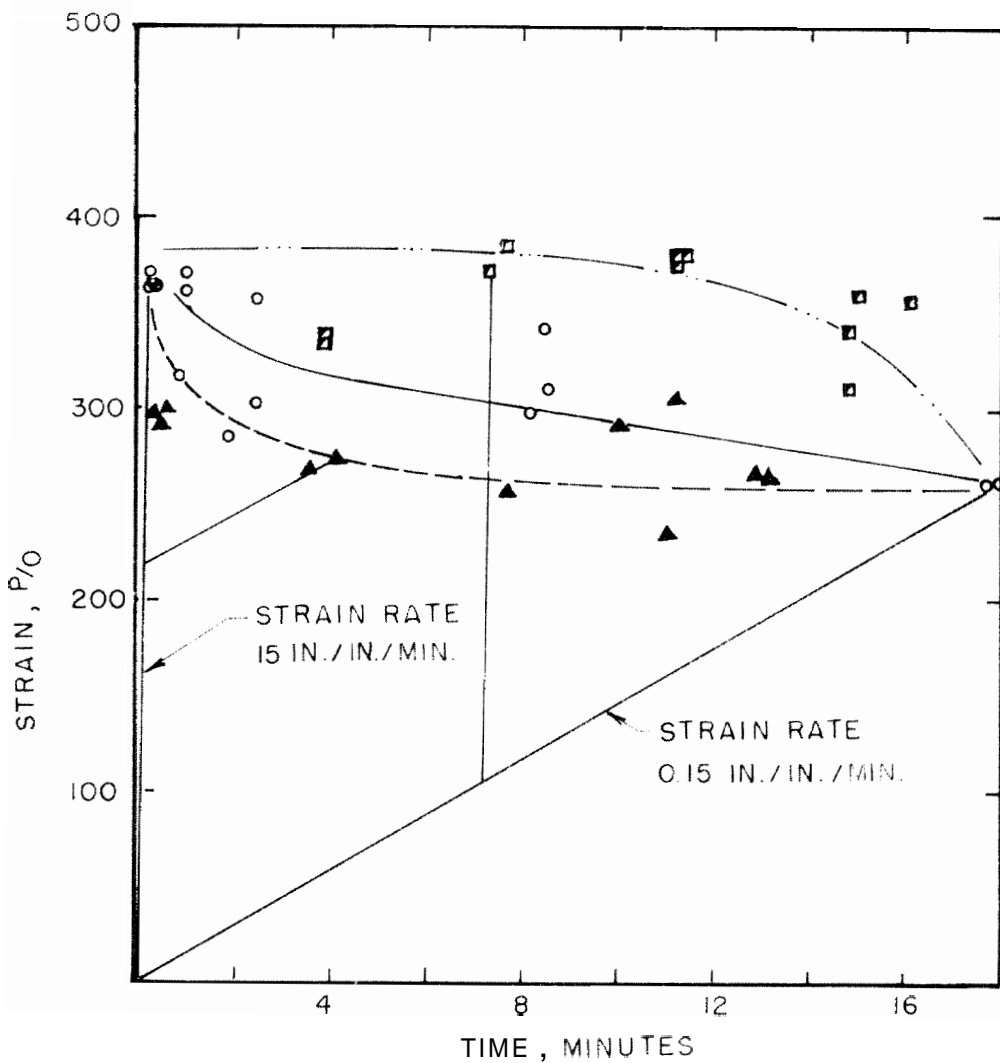


FIG. 20 EXPERIMENTALLY DETERMINED ULTIMATE STRAIN IN DUAL RATE TEST

- CONSTANT STRAIN RATE ———
- ▲ FAST - SLOW SEQUENCE
- SLOW - FAST SEQUENCE - - - - -

H-C RUBBER FORMULATION DIFFERENT
FROM PREVIOUS EXPERIMENTAL MATERIAL
TEMP = 20°C

(COURTESY K HARSTAD; REF. 61)

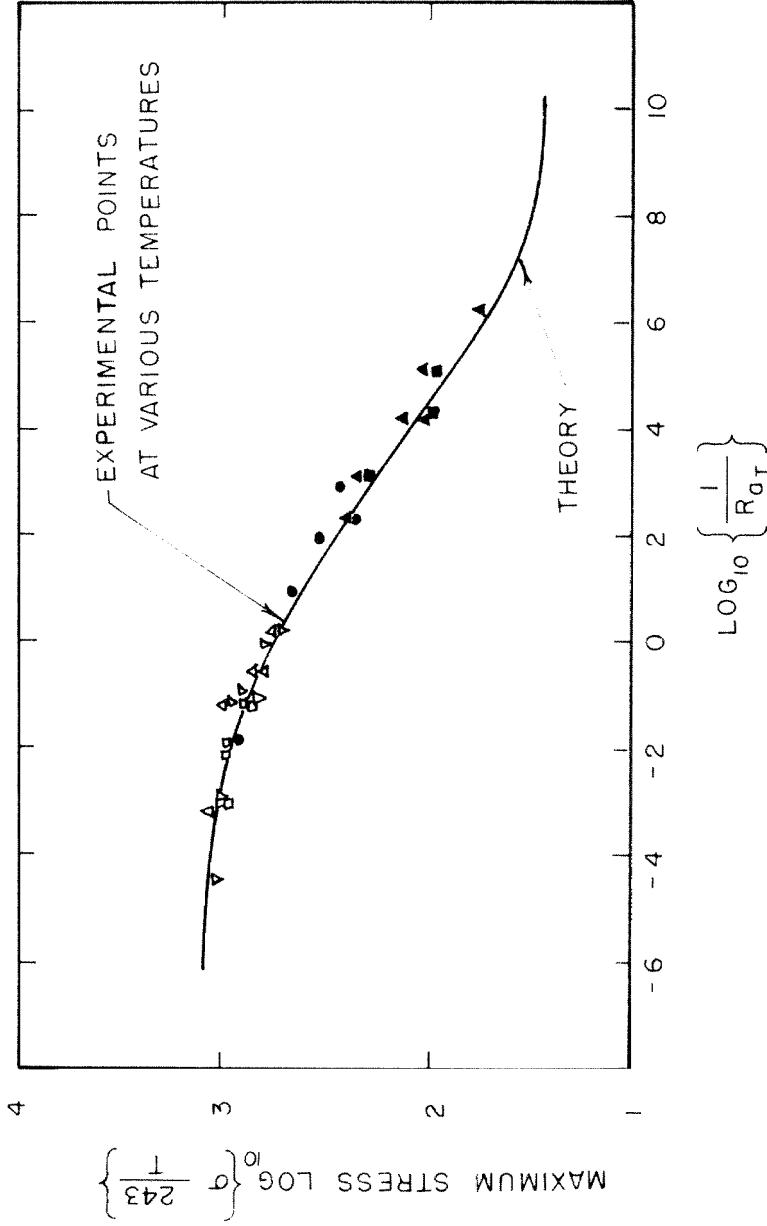


FIG. 21 VARIATION OF ULTIMATE TENSILE STRESS IN A CONSTANT STRAIN RATE TEST AS A FUNCTION OF STRAIN RATE (DATA TAKEN FROM REF.65)

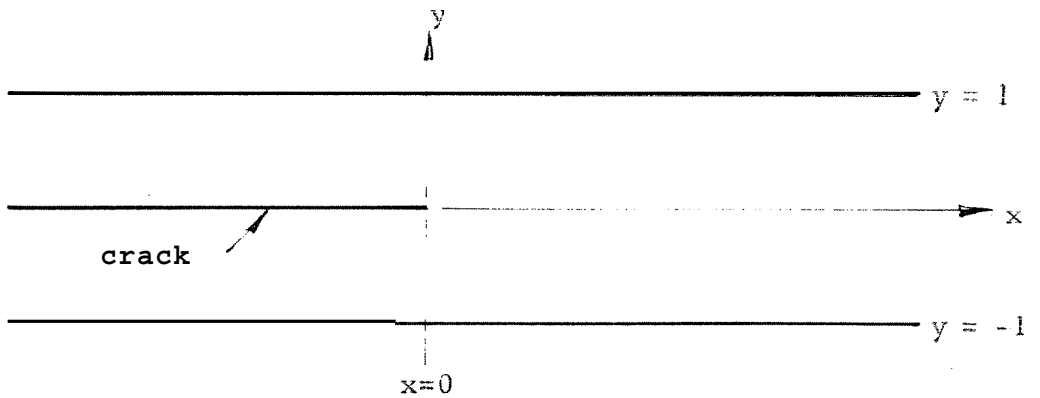


FIG. 22 GEOMETRY AND COORDINATE SYSTEM OF GRACKEU STRIP

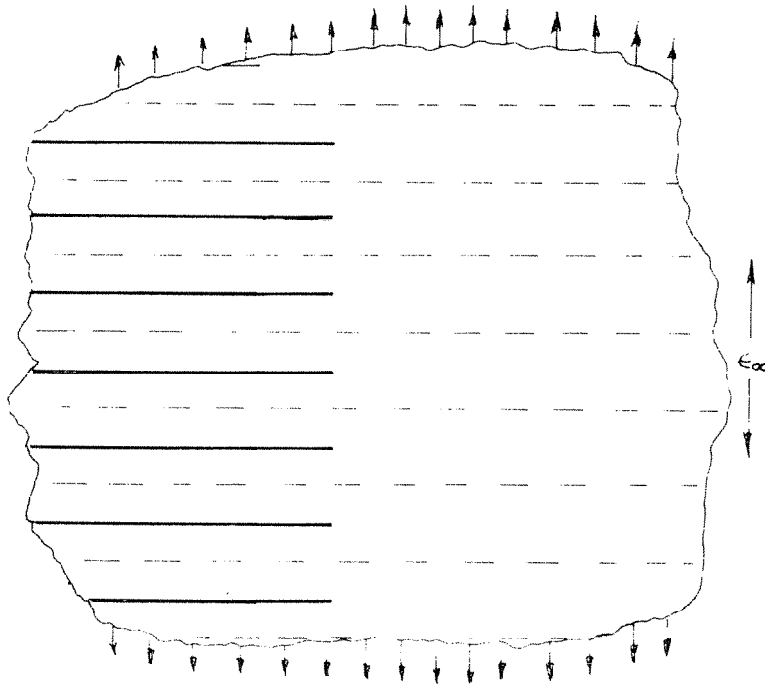


FIG. 23 EQUIVALENT GEOMETRY: THE DISPLACEMENTS v ARE APPLIED TO PRODUCE UNIFORM STRAIN ϵ_{∞} TO RIGHT OF CRACKS, DASHED LINES REMAINING STRAIGHT.

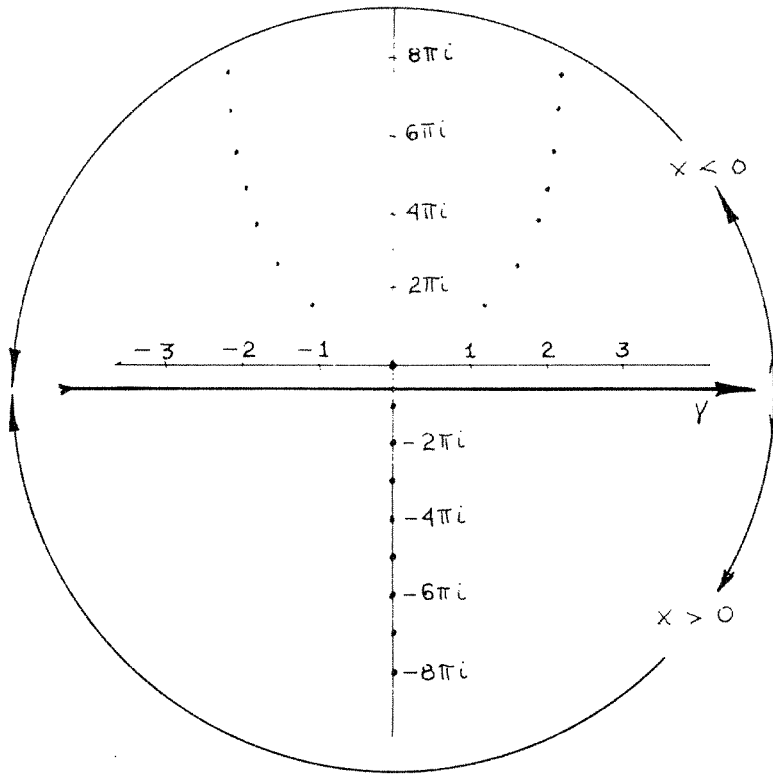


FIG. 24 LOCATION OF POLES AND CONTOURS OF INTEGRATION

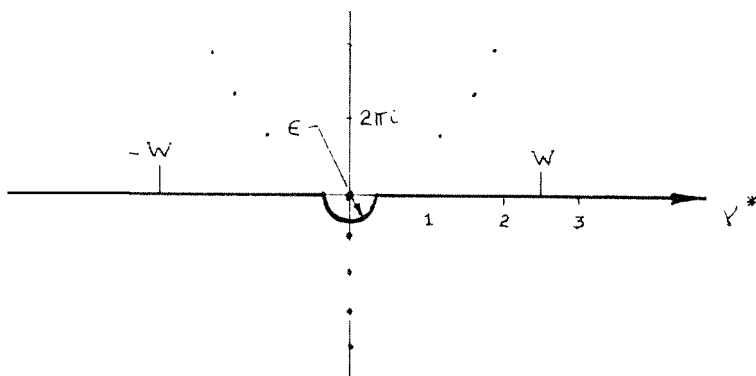


FIG. 25 INTEGRATION CONTOUR FOR ASYMPTOTIC EXPANSION

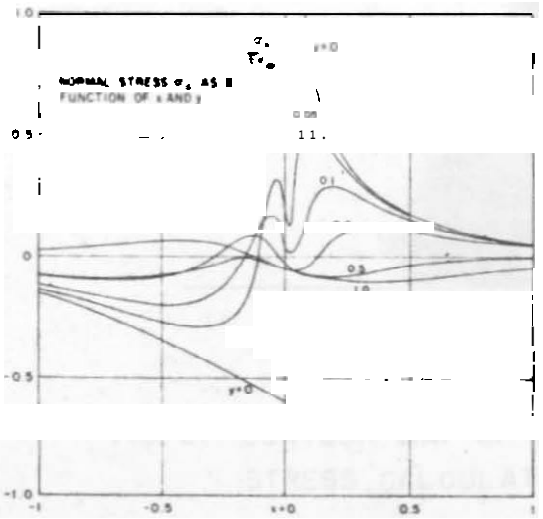
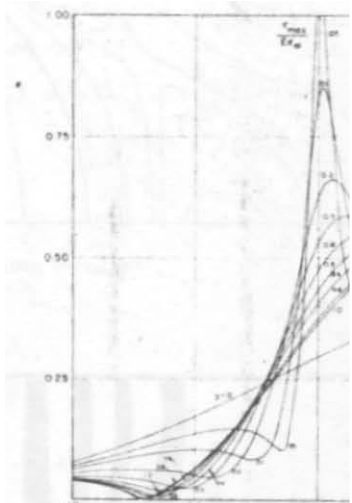
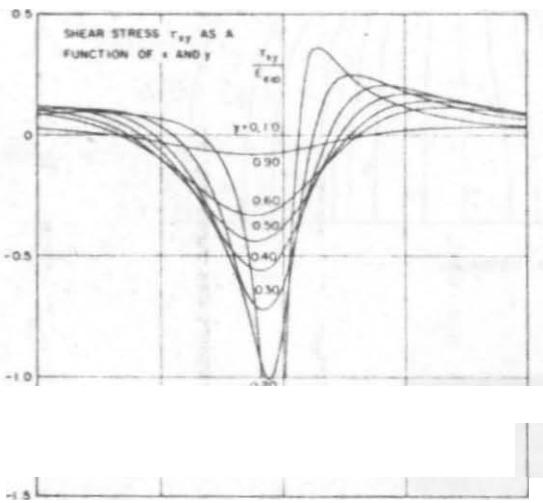
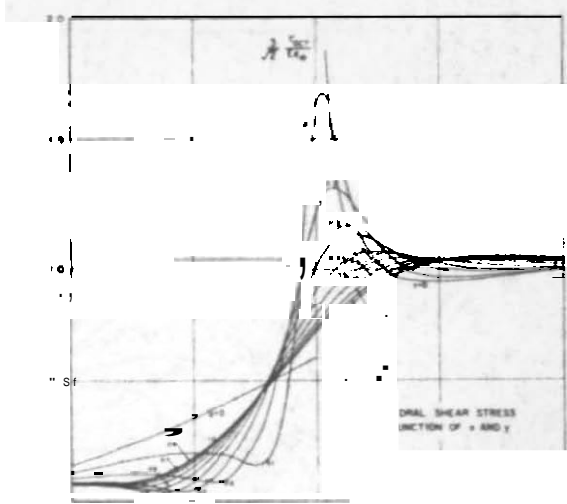
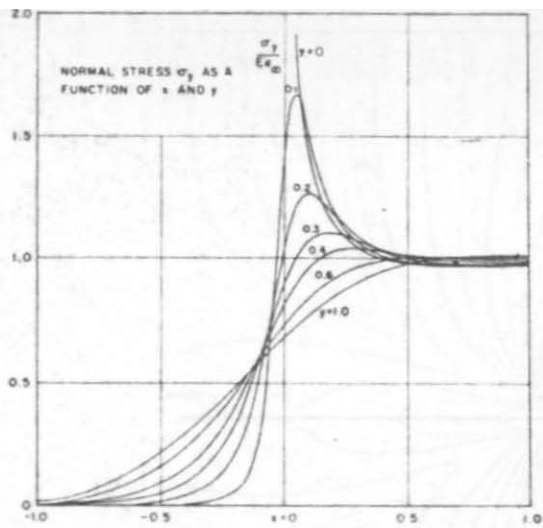


FIG. 26 STRESSES OF X AND Y

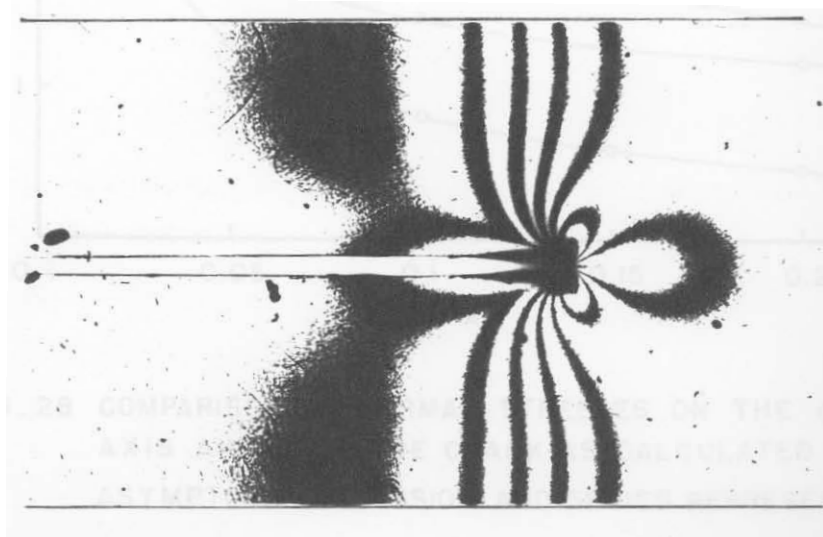
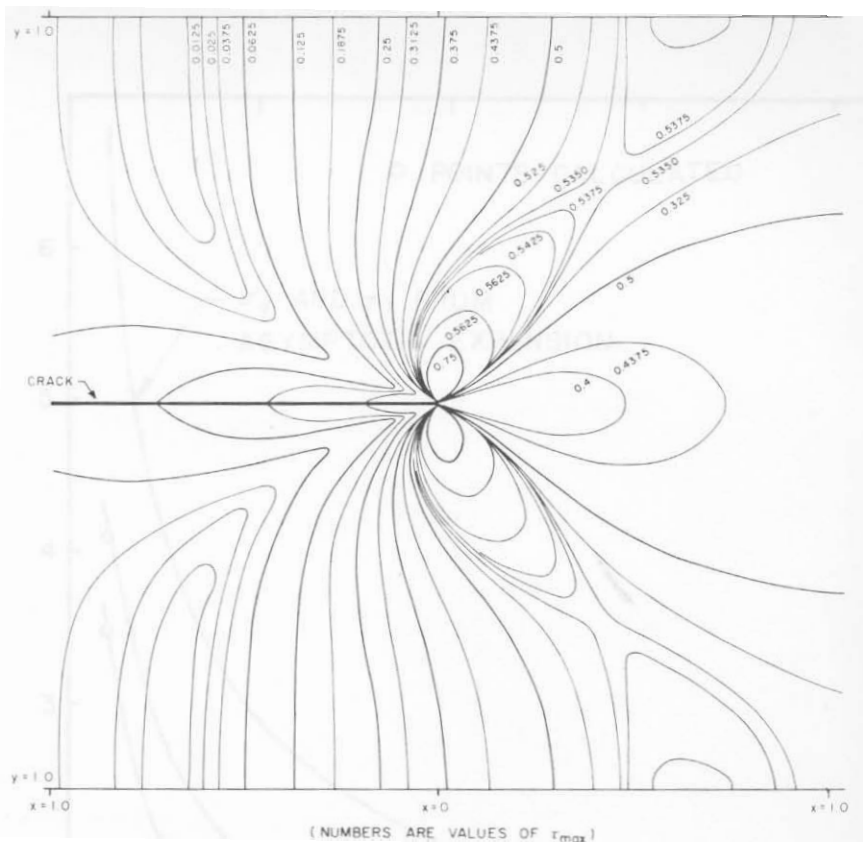


FIG. 27 CONTOUR MAP OF CONSTANT MAXIMUM SHEAR STRESS, CALCULATED AND EXPERIMENTAL

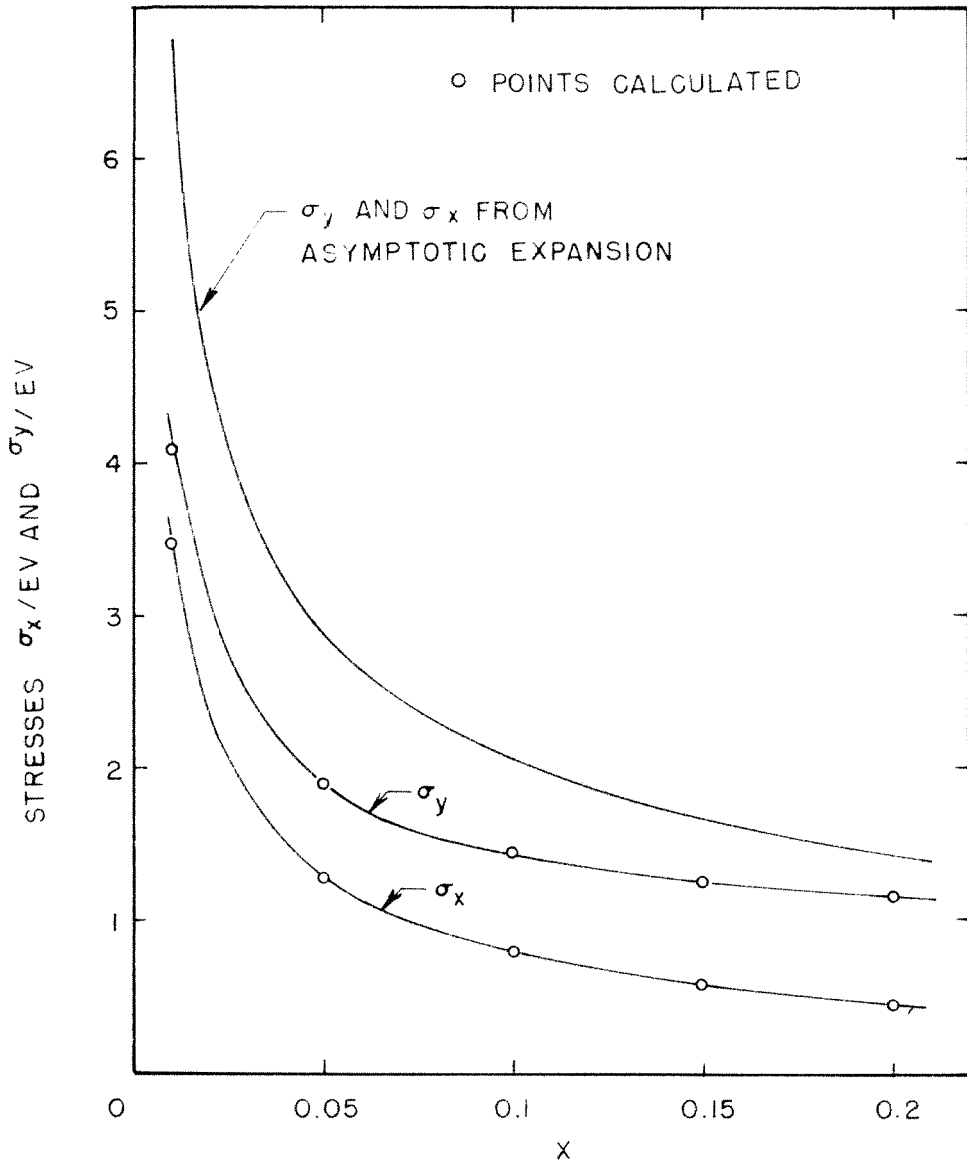


FIG. 28 COMPARISON OF NORMAL STRESSES ON THE CRACK AXIS AHEAD OF THE CRACK AS CALCULATED FROM ASYMPTOTIC EXPANSION AND SERIES REPRESENTATION

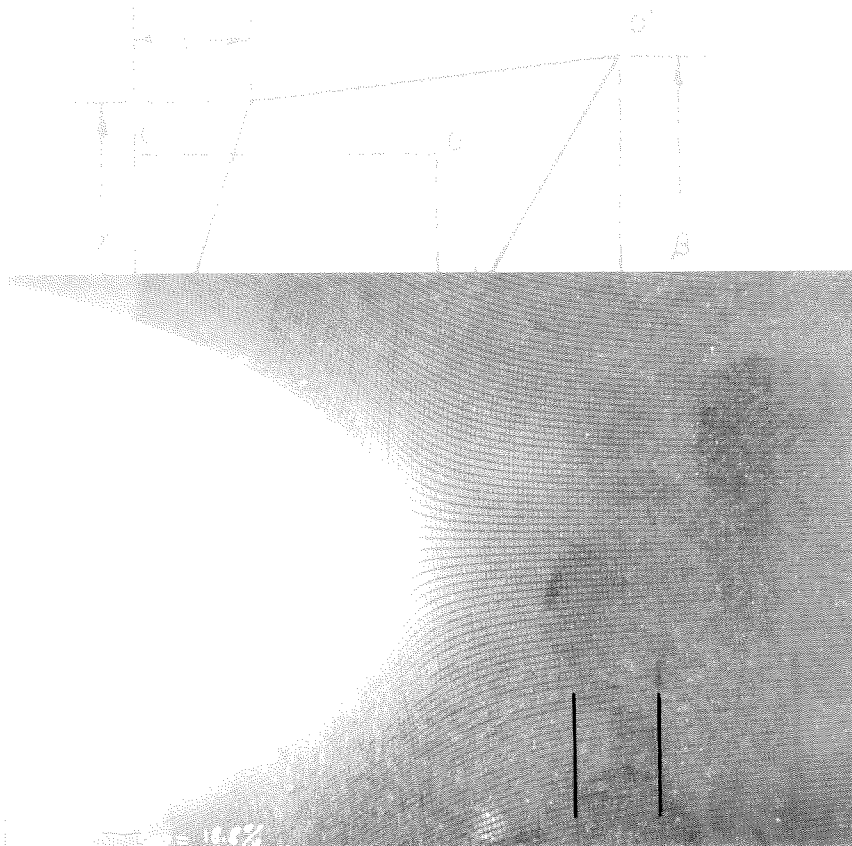


FIG. 29 DEFORMATION OF SQUARE GRID IN THE CRACK TIP VICINITY

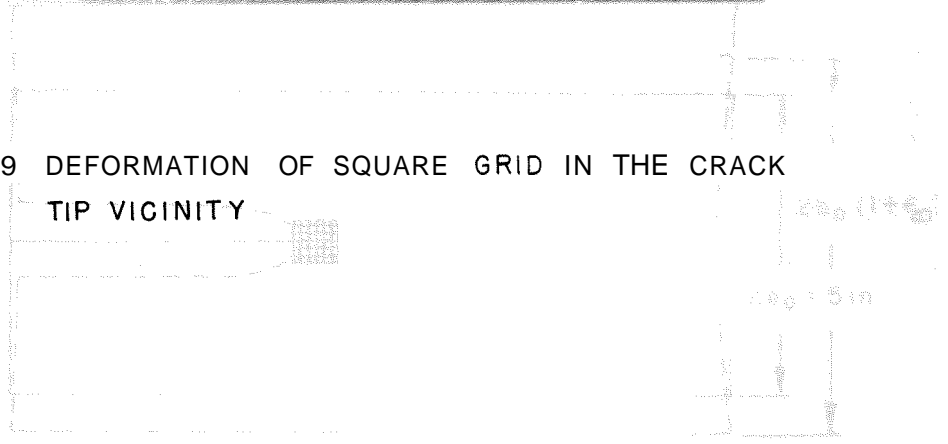


FIG. 30 SIZE OF SPECIMEN AND DIMENSIONS OF CRACK

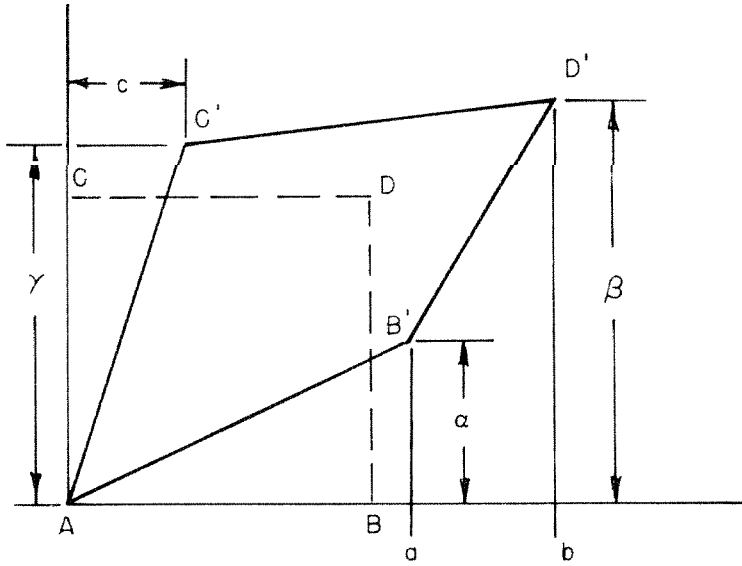


FIG. 30 ORIGINAL SQUARE, DEFORMED INTO QUADRILATERAL

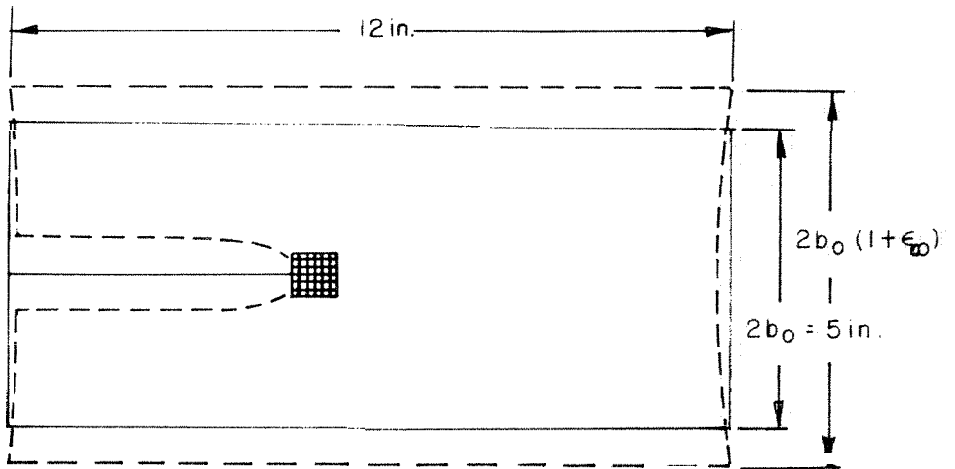


FIG. 31 SLIT SHEET GEOMETRY, AND DIMENSIONS ; THICKNESS = 0.01 in

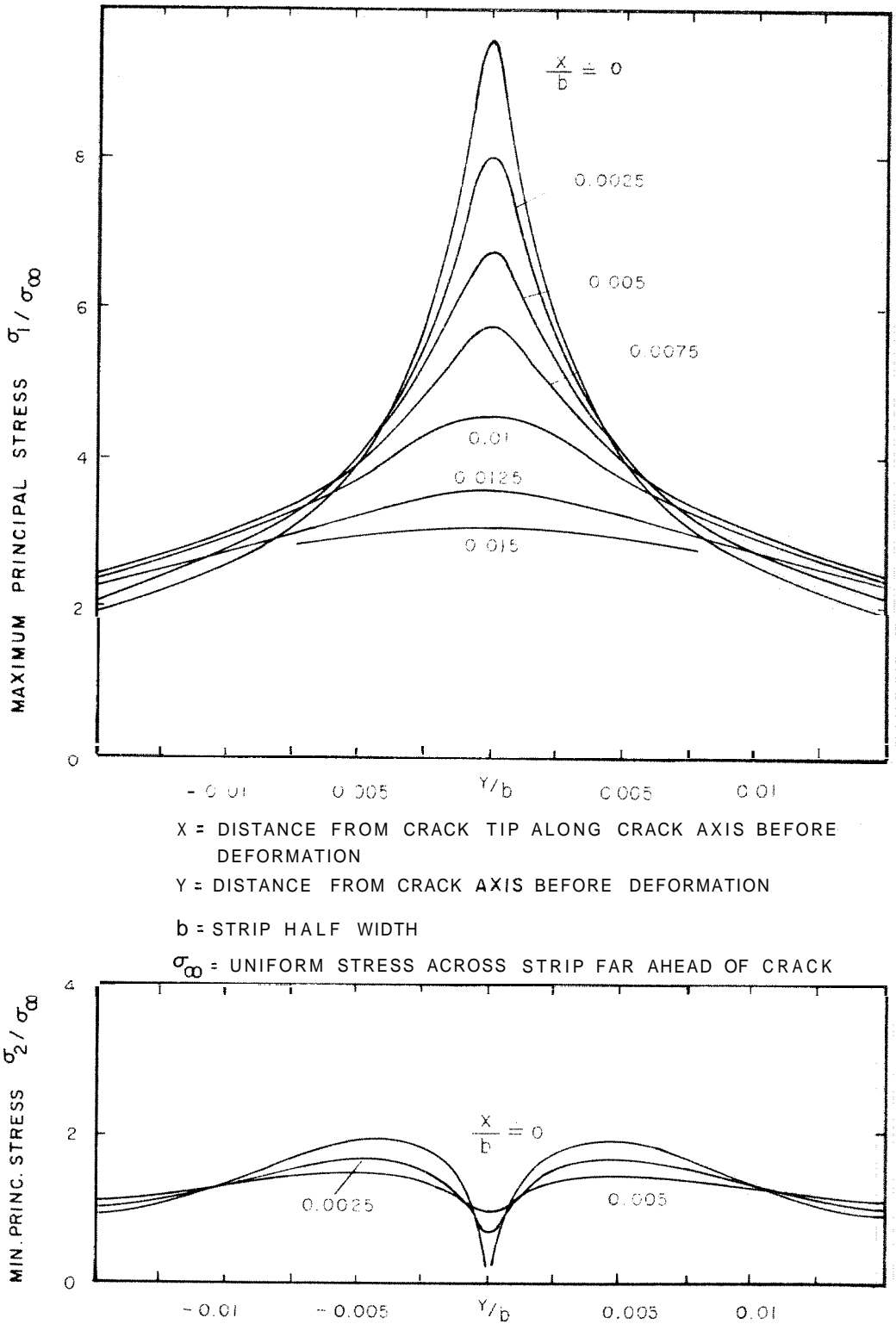


FIG.32 EXPERIMENTALLY DETERMINED PRINCIPAL STRESSES IN RUBBER STRIP AT A GROSS STRAIN $\epsilon_\infty = 19\%$

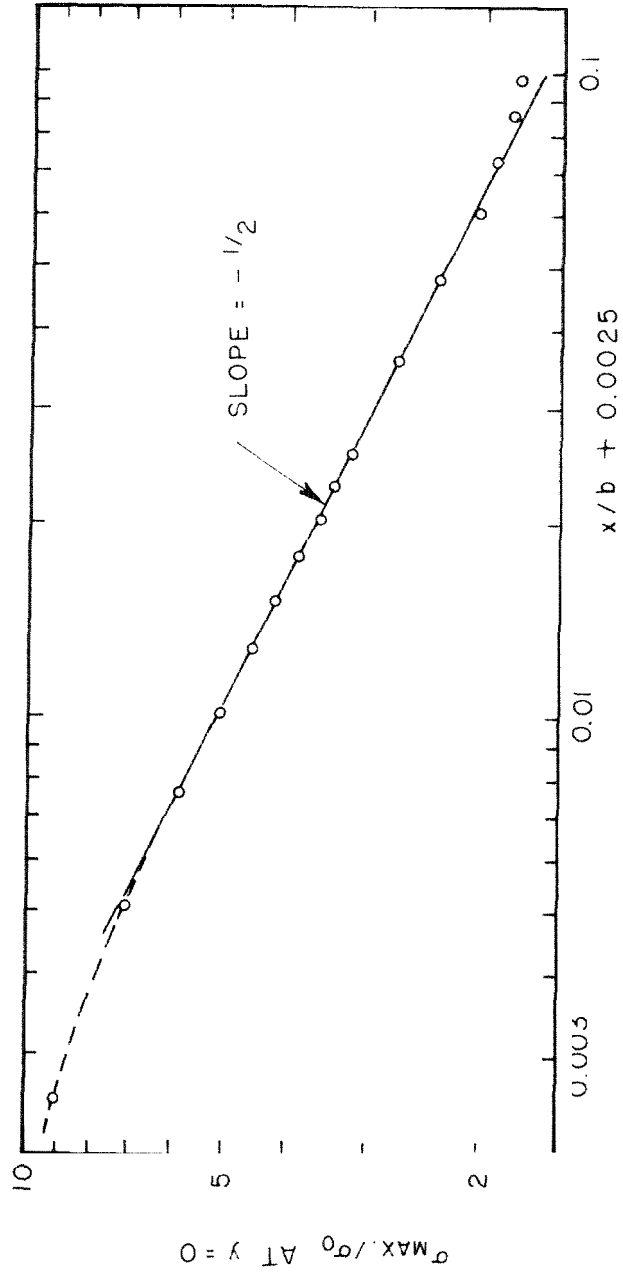


FIG. 33 MAXIMUM PRINCIPAL STRESS ON THE CRACK AXIS AS A FUNCTION OF THE UNDEFORMED COORDINATE X. CIRCLES DENOTE EXPERIMENTAL POINTS.

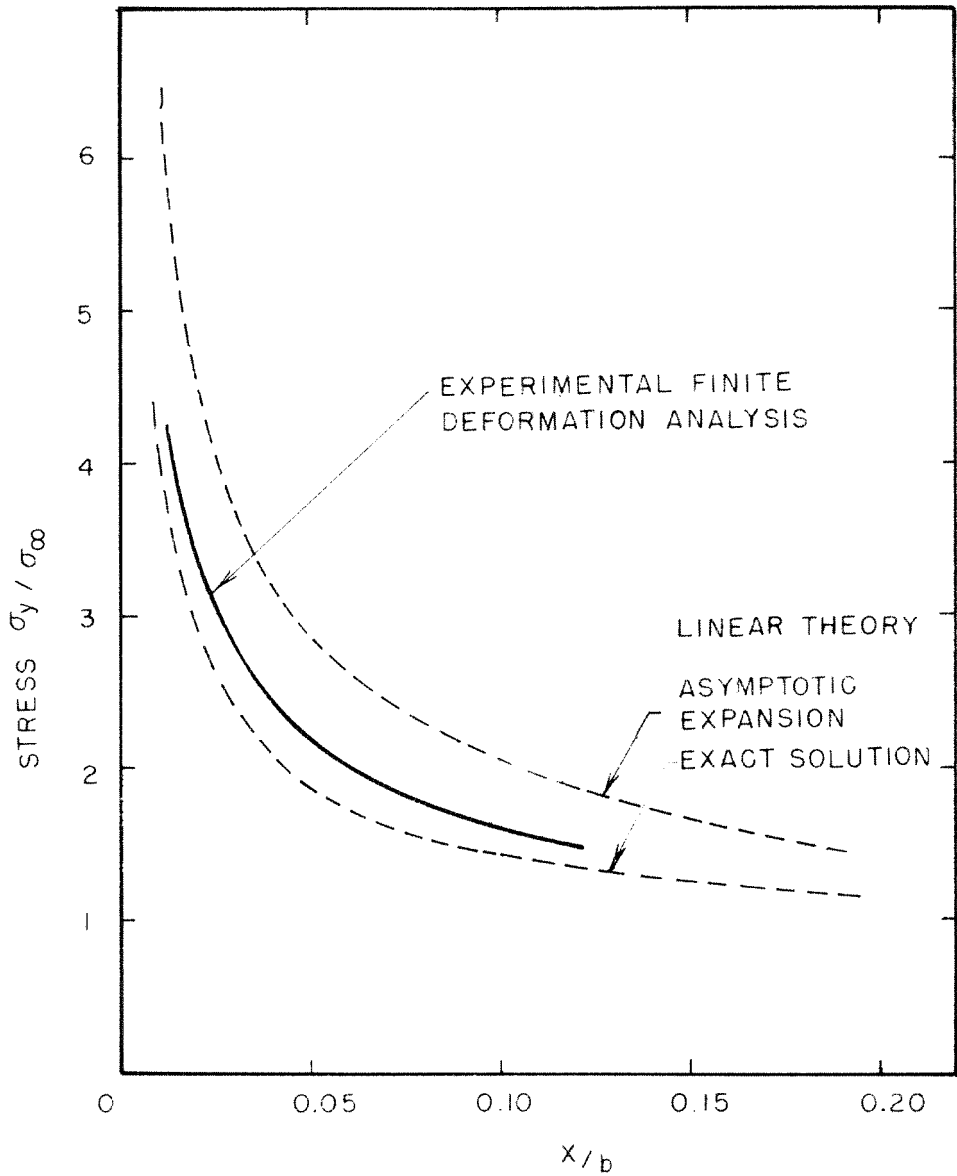


FIG 34 COMPARISON OF STRESS σ_y ON THE CRACK AXIS FOR LARGE DEFORMATION ANALYSIS AND INFINITESIMAL ELASTICITY SOLUTION

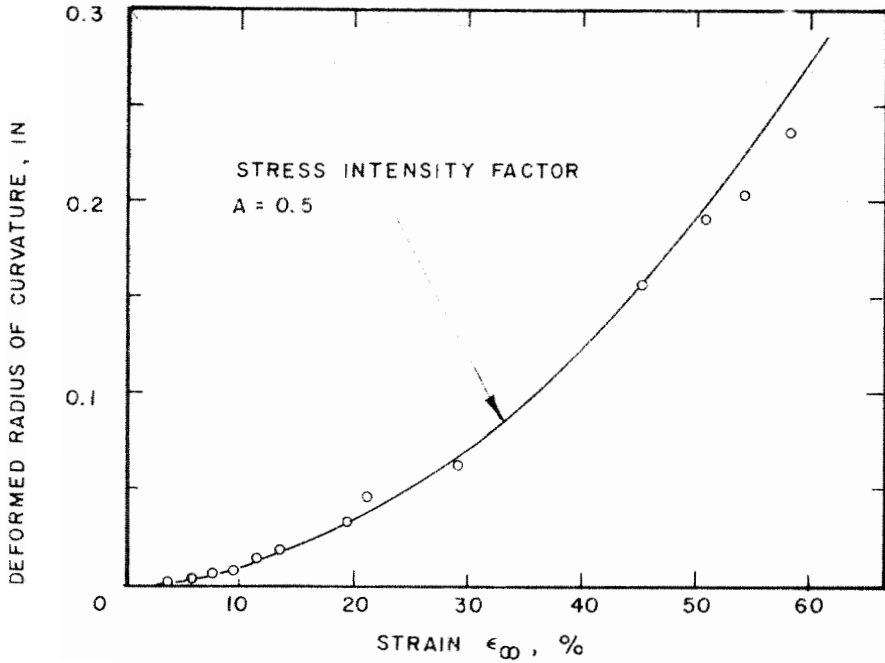


FIG.35 DEFORMED RADIUS OF CURVATURE AT THE CRACK TIP VS APPLIED GROSS STRAIN ϵ_{∞}

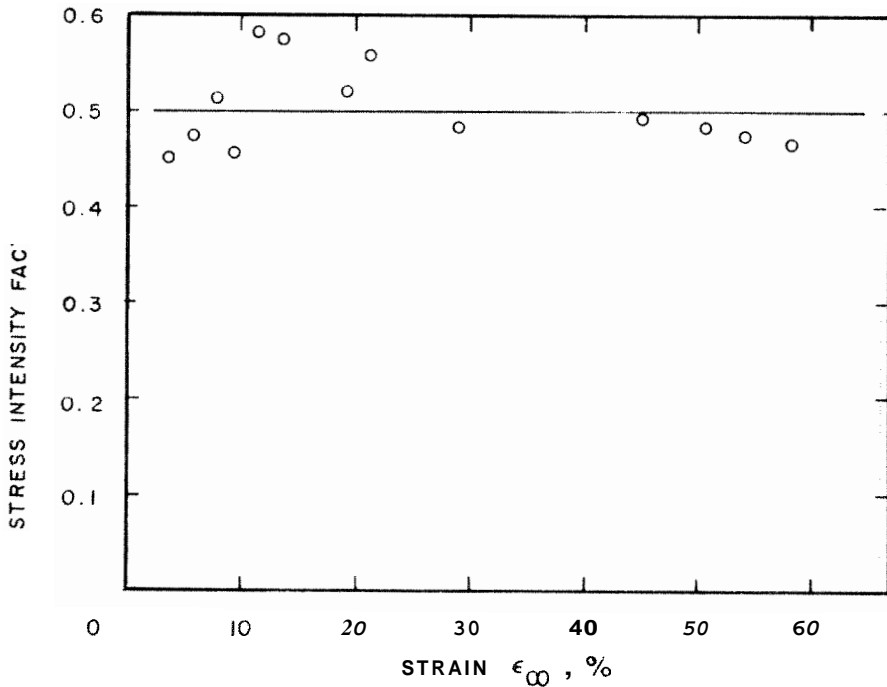


FIG.36 STRESS INTENSITY FACTOR A VS APPLIED GROSS STRAIN ϵ_{∞}

APPENDIX A

When a function $F(\omega)$ is to be written as the product of two functions the product functions are not unique, for if

$$F(\omega) = F^-(\omega) \cdot F^+(\omega) \tag{1A}$$

then also

$$F(\omega) = \{e^{g(\omega)} F^-(\omega)\} \cdot \{e^{-g(\omega)} F^+(\omega)\}. \tag{2A}$$

In the following F^- will be determined such that it behaves algebraically as $c \sim -\infty$.

Consider
$$f(\omega) = \frac{\sinh 2\omega}{4\omega} + \frac{1}{2} ; \tag{3A}$$

using Weierstrass' theorem on factorization of integral functions write

$$= \left\{ e^{C_1 \omega} \prod_{n=1}^{\infty} \left(1 - \frac{\omega}{\omega_n}\right) \left(1 - \frac{\omega}{\bar{\omega}_n}\right) e^{\frac{\omega}{\omega_n} - \frac{\omega}{\bar{\omega}_n}} \right\}^* \cdot \left\{ e^{-C_1 \omega} \prod_{n=1}^{\infty} \left(1 + \frac{\omega}{\omega_n}\right) \left(1 - \frac{\omega}{\bar{\omega}_n}\right) e^{-\frac{\omega}{\omega_n} - \frac{\omega}{\bar{\omega}_n}} \right\} \tag{4A}$$

where ω_n and $\bar{\omega}_n$ are the solutions of $f(\omega) = 0$ and their complex conjugates in the quadrant $0 < \arg \omega_n < \frac{\pi}{2}$. For further reference let

$\omega_n = w_n + i\beta_n$ and $R_n = |\omega_n|$. Writing (see reference 84)

$$\frac{\omega}{\sinh \omega} = \prod \left(1 - \frac{i\omega}{\pi}\right) \prod \left(1 - \frac{i\omega}{\pi}\right) \tag{5A}$$

with $\Gamma(x)$ denoting the Gamma function, the kernel function $F(\omega)$ can be expanded as

$$F(\omega) = \left\{ e^{C_1 \omega} \prod_{n=1}^{\infty} \left[\left(1 - \frac{\omega}{\omega_n}\right) \left(1 + \frac{\omega}{\omega_n}\right) e^{-2i \frac{\Omega_n}{R_n^2} \omega} \right] \Gamma^2\left(1 - \frac{i\omega}{\pi}\right) \right\}^* \tag{6A}$$

$$\& \left\{ e^{C_1 \omega} \prod_{n=1}^{\infty} \left[\left(1 + \frac{\omega}{\omega_n}\right) \left(1 - \frac{\omega}{\omega_n}\right) e^{2i \frac{\Omega_n}{R_n^2} \omega} \right] \Gamma^2\left(1 - \frac{i\omega}{\pi}\right) \right\}$$

from which, by identifying the factor which has singularities and zeros only in the upper half plane. $\text{Im}(\omega) > 0$ one chooses

$$F^-(\omega) = e^{C_1 \omega} \left\{ \prod_{n=1}^{\infty} \left[\left(1 - \frac{\omega}{\omega_n}\right) \left(1 - \frac{\omega}{\omega_n}\right) e^{-2i \frac{\Omega_n}{R_n^2} \omega} \right] \right\} \Gamma^2\left(1 - \frac{i\omega}{\pi}\right). \tag{7A}$$

It remains to determine the constant C_1 such that $F(\omega)$ has algebraic behavior at infinity.

Define $f^- \equiv \prod_{n=1}^{\infty} \left(1 - \frac{\omega}{\omega_n}\right) \left(1 - \frac{\omega}{\omega_n}\right) e^{-2i \frac{\Omega_n}{R_n^2} \omega}$ (8A)

and consider the product

$$P(\omega) = f^- \Gamma^2\left(\frac{3}{4} - \frac{i\omega}{\pi}\right) = \frac{\Gamma^2(3/4)}{e^{2i C_1 \frac{\omega}{\pi}}} \frac{\prod_{n=1}^{\infty} \left\{ \left(1 - \frac{\omega}{\omega_n}\right) \left(1 - \frac{\omega}{\omega_n}\right) e^{-2i \omega \frac{\Omega_n}{R_n^2}} \right\}}{\prod_{n=1}^{\infty} \left\{ \left(1 - \frac{i\omega}{(n-\frac{1}{4})\pi}\right)^2 e^{-2i \frac{\omega}{n\pi}} \right\}} \tag{9A}$$

where use has been made of the relation (cf. ref. 84)

$$\frac{1}{\alpha \Gamma(\alpha)} = e^{C\alpha} \prod_{n=1}^{\infty} \left(1 + \frac{\alpha}{n}\right) e^{-\frac{\alpha}{n}} \quad (10A)$$

with Euler's constant $C = 0.5772 \dots$. Now $P(\omega)$ is convergent when the products in

$$P(\omega) = \frac{\Gamma^2(3/4)}{e^{2iC\frac{\omega}{\pi}}} \left\{ \prod_{n=1}^{\infty} \frac{\left(1 - \frac{\omega}{\omega_n}\right)\left(1 + \frac{\omega}{\omega_n}\right)}{\left(1 - \frac{\omega}{(n-\frac{1}{4})\pi}\right)^2} \right\} \left\{ \prod_{n=1}^{\infty} e^{-2i\omega\left(\frac{\mathcal{R}_n}{R_n^2} - \frac{1}{n\pi}\right)} \right\} \quad (11A)$$

converge separately which is readily shown to hold true under consideration of the behavior of the roots for large n ,

$$\mathcal{R}_n \sim \left(n - \frac{1}{4}\right)\pi - \frac{\ln\sqrt{(4n-1)\pi}}{(4n-1)\pi} \quad (12A)$$

$$\omega_n \sim \ln\sqrt{(4n-1)\pi}$$

The first product in equation 11A approaches a constant as $\omega \rightarrow \infty$ and the second factor tends toward $e^{-2i\omega\Phi}$, Φ being a real constant. Hence it follows from equation 9A that $f^-(\omega)$ behaves asymptotically as

$$f^-(\omega) \underset{\omega \rightarrow \infty}{\sim} \prod_{n=1}^{\infty} \left\{ \frac{(4n-1)\pi}{4|\omega_n|} \right\}^2 \frac{\Gamma^2(3/4)}{\Gamma^2\left(\frac{3}{4} - \frac{i\omega}{\pi}\right)} e^{-2i\omega\left(\frac{C}{\pi} - \Phi\right)} \quad (13A)$$

and consequently, from equation 7A that

$$F^-(\omega) \underset{\omega \rightarrow \infty}{\sim} e^{C_1 \omega} \Gamma^2\left(\frac{3}{4}\right) \prod_{n=1}^{\infty} \left\{ \frac{(4n-1)\pi}{4|\omega_n|} \right\}^2 \frac{\Gamma^2\left(1 - \frac{i\omega}{\pi}\right)}{\Gamma^2\left(\frac{3}{4} - \frac{i\omega}{\pi}\right)} e^{-2i\omega\left(\frac{C}{\pi} + \Phi\right)} \quad (14A)$$

Since with the help of Stirling's approximation of Gamma functions this can be shown to behave asymptotically as

$$F^-(\omega) \underset{\omega \rightarrow \infty}{\sim} \Gamma^2\left(\frac{3}{4}\right) \prod_{n=1}^{\infty} \left\{ \frac{(4n-1)\pi}{4|\omega_n|} \right\}^2 \sqrt{\frac{i\omega}{e\pi}} e^{[C_1 - 2i\left(\frac{C}{\pi} + \Phi\right)]\omega} \quad (15A)$$

choose $C_1 = 2i\left(\frac{C}{\pi} + \Phi\right)$ (16A)

so that

$$F^-(\omega) = \prod_{n=1}^{\infty} \frac{\left(1 - \frac{\omega}{\omega_n}\right)\left(1 + \frac{\omega}{\omega_n}\right)}{\left(1 - \frac{i\omega}{n\pi}\right)^2} \quad (17A)$$

and

$$F^-(\omega) \underset{\omega \rightarrow \infty}{\sim} \Gamma^2\left(\frac{3}{4}\right) \prod_{n=1}^{\infty} \left\{ \frac{(4n-1)\pi}{4|\omega_n|} \right\}^2 \sqrt{\frac{i\omega}{e\pi}} \quad ; \quad (18A)$$

$\omega \rightarrow \infty$
 $-\pi < \arg \omega < \pi$

APPENDIX B

After addition of the uniform stress field to that of the pressure crack problem, the stresses and displacements are, for

$x > 0$

$$\frac{\sigma_y(x,y)}{E} = 1 - \frac{1}{2} \sum_{m=1}^{\infty} [1 - m\pi(F_m + x)] \cos m\pi y \varphi_m e^{-m\pi x}$$

$$\frac{\sigma_x(x,y)}{E} = \frac{1}{2} \sum_{m=1}^{\infty} [1 + m\pi(F_m + x)] \cos m\pi y \varphi_m e^{-m\pi x}$$

$$\frac{\tau_{xy}(x,y)}{E} = \frac{1}{2} \sum_{m=1}^{\infty} [m\pi(F_m + x)] \sin m\pi y \varphi_m e^{-m\pi x}$$

$$u(x,y) = -\nu x - \frac{1}{2} \sum_{m=1}^{\infty} \left[\frac{2}{m\pi} + (1+\nu)(F_m + x) \right] \cos m\pi y \varphi_m e^{-m\pi x}$$

$$v(x,y) = y + \frac{1}{2} \sum_{m=1}^{\infty} \left[\frac{1-\nu}{m\pi} - (1+\nu)(F_m + x) \right] \sin m\pi y \varphi_m e^{-m\pi x},$$

...

$$F_m = \frac{2}{\pi} \sum_{n=1}^{\infty} \left\{ \frac{\Omega_n + m\pi}{R_n^2 + 2m\pi\Omega_n + (m\pi)^2} - \frac{1}{n+m} \right\} - \frac{1}{m\pi}$$

$$\varphi_m = \varphi(-im\pi).$$

For $x < 0$ there results

$$\frac{\bar{\sigma}_y(x,y)}{E} = -\operatorname{Re} \sum_{n=1}^{\infty} \left\{ \omega_n y \frac{\sinh \omega_n (1-y)}{\sinh \omega_n} - \sinh \omega_n y \right\} \psi_n e^{-i\omega_n x}$$

$$\frac{\bar{\sigma}_x(x,y)}{E} = \operatorname{Re} \sum_{n=1}^{\infty} \left\{ \omega_n y \frac{\sinh \omega_n (1-y)}{\sinh \omega_n} + \sinh \omega_n y + 2\omega_n \frac{\cosh \omega_n y}{\sinh^2 \omega_n} \right\} \psi_n e^{-i\omega_n x}$$

$$\frac{\bar{\tau}_{xy}(x,y)}{E} = -\operatorname{Re} \sum_{n=1}^{\infty} i \left\{ \omega_n y \frac{\cosh \omega_n (1-y)}{\sinh \omega_n} - \omega_n \frac{\sinh \omega_n y}{\sinh^2 \omega_n} \right\} \psi_n e^{-i\omega_n x}$$

$$u(x,y) = -\operatorname{Re} \sum_{n=1}^{\infty} i \left\{ (1-\nu) \frac{\cosh \omega_n (1-y)}{\omega_n \sinh \omega_n} - (1+\nu) \left[y \frac{\sinh \omega_n (1-y)}{\sinh \omega_n} + \frac{\cosh \omega_n y}{\sinh^2 \omega_n} \right] \right\} \psi_n e^{-i\omega_n x}$$

$$v(x,y) = 1 + \operatorname{Re} \sum_{n=1}^{\infty} \left\{ 2 \frac{\sinh \omega_n (1-y)}{\omega_n \sinh \omega_n} - (1-\nu) \left[y \frac{\cosh \omega_n (1-y)}{\sinh \omega_n} - \frac{\sinh \omega_n y}{\sinh^2 \omega_n} \right] \right\} \psi_n e^{-i\omega_n x}$$

where

$$\psi_n = -\omega_n \frac{\left(1 - \frac{i\omega_n}{n\pi}\right)^2}{\left(1 + \frac{i\omega_n}{\omega_n}\right)} \quad \begin{matrix} \infty \\ m=1 \\ m \neq n \end{matrix} \frac{\left(1 - \frac{i\omega_n}{m\pi}\right)^2}{\left(1 - \frac{\omega_n}{\omega_m}\right)\left(1 + \frac{\omega_n}{\omega_m}\right)}$$